# The SOFIA Massive (SOMA) Star Formation Survey


Jonathan C. Tan

James M. De Buizer
Mengyao Liu
Yichen Zhang

Jan E. Staff
Maria T. Beltrán
Kei Tanaka
Barbara Whitney
Ralph Shuping

Nicola Da Rio
Viviana Rosero
Maria Drozdovskaya


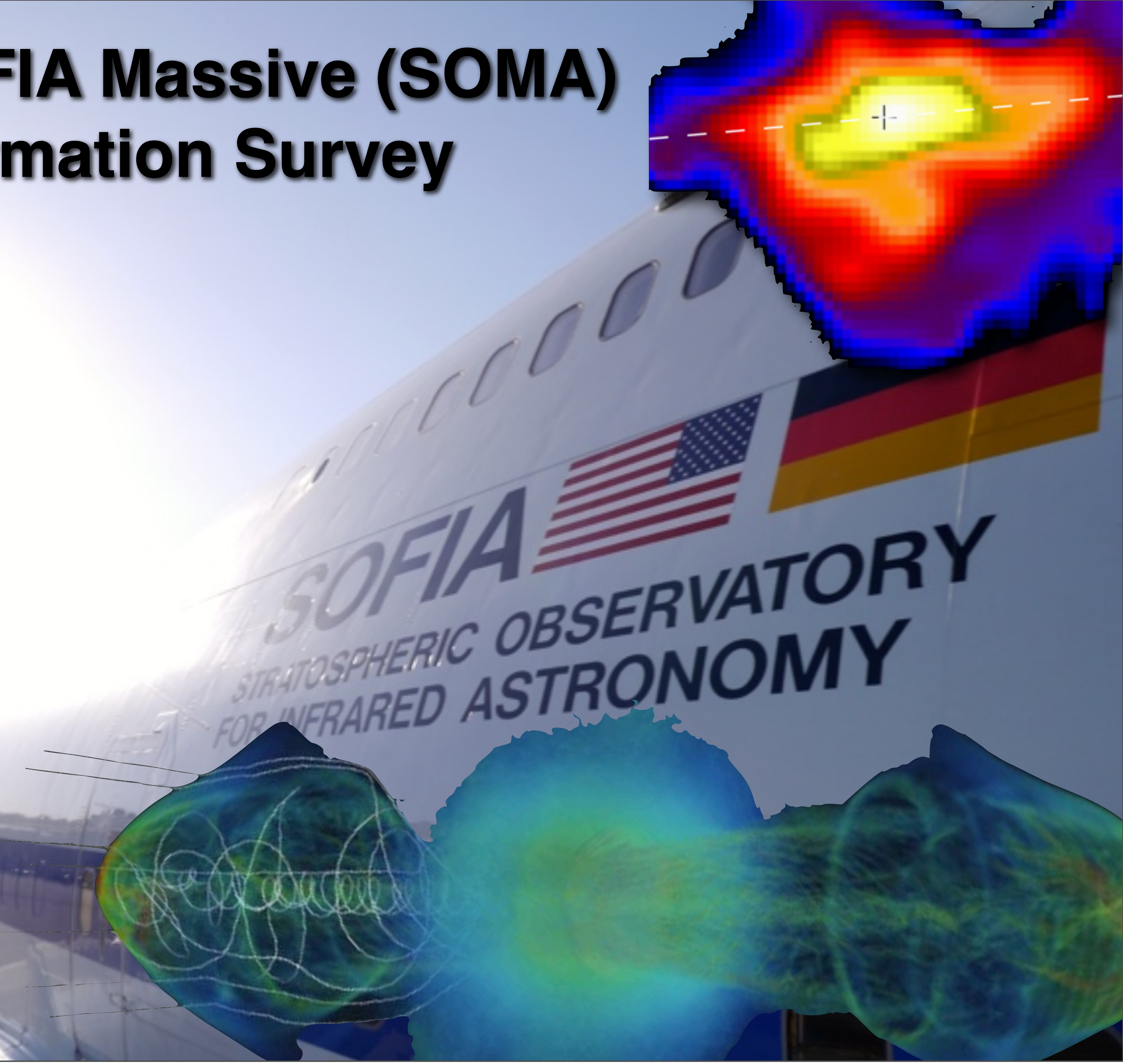

# The Importance of Massive Stars

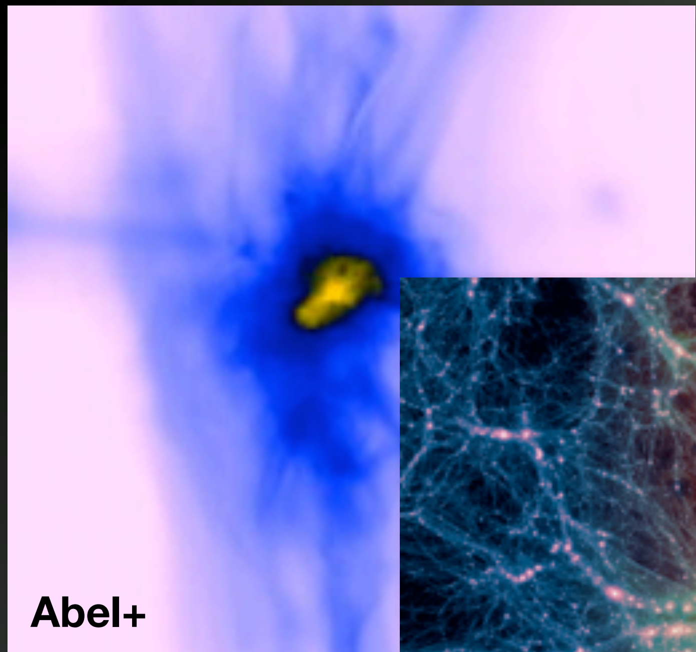


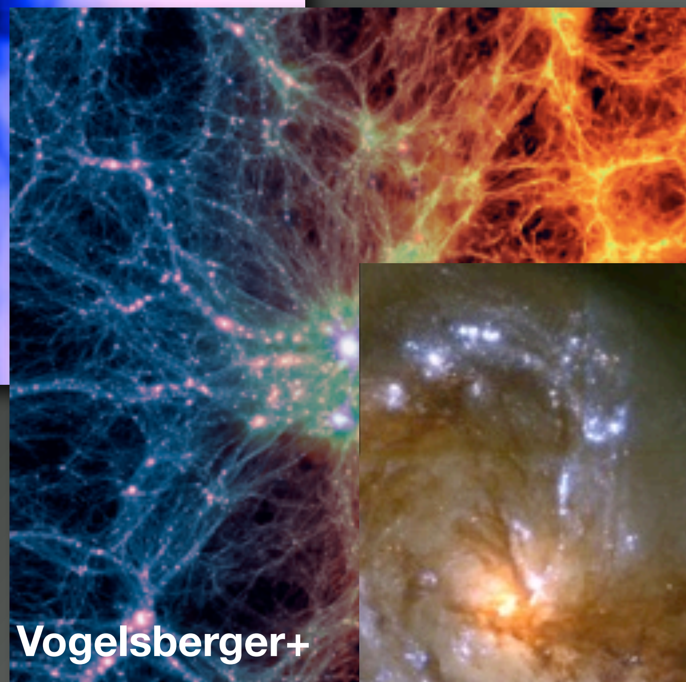






**Zinnecker & Yorke (2007)**
**Tan et al. (2014)**

# The Physics of High-Mass Star Formation

## A complicated, nonlinear process:

- Gravity vs pressure (thermal, magnetic, turbulence, radiation, cosmic rays) and shear.
- Heating and cooling, generation and decay of turbulence, generation (dynamo) and diffusion of B-fields.
- Chemical evolution of dust and gas.
- Fragmentation
- Stellar structure and evolution
- Feedback

- Wide range of scales (~12 dex in space, time) and multidimensional.
- Uncertain/unconstrained initial conditions/boundary conditions.

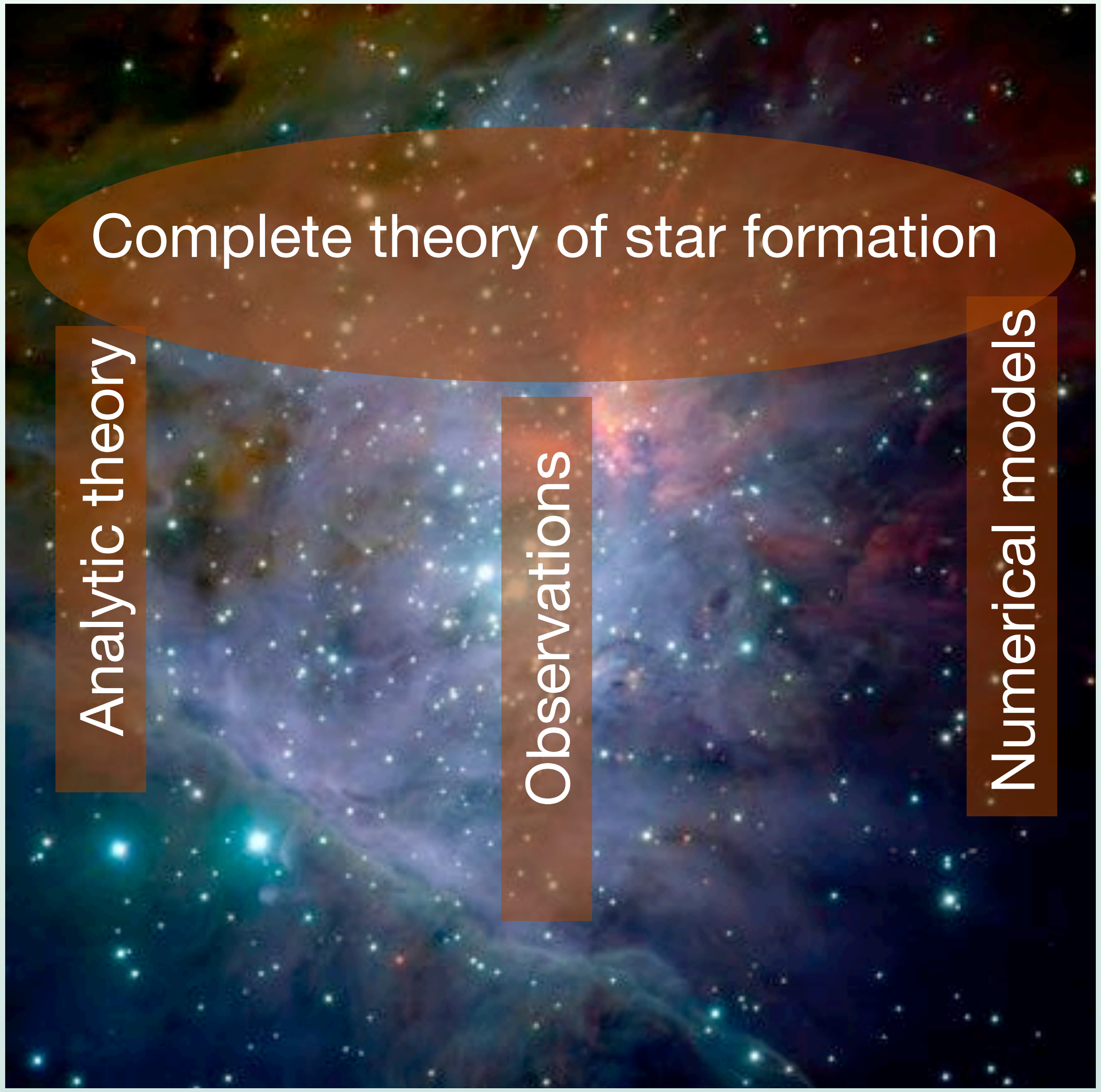


Notation for gas structures:
Core -> star or close binary
Clump -> star cluster

# (Massive) Star Formation: Open Questions

- Causation: external triggering or spontaneous gravitational instability?
- Initial conditions: how close to equilibrium?
- Accretion mechanism: [turbulent/magnetic/thermal-pressure]-regulated fragmentation to form **cores** vs **competitive accretion / mergers**
- Timescale: fast or slow (# of dynamical times)?
- End result
  - Initial mass function (IMF)
  - Binary fraction and properties

Salpeter (1955)
$dN_*/dm_* = A\, m_*^{-2.35}$

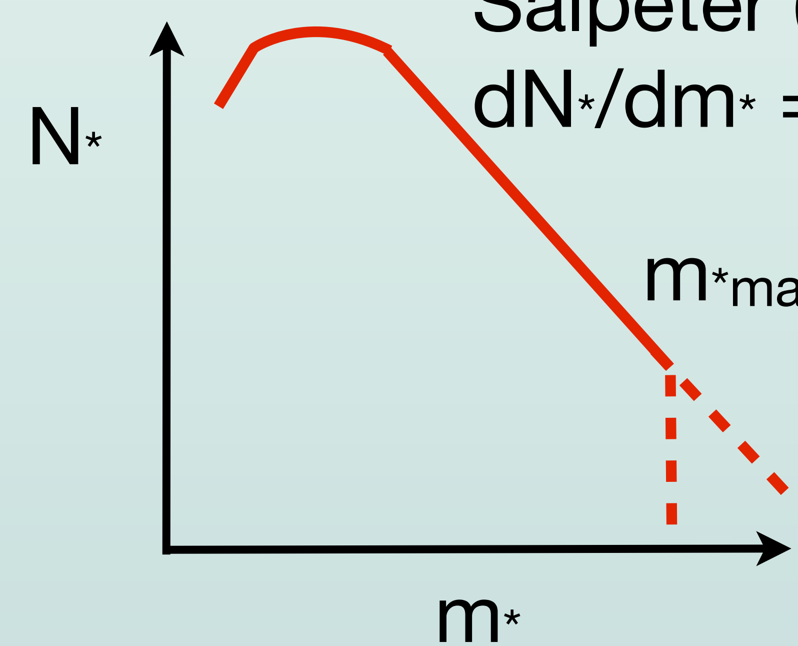


**How do these properties vary with environment?**

**Subgrid model of SF? Threshold $n_{H*}$? Efficiency $\varepsilon_{ff}$?**

# The Environments of Massive Star Formation

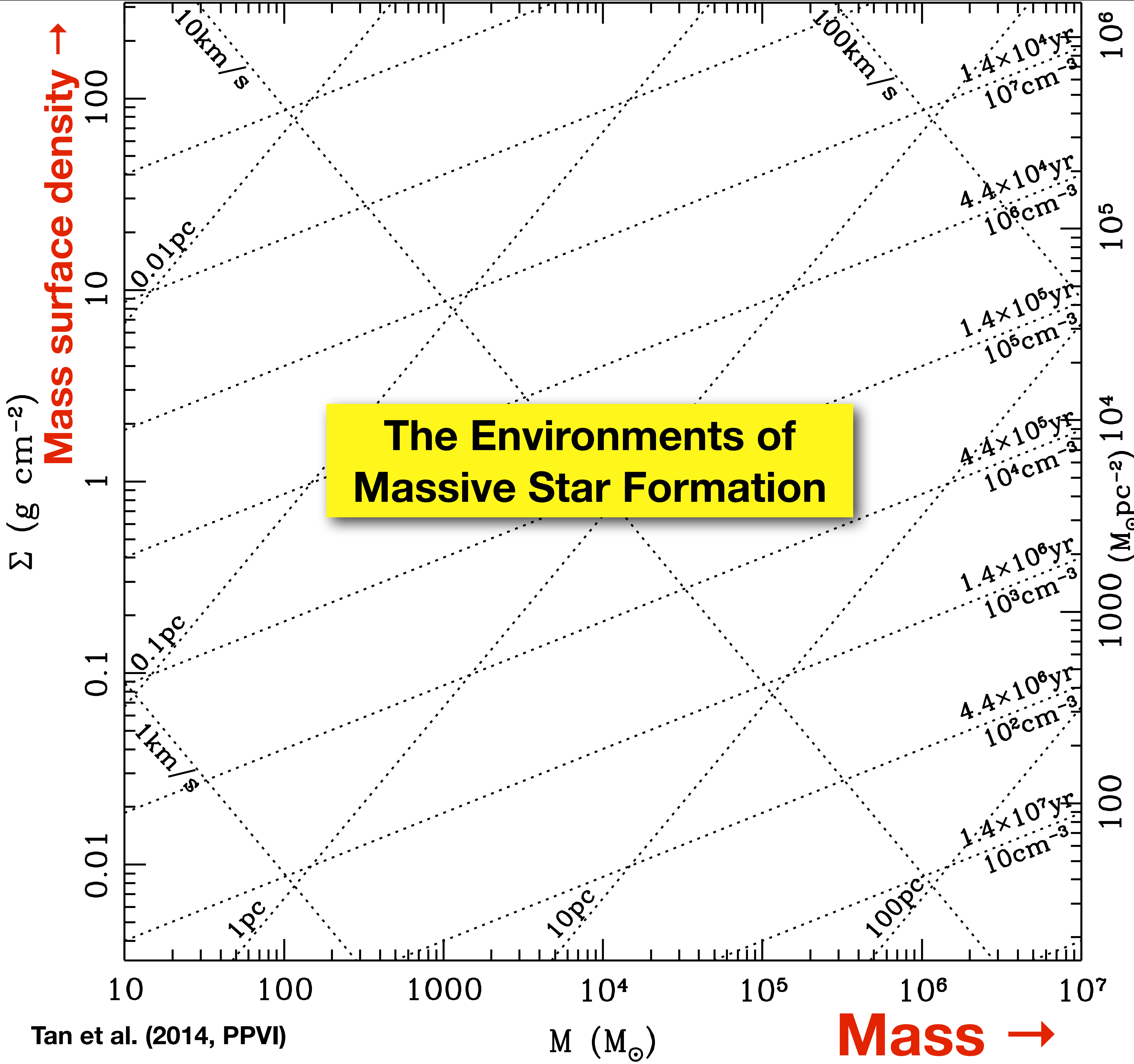


Tan et al. (2014, PPVI)

## Σ - M Diagram

Physical Properties of Star-Forming Regions

$$\Sigma \equiv \frac{M}{\pi R^2}$$

$$\bar{P} \simeq G\Sigma^2$$

$$\bar{P}/k = 4.3 \times 10^8 \Sigma^2 \, K \, cm^{-3}$$

$$t_{ff} = \left(\frac{3\pi}{32 G\rho}\right)^{1/2}$$

# Σ - M Diagram

Physical Properties of Star-Forming Regions

$$\Sigma \equiv \frac{M}{\pi R^2}$$

$$\bar{P} \simeq G\Sigma^2$$

$$\bar{P}/k = 4.3 \times 10^8 \Sigma^2 \, K\, cm^{-3}$$

$$t_{ff} = \left(\frac{3\pi}{32G\rho}\right)^{1/2}$$

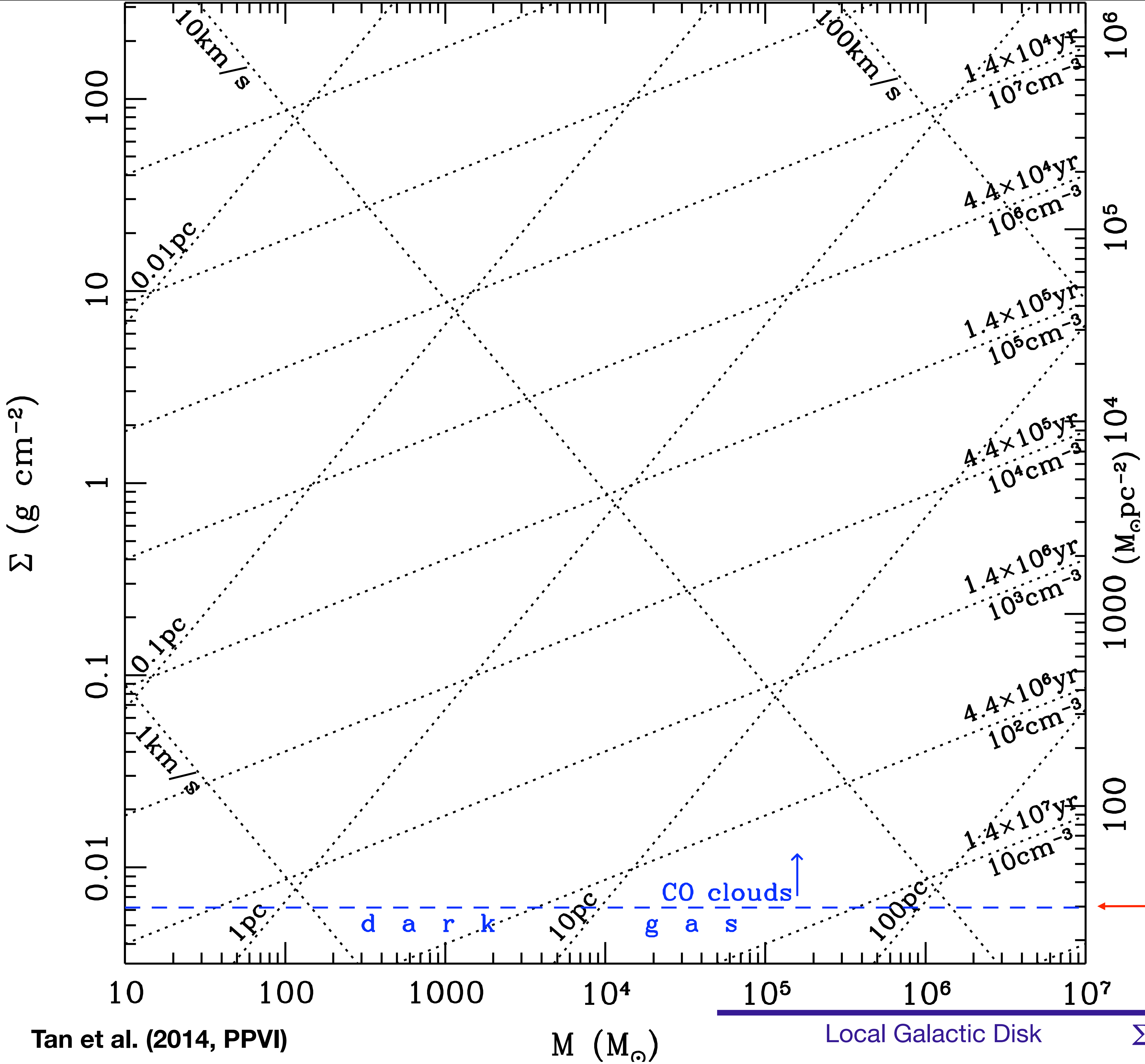


$A_V=1.4$

$N_H=3.0\times10^{21} cm^{-2}$

$\Sigma=34\ M_\odot\ pc^{-2}$

Local Galactic Disk $\Sigma \sim 10\ M_\odot\ pc^{-2}$

**Tan et al. (2014, PPVI)**

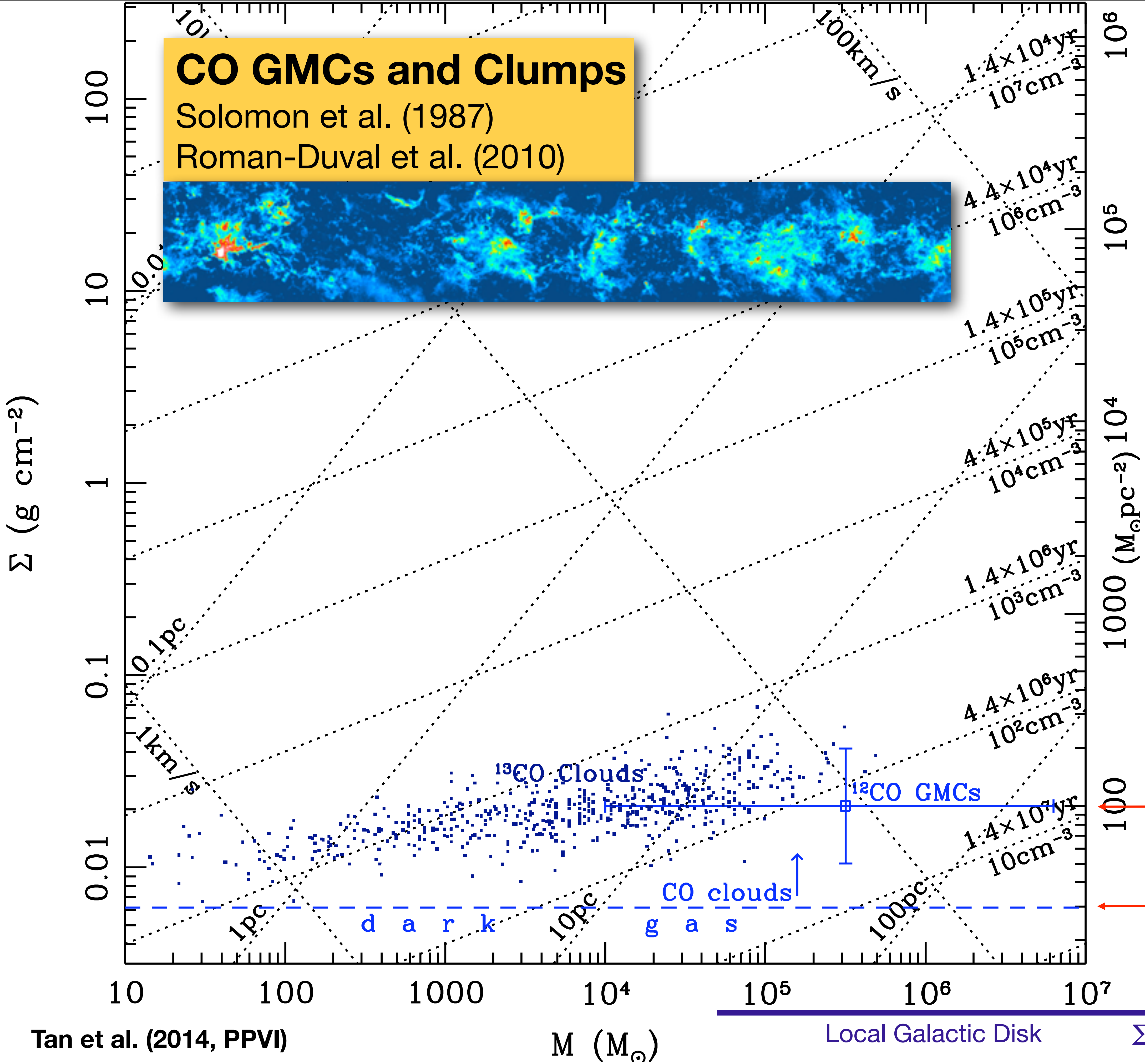


# Σ - M Diagram

Physical Properties of Star-Forming Regions

$$\Sigma \equiv \frac{M}{\pi R^2}$$

$$\bar{P} \simeq G\Sigma^2$$

$$\bar{P}/k = 4.3 \times 10^8 \Sigma^2\, K\, cm^{-3}$$

$$t_{ff} = \left(\frac{3\pi}{32G\rho}\right)^{1/2}$$

$A_V = 7.5$
$A_{8\mu m} = 0.30$
$N_H = 1.6 \times 10^{22} cm^{-2}$
$\Sigma = 180\ M_\odot\ pc^{-2}$

$A_V = 1.4$
$N_H = 3.0 \times 10^{21} cm^{-2}$
$\Sigma = 34\ M_\odot\ pc^{-2}$

Local Galactic Disk $\Sigma \sim 10\ M_\odot\ pc^{-2}$

Tan et al. (2014, PPVI)

# Σ - M Diagram

Physical Properties of Star-Forming Regions

$$\Sigma \equiv \frac{M}{\pi R^2}$$

$$\bar{P} \simeq G\Sigma^2$$

$$\bar{P}/k = 4.3 \times 10^8 \Sigma^2 \, K\, cm^{-3}$$

$$t_{ff} = \left(\frac{3\pi}{32 G\rho}\right)^{1/2}$$

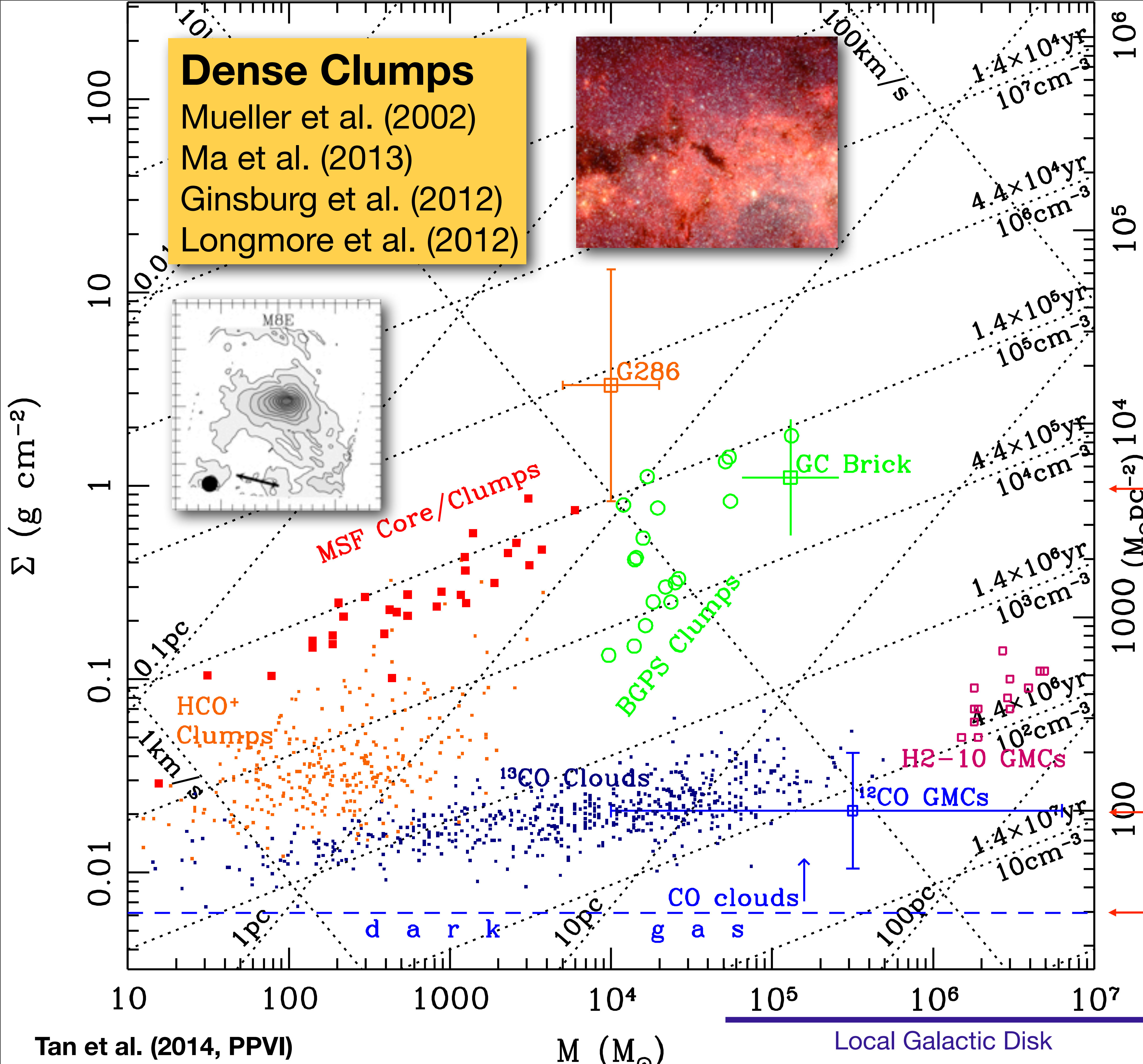


$A_V$=230
$A_{8\mu m}$=8.1
$N_H$=4.2x10$^{23}$cm$^{-2}$
Σ=4800 $M_\odot$ pc$^{-2}$

$A_V$=7.5
$A_{8\mu m}$=0.30
$N_H$=1.6x10$^{22}$cm$^{-2}$
Σ=180 $M_\odot$ pc$^{-2}$

$A_V$=1.4
$N_H$=3.0x10$^{21}$cm$^{-2}$
Σ=34 $M_\odot$ pc$^{-2}$

**Tan et al. (2014, PPVI)**

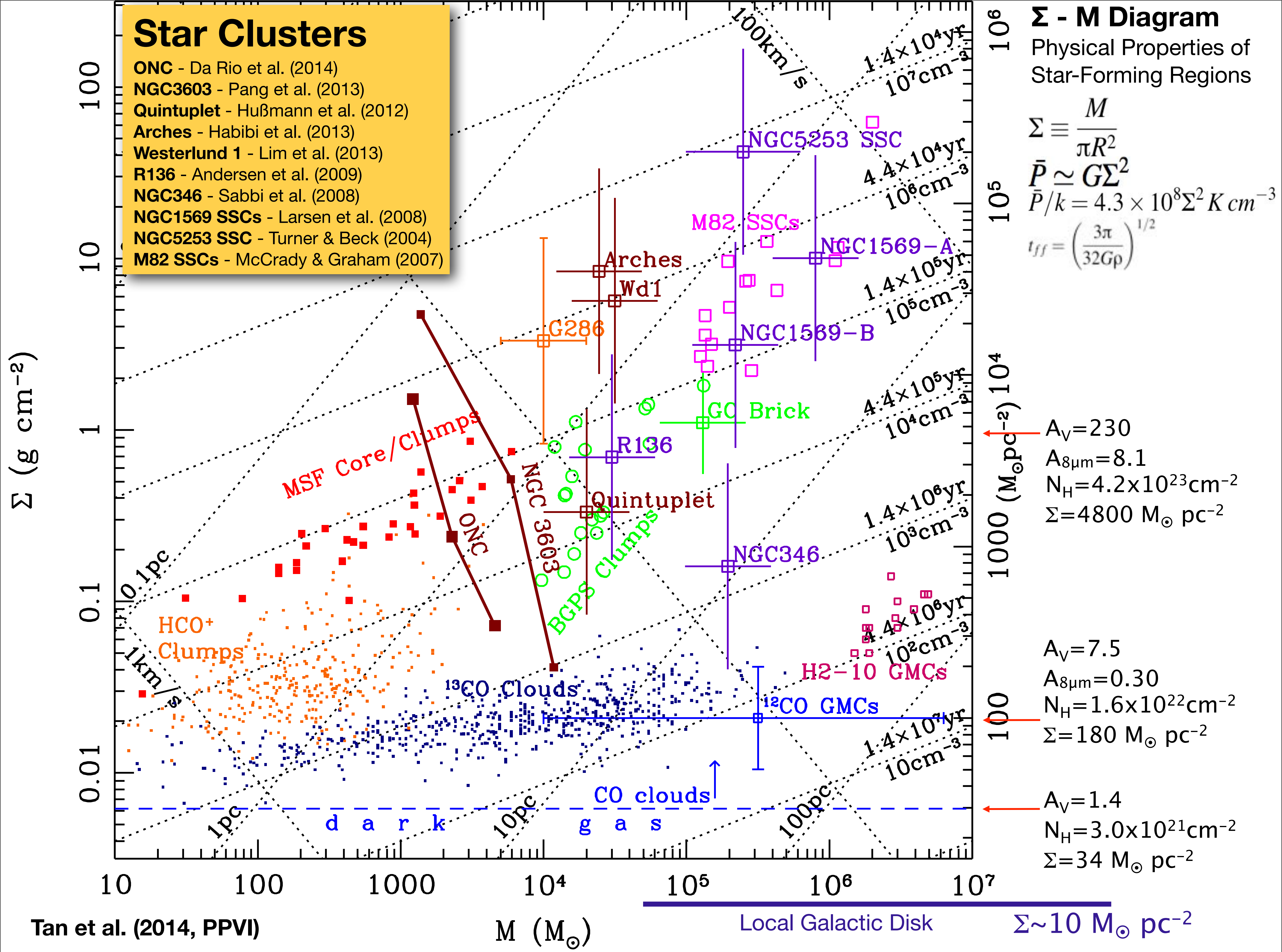
Star Clusters
ONC - Da Rio et al. (2014)
NGC3603 - Pang et al. (2013)
Quintuplet - Hußmann et al. (2012)
Arches - Habibi et al. (2013)
Westerlund 1 - Lim et al. (2013)
R136 - Andersen et al. (2009)
NGC346 - Sabbi et al. (2008)
NGC1569 SSCs - Larsen et al. (2008)
NGC5253 SSC - Turner & Beck (2004)
M82 SSCs - McCrady & Graham (2007)
Σ - M Diagram
Physical Properties of Star-Forming Regions
$\Sigma \equiv \frac{M}{\pi R^2}$
$\bar{P} \simeq G\Sigma^2$
$\bar{P}/k = 4.3 \times 10^8 \Sigma^2 \, K \, cm^{-3}$
$t_{ff} = \left(\frac{3\pi}{32 G\rho}\right)^{1/2}$
$\Sigma$ (g cm$^{-2}$)
$\Sigma$ ($M_\odot$ pc$^{-2}$)
M ($M_\odot$)
100km/s
1km/s
0.1pc
1pc
10pc
100pc
1.4x10⁴yr 10⁷cm⁻³
4.4x10⁴yr 10⁶cm⁻³
1.4x10⁵yr 10⁵cm⁻³
4.4x10⁵yr 10⁴cm⁻³
1.4x10⁶yr 10³cm⁻³
4.4x10⁶yr 10²cm⁻³
1.4x10⁷yr 10cm⁻³
NGC5253 SSC
M82 SSCs
NGC1569-A
NGC1569-B
Arches
Wd1
G286
GC Brick
R136
Quintuplet
NGC346
MSF Core/Clumps
NGC 3603
ONC
BGPS Clumps
HCO⁺ Clumps
¹³CO Clouds
¹²CO GMCs
H2-10 GMCs
CO clouds
d a r k g a s
$A_V$=230
$A_{8\mu m}$=8.1
$N_H$=4.2x10²³cm⁻²
Σ=4800 $M_\odot$ pc⁻²
$A_V$=7.5
$A_{8\mu m}$=0.30
$N_H$=1.6x10²²cm⁻²
Σ=180 $M_\odot$ pc⁻²
$A_V$=1.4
$N_H$=3.0x10²¹cm⁻²
Σ=34 $M_\odot$ pc⁻²
Local Galactic Disk
Σ~10 $M_\odot$ pc⁻²
Tan et al. (2014, PPVI)

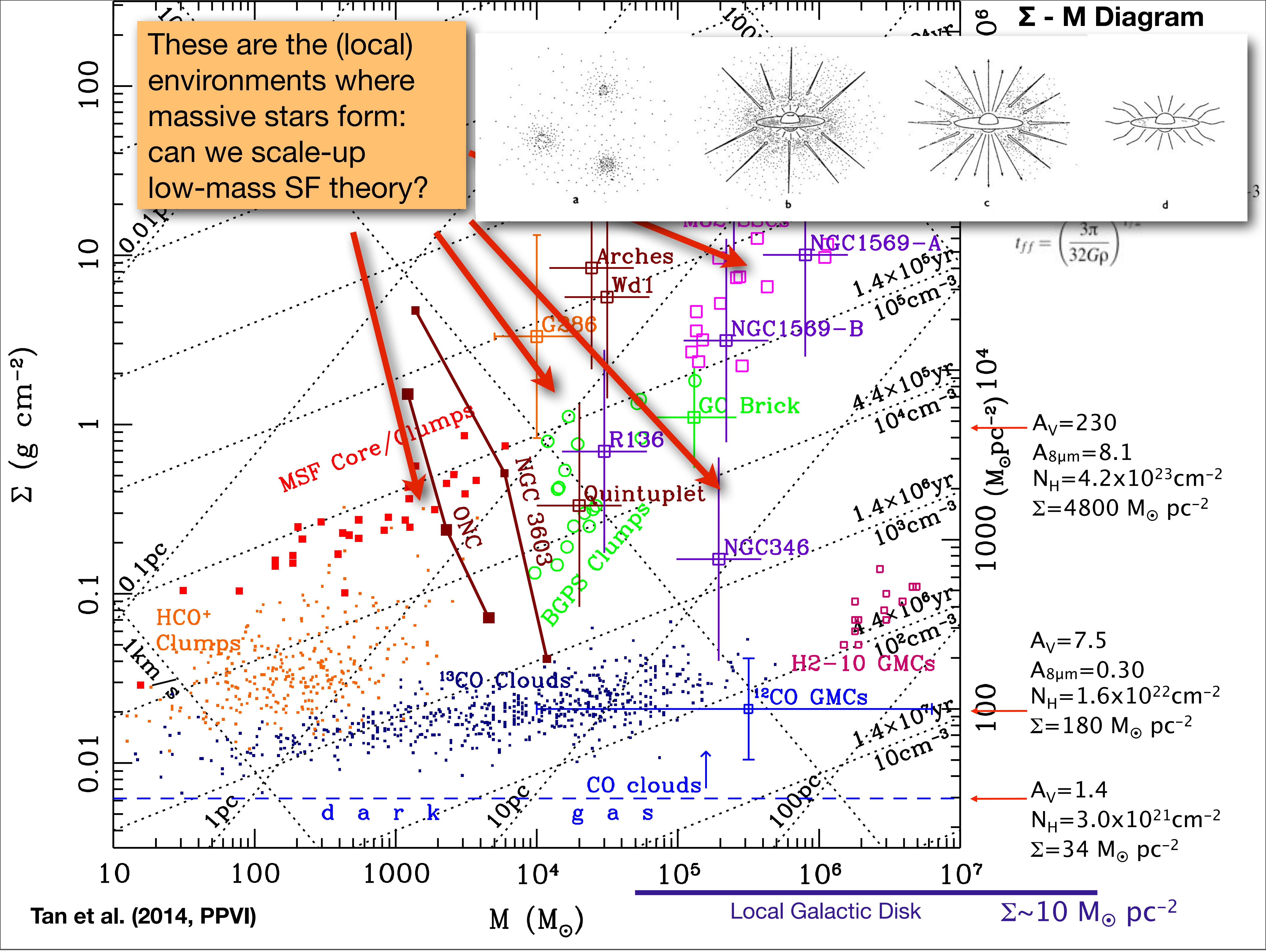

These are the (local) environments where massive stars form: can we scale-up low-mass SF theory?
Σ - M Diagram
a
b
c
d
$t_{ff} = \left(\frac{3\pi}{32G\rho}\right)^{1/2}$
Σ (g cm⁻²)
M (M⊙)
Σ (M⊙ pc⁻²)
Arches
Wd1
G286
NGC1569−A
NGC1569−B
GC Brick
R136
Quintuplet
NGC346
MSF Core/Clumps
ONC
NGC 3603
BGPS Clumps
HCO⁺ Clumps
¹³CO Clouds
¹²CO GMCs
H2−10 GMCs
CO clouds
d a r k g a s
1.4x10⁵yr
10⁵cm⁻³
4.4x10⁵yr
10⁴cm⁻³
1.4x10⁶yr
10³cm⁻³
4.4x10⁶yr
10²cm⁻³
1.4x10⁷yr
10cm⁻³
0.1pc
1pc
10pc
100pc
1km/s
A_V=230
A_8μm=8.1
N_H=4.2x10²³cm⁻²
Σ=4800 M⊙ pc⁻²
A_V=7.5
A_8μm=0.30
N_H=1.6x10²²cm⁻²
Σ=180 M⊙ pc⁻²
A_V=1.4
N_H=3.0x10²¹cm⁻²
Σ=34 M⊙ pc⁻²
Local Galactic Disk
Σ~10 M⊙ pc⁻²
Tan et al. (2014, PPVI)

# Massive Star Formation Theories

**Core Accretion:**

wide range of $dm_*/dt \sim 10^{-5}$ - $10^{-2}\ M_\odot\ yr^{-1}$

(e.g. Myers & Fuller 1992; Caselli & Myers 1995; McLaughlin & Pudritz 1997; Osorio+ 1999; Nakano+ 2000; Behrend & Maeder 2001)

**Turbulent Core Model:**

(McKee & Tan 2002, 2003)

Stars form from **"cores"** that fragment from the **"clump"**

**$\Sigma \sim 1$ g cm$^{-2}$**

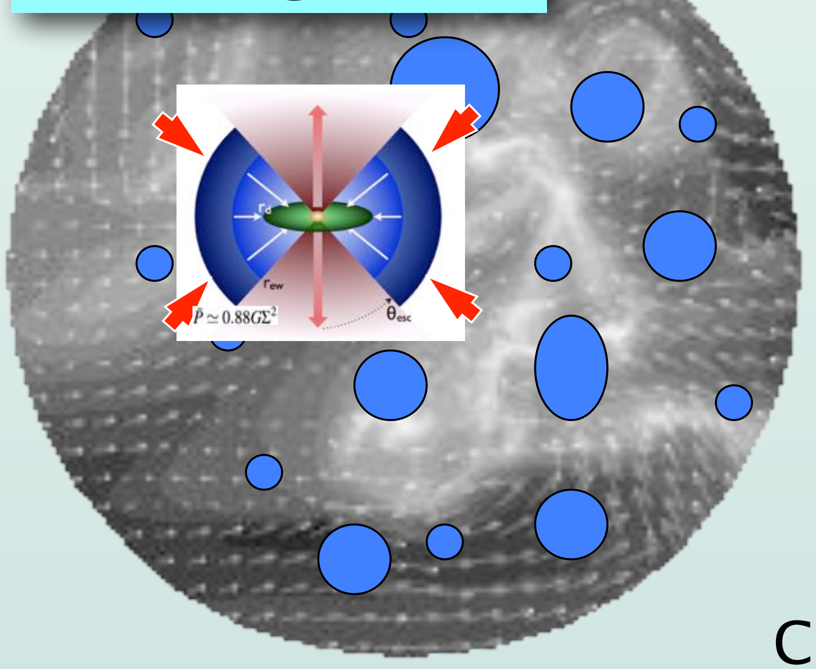

$$\bar{P} = \phi_P G \Sigma^2$$

If in **equilibrium**, then **self-gravity** is balanced by **internal pressure**: B-field, turbulence, radiation pressure (thermal P is small)

Cores form from this turbulent/magnetized medium: at any instant there is a small mass fraction in cores. These cores collapse quickly to feed a central disk to form individual stars or binaries.

$$\dot{m}_* \sim M_{\rm core}/t_{\rm ff}$$

# Massive Star Formation Theories

**Core Accretion:**

wide range of $dm_*/dt \sim 10^{-5} - 10^{-2}\ M_\odot\ yr^{-1}$

(e.g. Myers & Fuller 1992; Caselli & Myers 1995; McLaughlin & Pudritz 1997; Osorio+ 1999; Nakano+ 2000; Behrend & Maeder 2001)

**Turbulent Core Model:**

(McKee & Tan 2002, 2003)

Stars form from **"cores"** that fragment from the **"clump"**

**$\Sigma \sim 1$ g cm$^{-2}$**

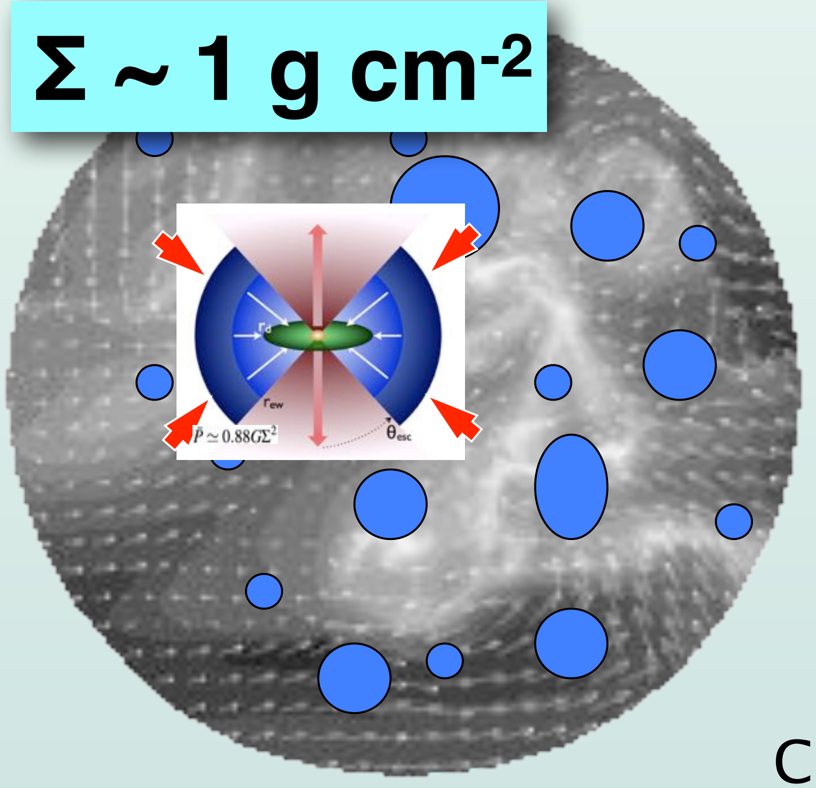

$$\bar{P} = \phi_P G \Sigma^2$$

If in **equilibrium**, then **self-gravity** is balanced by **internal pressure**: B-field, turbulence, radiation pressure (thermal P is small)

Cores form from this turbulent/magnetized medium: at any instant there is a small mass fraction in cores. These cores collapse quickly to feed a central disk to form individual stars or binaries.

$$\dot{m}_* \sim M_{\rm core}/t_{\rm ff}$$

**Competitive (Clump-fed) Accretion:**

(Bonnell, Clarke, Bate, Pringle 2001;
Bonnell, Vine, & Bate 2004;
Schmeja & Klessen 2004;
Wang, Li, Abel, Nakamura 2010; ...)

Massive stars gain most mass by Bondi-Hoyle accretion of ambient clump gas

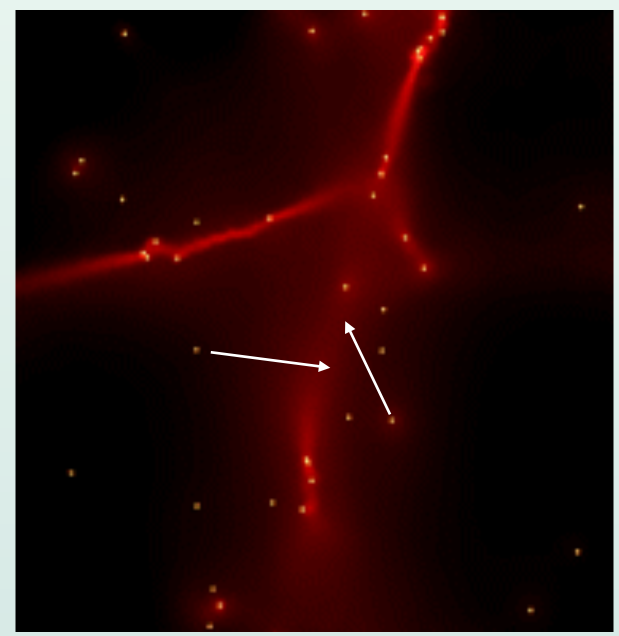

Originally based on simulations including only thermal pressure.

Massive stars form on the timescale of the star cluster, with relatively low accretion rates.

**Violent interactions? Mergers?**

(Bonnell, Bate & Zinnecker 1998;
Bally & Zinnecker 2005
Bally et al. 2011)

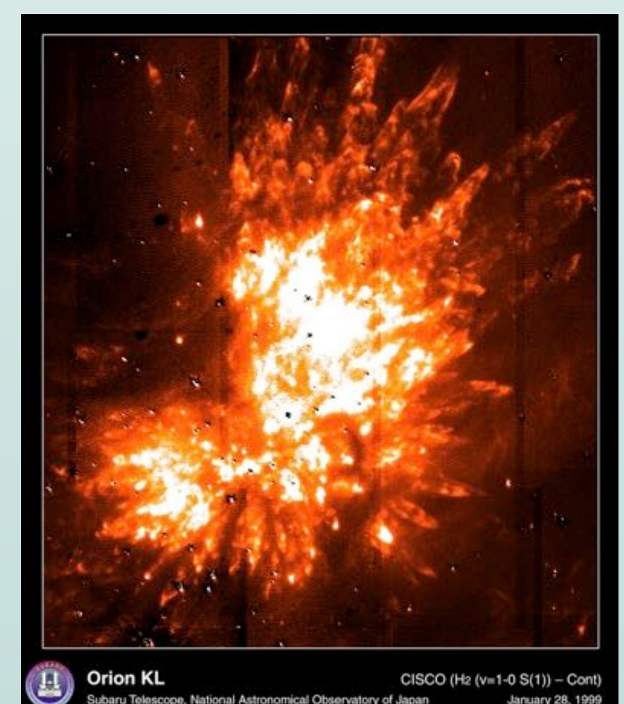

# Massive Star Formation Theories

**Core Accretion:**
wide range of $dm_*/dt \sim 10^{-5} - 10^{-2}\ M_\odot\ yr^{-1}$
(e.g. Myers & Fuller 1992; Caselli & Myers 1995; McLaughlin & Pudritz 1997; Osorio+ 1999; Nakano+ 2000; Behrend & Maeder 2001)

**Turbulent Core Model:**
(McKee & Tan 2002, 2003)
Stars form from **"cores"** that fragment from the **"clump"**

**$\Sigma \sim 1$ g cm$^{-2}$**

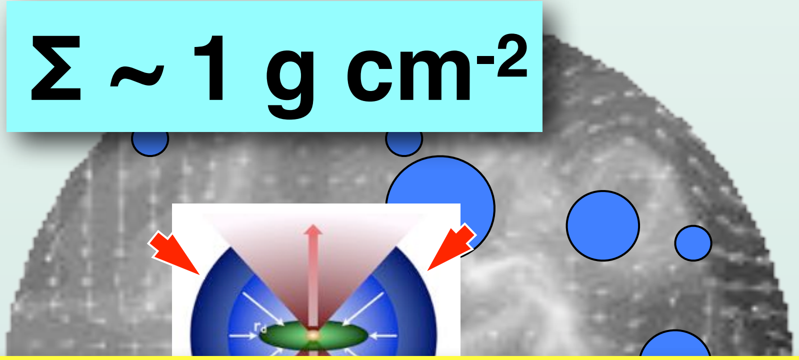

$$\bar{P} = \phi_P G \Sigma^2$$

If in **equilibrium**, then **self-gravity** is balanced by

**SOFIA measurement of Clump Infall**

**$v_{infall} \sim 0.1\ v_{ff}$**

**(Wyrowski et al. 2016)**

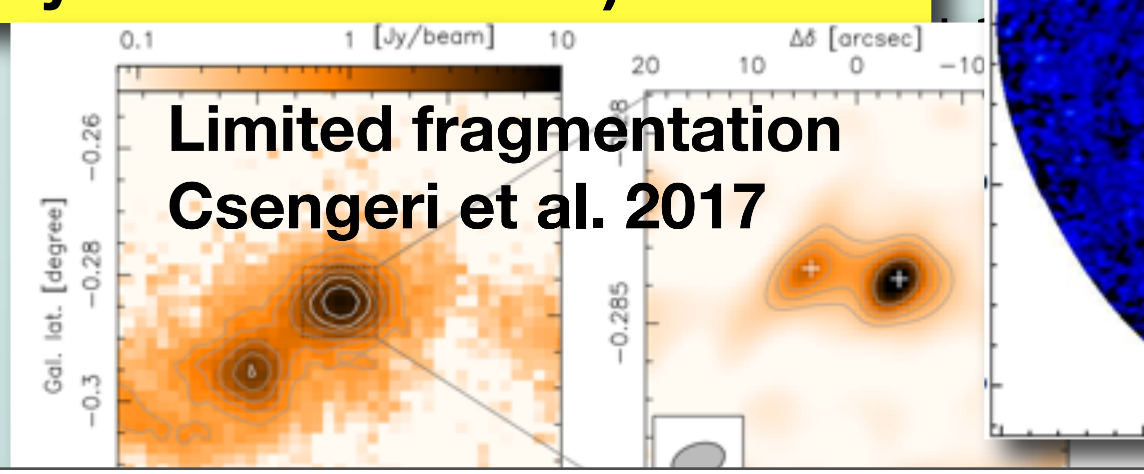


**Limited fragmentation**
**Csengeri et al. 2017**

**Competitive (Clump-fed) Accretion:**
(Bonnell, Clarke, Bate, Pringle 2001;
Bonnell, Vine, & Bate 2004;
Schmeja & Klessen 2004;
Wang, Li, Abel, Nakamura 2010; ...)
Massive stars gain most mass by Bondi-Hoyle accretion of ambient clump gas

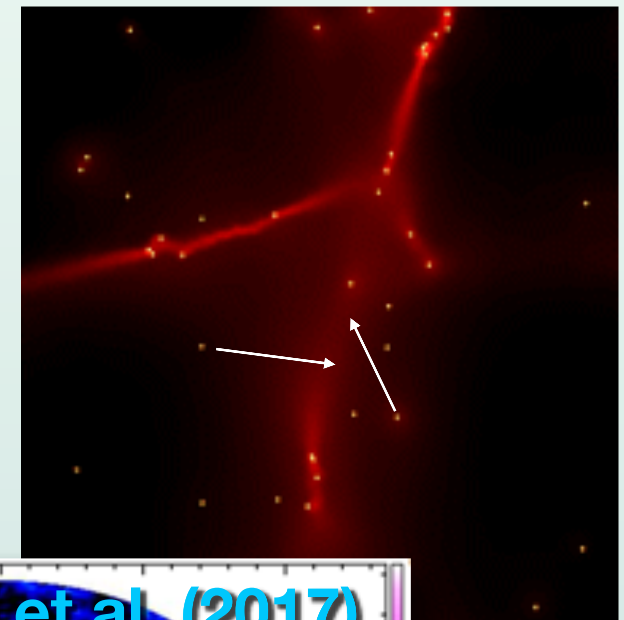

Originally based on simulations including only thermal pressure.

Massive stars form on the timescale of the star cluster, with relatively low accretion rates.

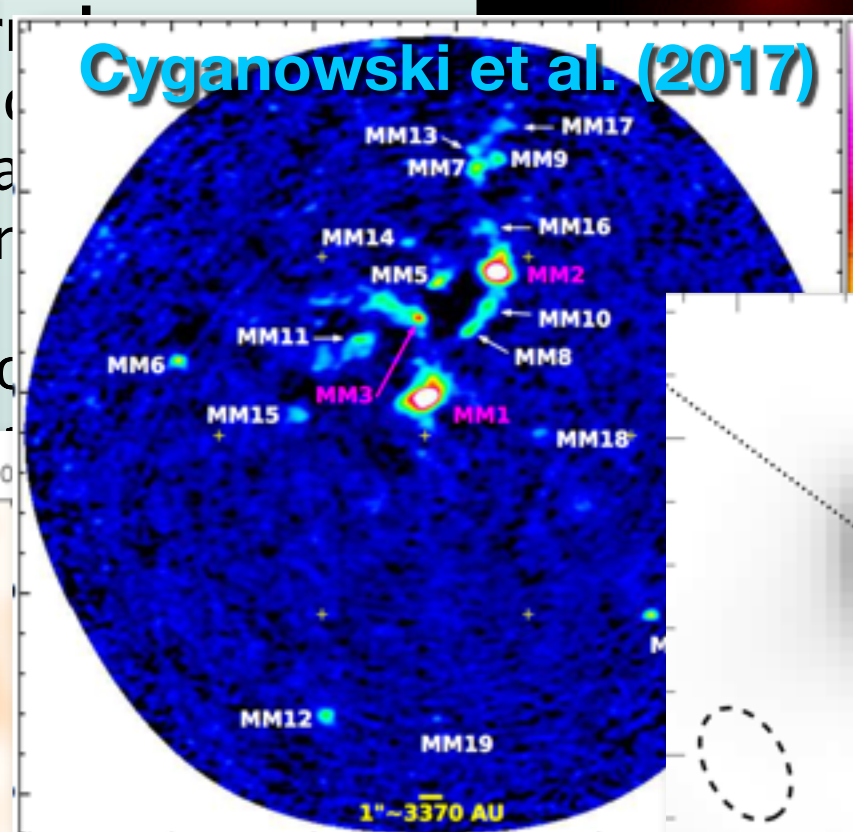


**Cyganowski et al. (2017)**

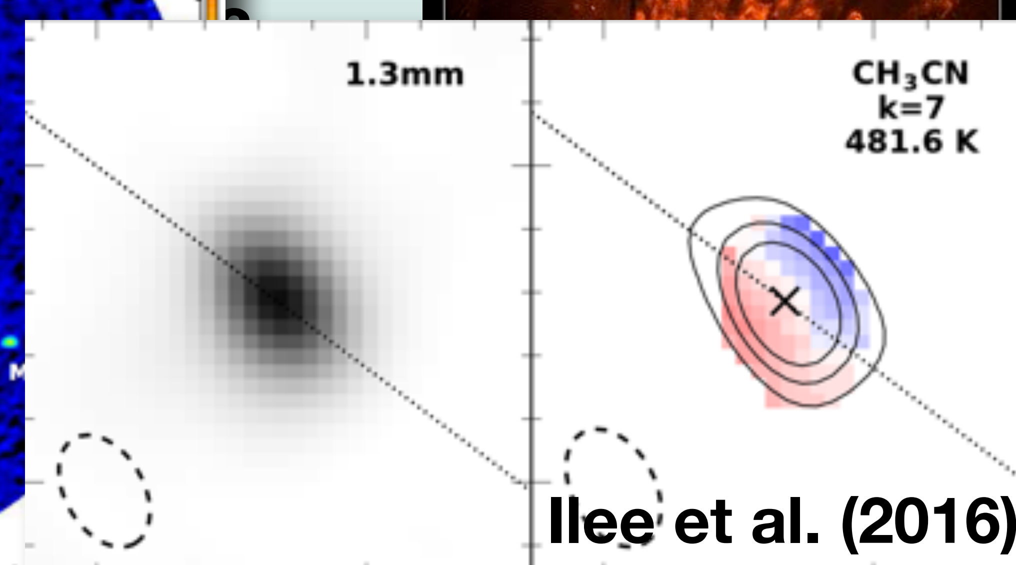


**Ilee et al. (2016)**

# Schematic Differences Between Massive Star Formation Theories

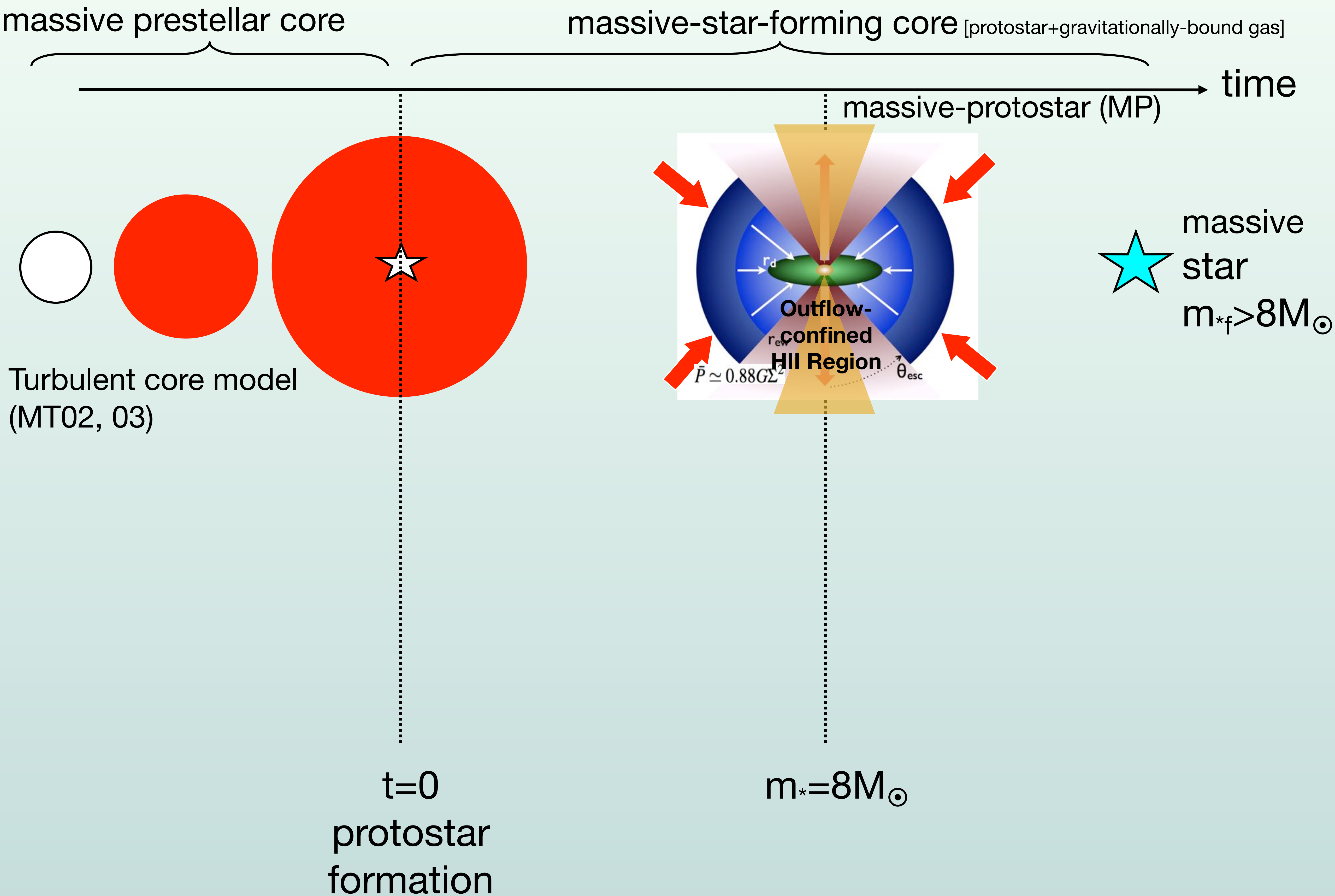

# Schematic Differences Between Massive Star Formation Theories

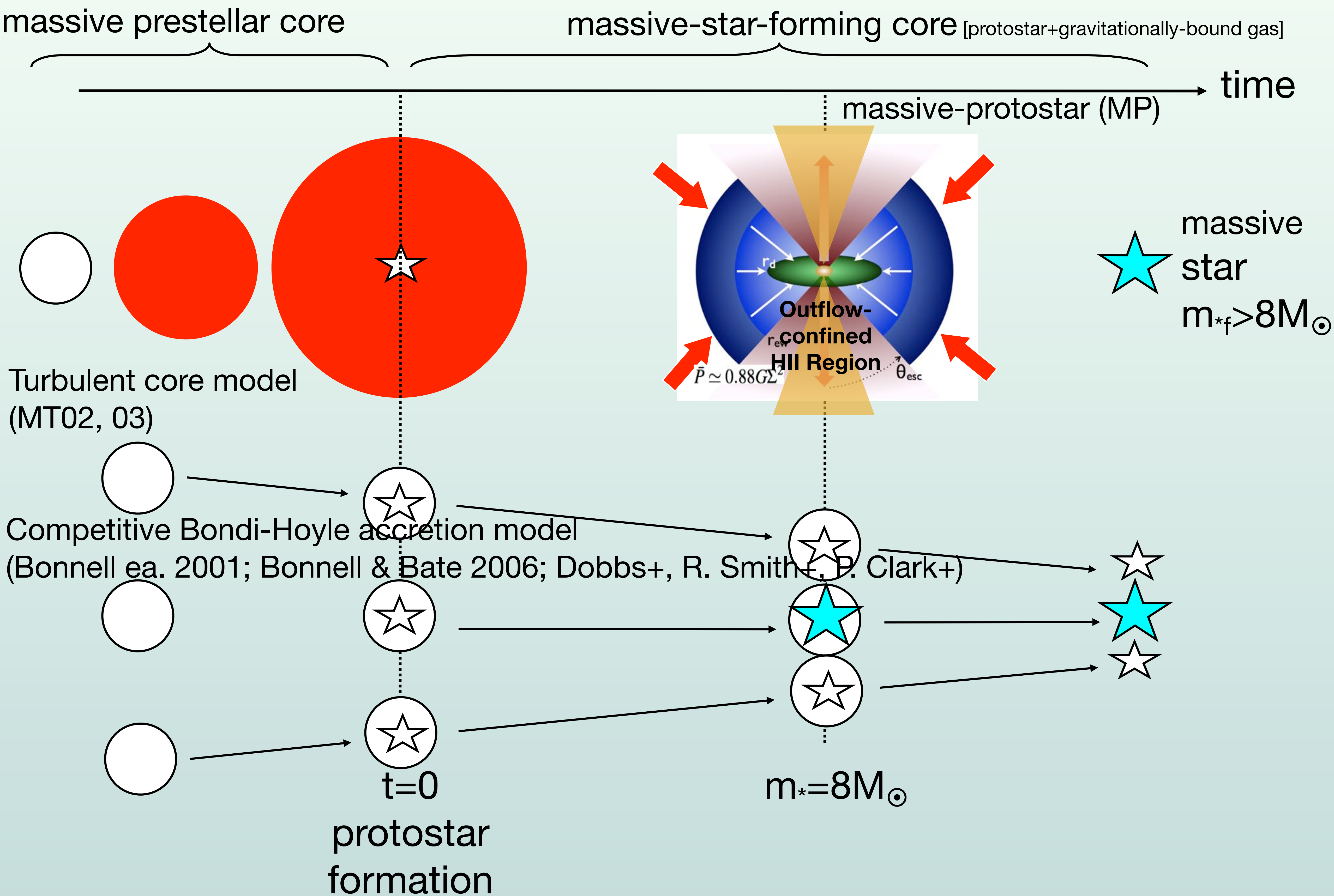

# Schematic Differences Between Massive Star Formation Theories

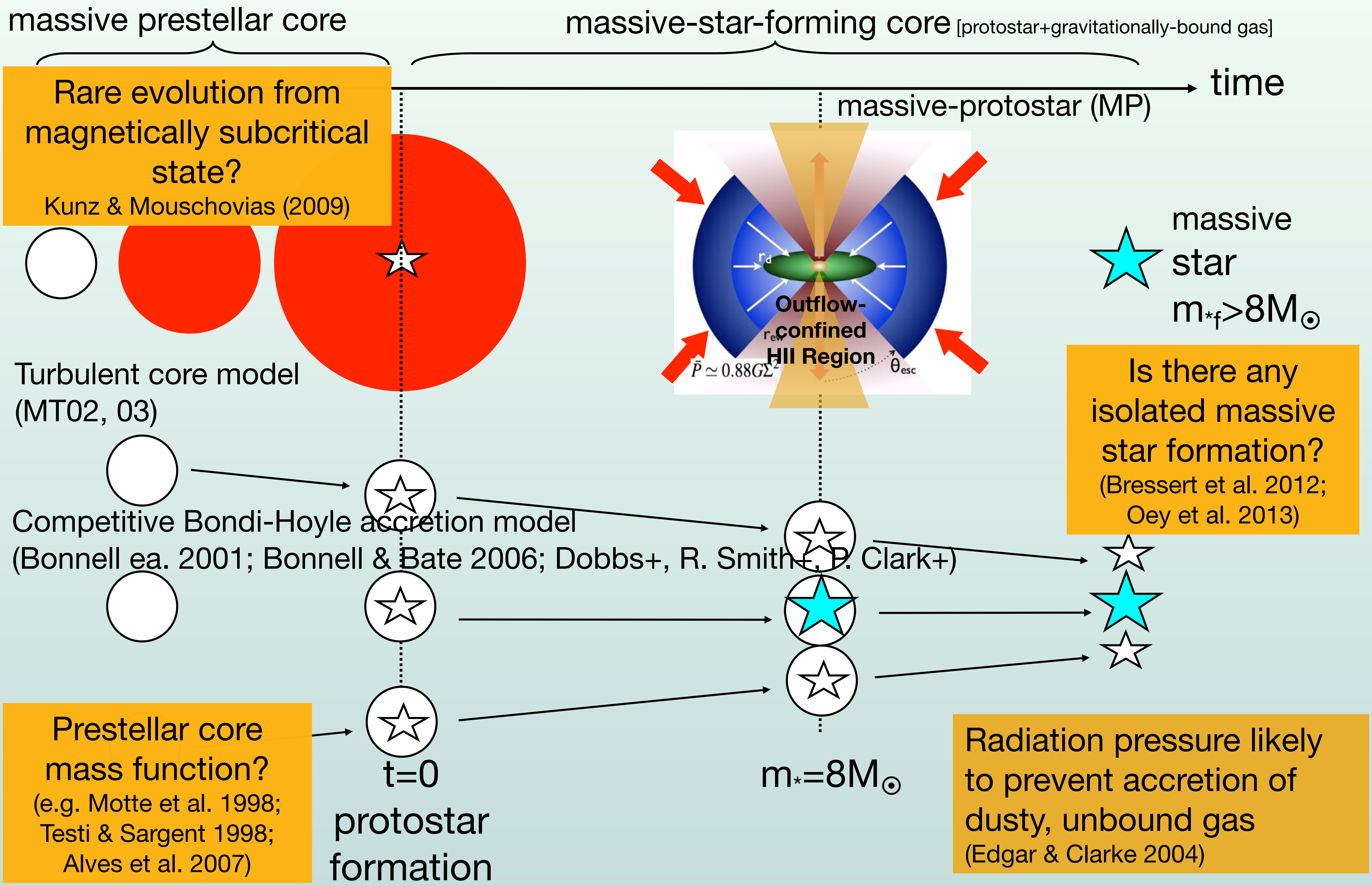

# The Initial Conditions of Massive Star Formation

## Do massive starless cores exist?
## Are they close to virial equilibrium?

$$R_{c,\mathrm{vir}} \rightarrow 0.0574 \left(\frac{M_c}{60\,M_\odot}\right)^{1/2} \left(\frac{\Sigma_{\mathrm{cl}}}{1\ \mathrm{g\ cm^{-2}}}\right)^{-1/2} \mathrm{pc}$$

$$\sigma_{c,\mathrm{vir}} \rightarrow 1.09 \left(\frac{M_c}{60 M_\odot}\right)^{1/4} \left(\frac{\Sigma_{\mathrm{cl}}}{1\ \mathrm{g\ cm^{-2}}}\right)^{1/4} \mathrm{km\ s^{-1}}$$

McKee & Tan (2003)

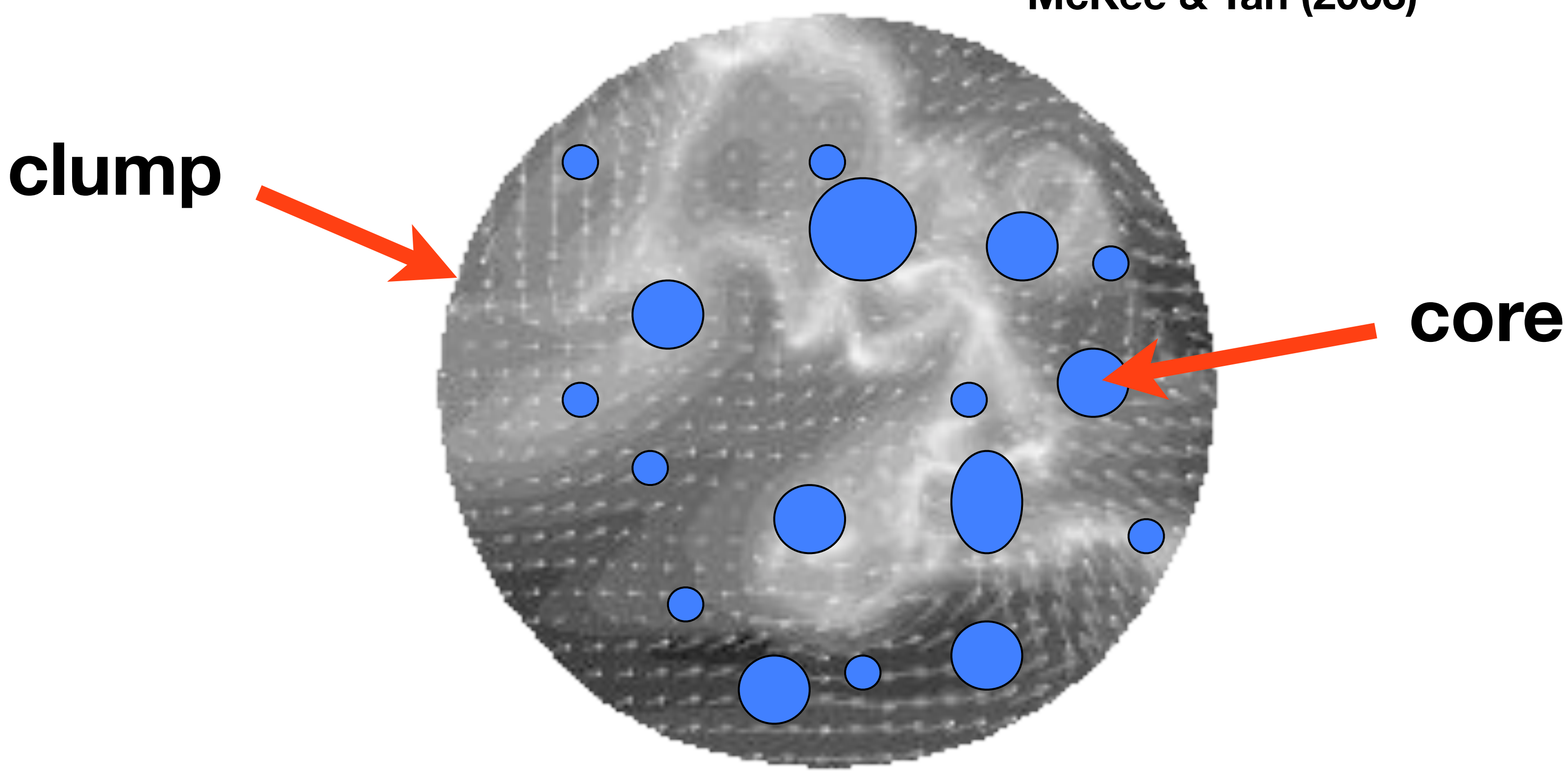

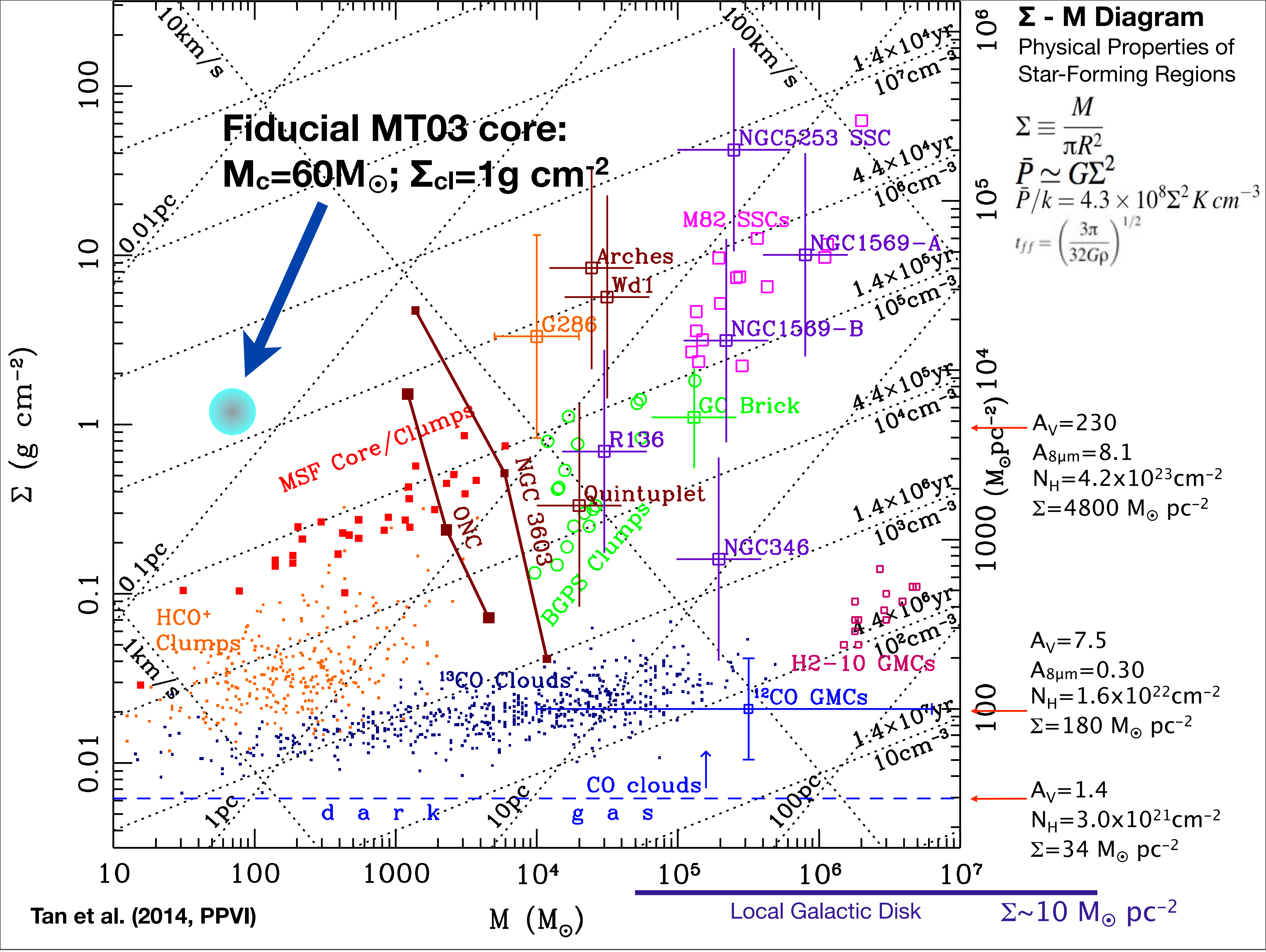
Σ - M Diagram
Physical Properties of Star-Forming Regions
$\Sigma \equiv \frac{M}{\pi R^2}$
$\bar{P} \simeq G\Sigma^2$
$\bar{P}/k = 4.3 \times 10^8 \Sigma^2\, K\, cm^{-3}$
$t_{ff} = \left(\frac{3\pi}{32G\rho}\right)^{1/2}$
Fiducial MT03 core:
$M_c$=60$M_\odot$; $\Sigma_{cl}$=1g cm$^{-2}$
NGC5253 SSC
M82 SSCs
NGC1569−A
NGC1569−B
Arches
Wd1
G286
GC Brick
R136
Quintuplet
NGC346
MSF Core/Clumps
ONC
NGC 3603
BGPS Clumps
HCO+ Clumps
13CO Clouds
12CO GMCs
H2−10 GMCs
CO clouds
d a r k g a s
10km/s
100km/s
1km/s
0.01pc
0.1pc
1pc
10pc
100pc
1.4×10⁴yr 10⁷cm⁻³
4.4×10⁴yr 10⁶cm⁻³
1.4×10⁵yr 10⁵cm⁻³
4.4×10⁵yr 10⁴cm⁻³
1.4×10⁶yr 10³cm⁻³
4.4×10⁶yr 10²cm⁻³
1.4×10⁷yr 10cm⁻³
Σ (g cm⁻²)
M (M⊙)
(M⊙pc⁻²)
AV=230
A8μm=8.1
NH=4.2x10²³cm⁻²
Σ=4800 M⊙ pc⁻²
AV=7.5
A8μm=0.30
NH=1.6x10²²cm⁻²
Σ=180 M⊙ pc⁻²
AV=1.4
NH=3.0x10²¹cm⁻²
Σ=34 M⊙ pc⁻²
Local Galactic Disk
Σ~10 M⊙ pc⁻²
Tan et al. (2014, PPVI)

# Mid-IR Extinction Mapping of Infrared Dark Clouds

**(Butler & Tan 2009, 2012; see also Peretto & Fuller 2009; Ragan et al. 2009; Battersby et al. 2010)**

**G28.37+00.07**

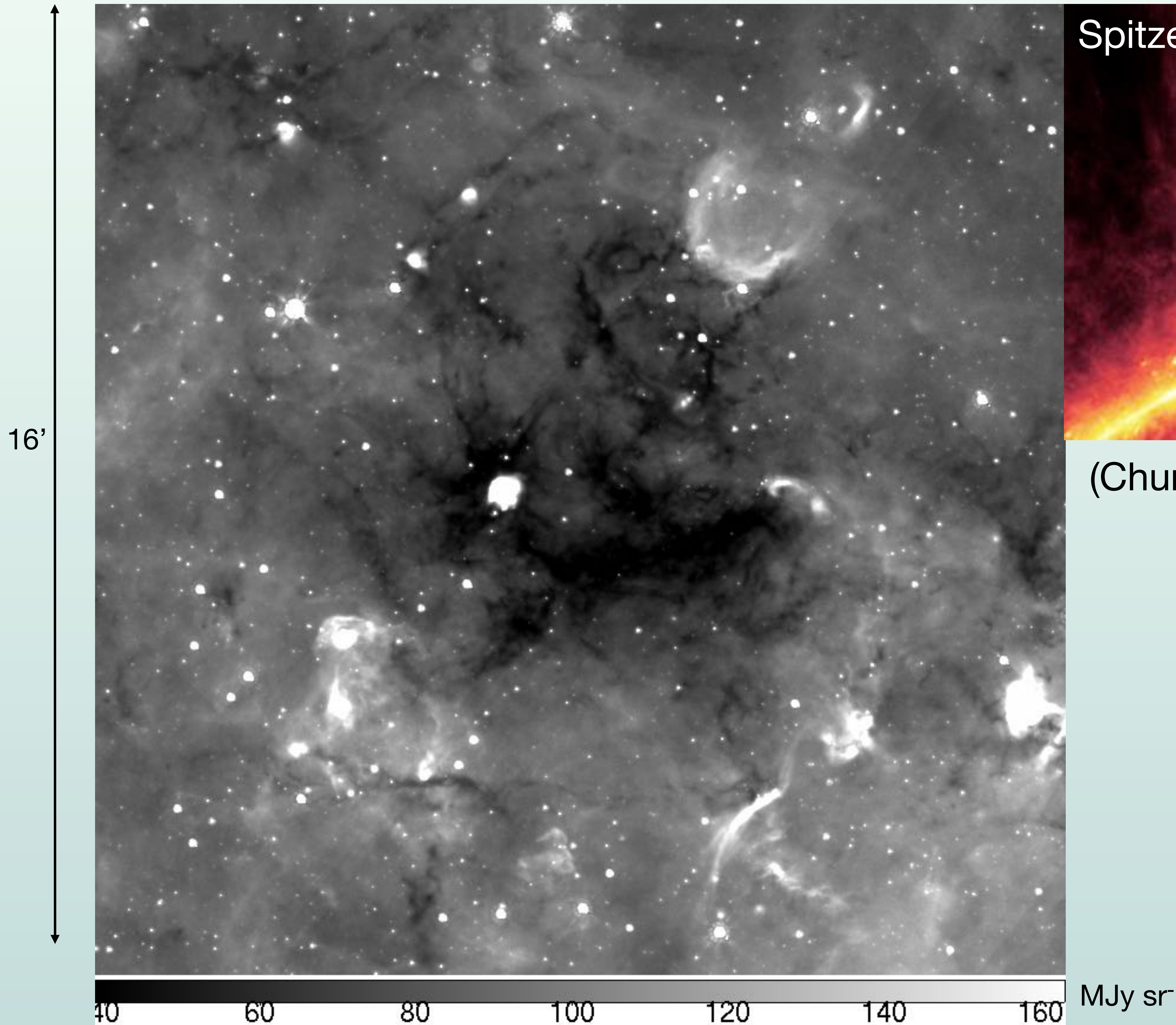



(Churchwell et al. 2009)

# Mid-IR Extinction Mapping of Infrared Dark Clouds

**(Butler & Tan 2009, 2012; see also Peretto & Fuller 2009; Ragan et al. 2009; Battersby et al. 2010)**

**G28.37+00.07**

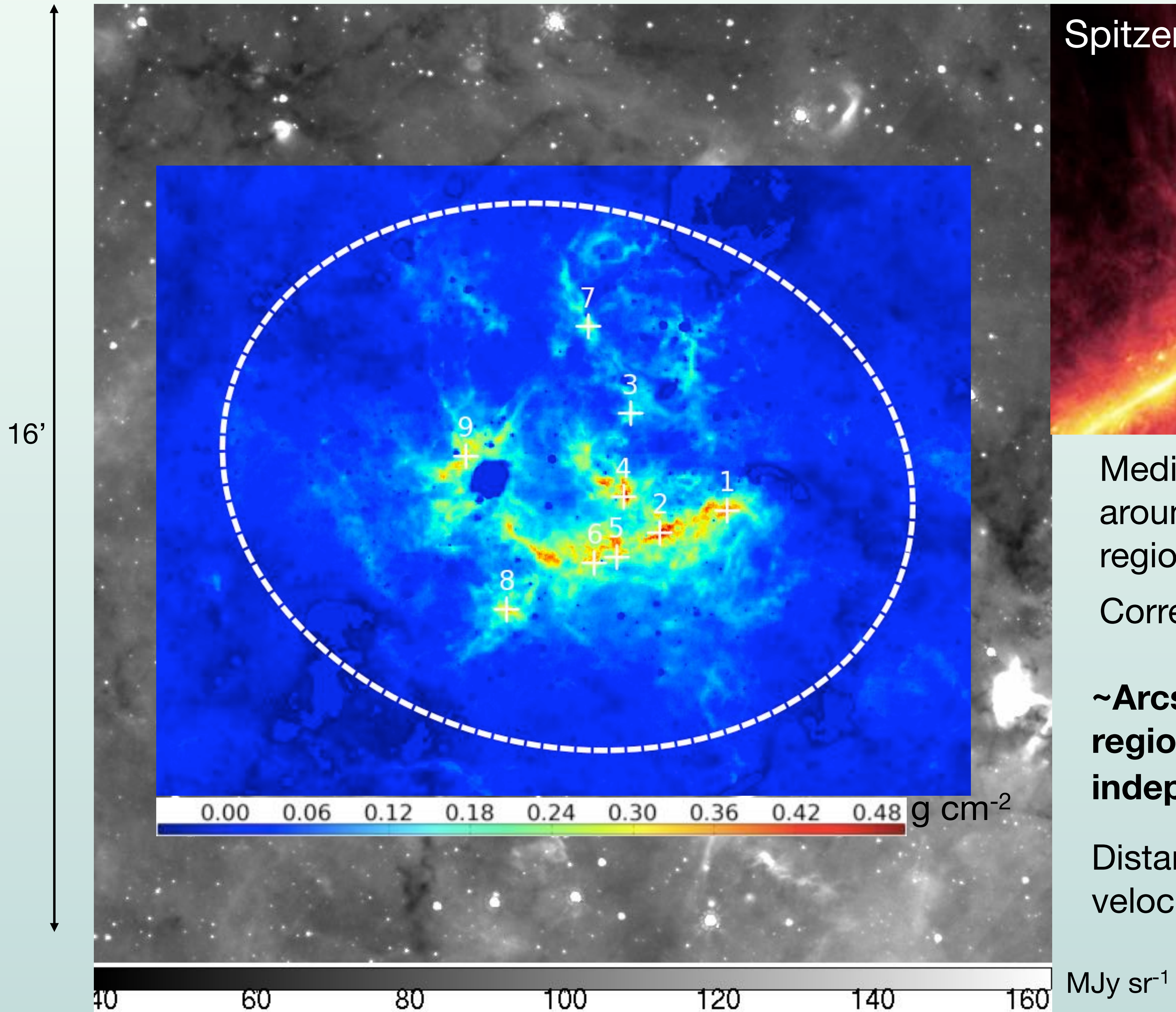



Median filter for background around IRDC; interpolate for region behind the IRDC

Correct for foreground

**~Arcsecond scale maps of regions up to $\Sigma$ ~0.5 g cm$^{-2}$; independent of dust temp.**

Distance from molecular line velocities -> M($\Sigma$)

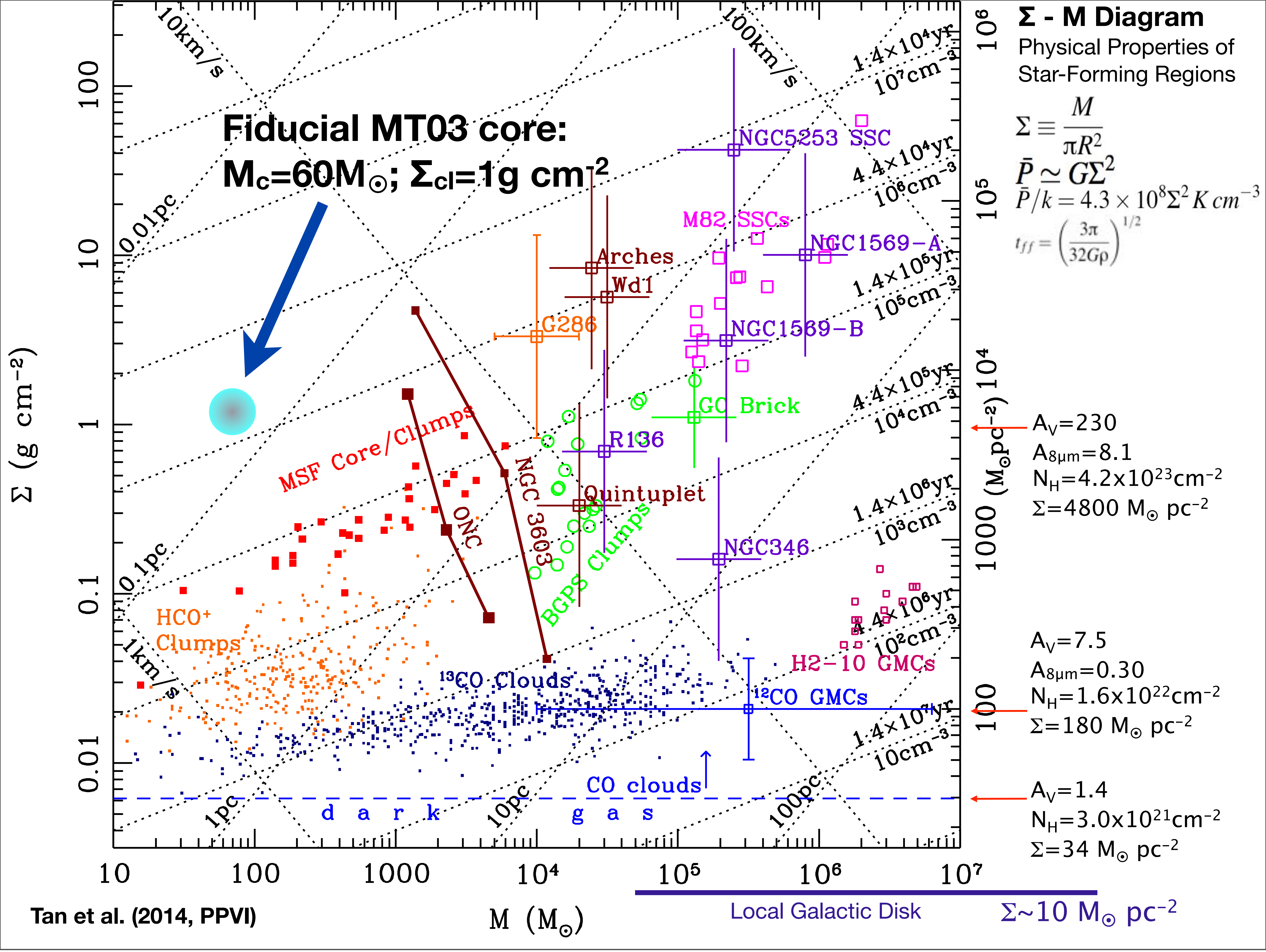

Σ - M Diagram
Physical Properties of Star-Forming Regions
$\Sigma \equiv \frac{M}{\pi R^2}$
$\bar{P} \simeq G\Sigma^2$
$\bar{P}/k = 4.3 \times 10^8 \Sigma^2\, K\, cm^{-3}$
$t_{ff} = \left(\frac{3\pi}{32G\rho}\right)^{1/2}$
Fiducial MT03 core:
$M_c=60M_\odot$; $\Sigma_{cl}=1$g cm$^{-2}$
Σ (g cm$^{-2}$)
(M$_\odot$pc$^{-2}$)
M (M$_\odot$)
10km/s
100km/s
1km/s
0.01pc
0.1pc
1pc
10pc
100pc
1.4x10$^4$yr 10$^7$cm$^{-3}$
4.4x10$^4$yr 10$^6$cm$^{-3}$
1.4x10$^5$yr 10$^5$cm$^{-3}$
4.4x10$^5$yr 10$^4$cm$^{-3}$
1.4x10$^6$yr 10$^3$cm$^{-3}$
4.4x10$^6$yr 10$^2$cm$^{-3}$
1.4x10$^7$yr 10cm$^{-3}$
NGC5253 SSC
M82 SSCs
NGC1569−A
NGC1569−B
Arches
Wd1
G286
GC Brick
R136
Quintuplet
NGC346
MSF Core/Clumps
ONC
NGC 3603
BGPS Clumps
HCO$^+$ Clumps
$^{13}$CO Clouds
$^{12}$CO GMCs
H2−10 GMCs
CO clouds
d a r k g a s
A$_V$=230
A$_{8\mu m}$=8.1
N$_H$=4.2x10$^{23}$cm$^{-2}$
Σ=4800 M$_\odot$ pc$^{-2}$
A$_V$=7.5
A$_{8\mu m}$=0.30
N$_H$=1.6x10$^{22}$cm$^{-2}$
Σ=180 M$_\odot$ pc$^{-2}$
A$_V$=1.4
N$_H$=3.0x10$^{21}$cm$^{-2}$
Σ=34 M$_\odot$ pc$^{-2}$
Local Galactic Disk
Σ~10 M$_\odot$ pc$^{-2}$
Tan et al. (2014, PPVI)

# IRDC Studies

**Butler & Tan (2009; 2012) - MIREX maps**

**Fiducial MT03 core:**

**$M_c$=60$M_\odot$; $\Sigma_{cl}$=1g cm$^{-2}$**

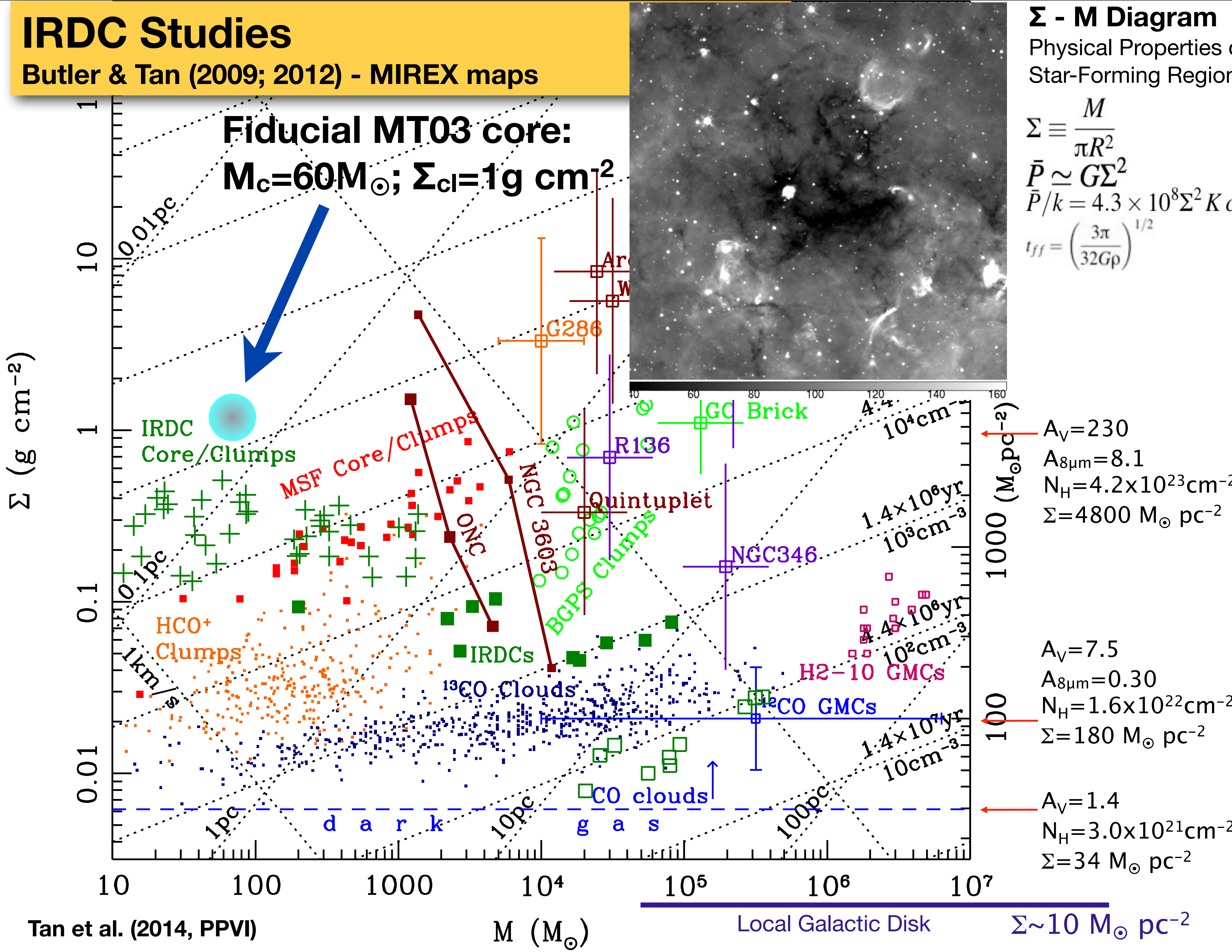


**Σ - M Diagram**

Physical Properties of Star-Forming Regions

$$\Sigma \equiv \frac{M}{\pi R^2}$$

$$\bar{P} \simeq G\Sigma^2$$

$$\bar{P}/k = 4.3 \times 10^8 \Sigma^2\, K\, cm^{-3}$$

$$t_{ff} = \left(\frac{3\pi}{32G\rho}\right)^{1/2}$$

Tan et al. (2014, PPVI)

# SOFIA Capabilities

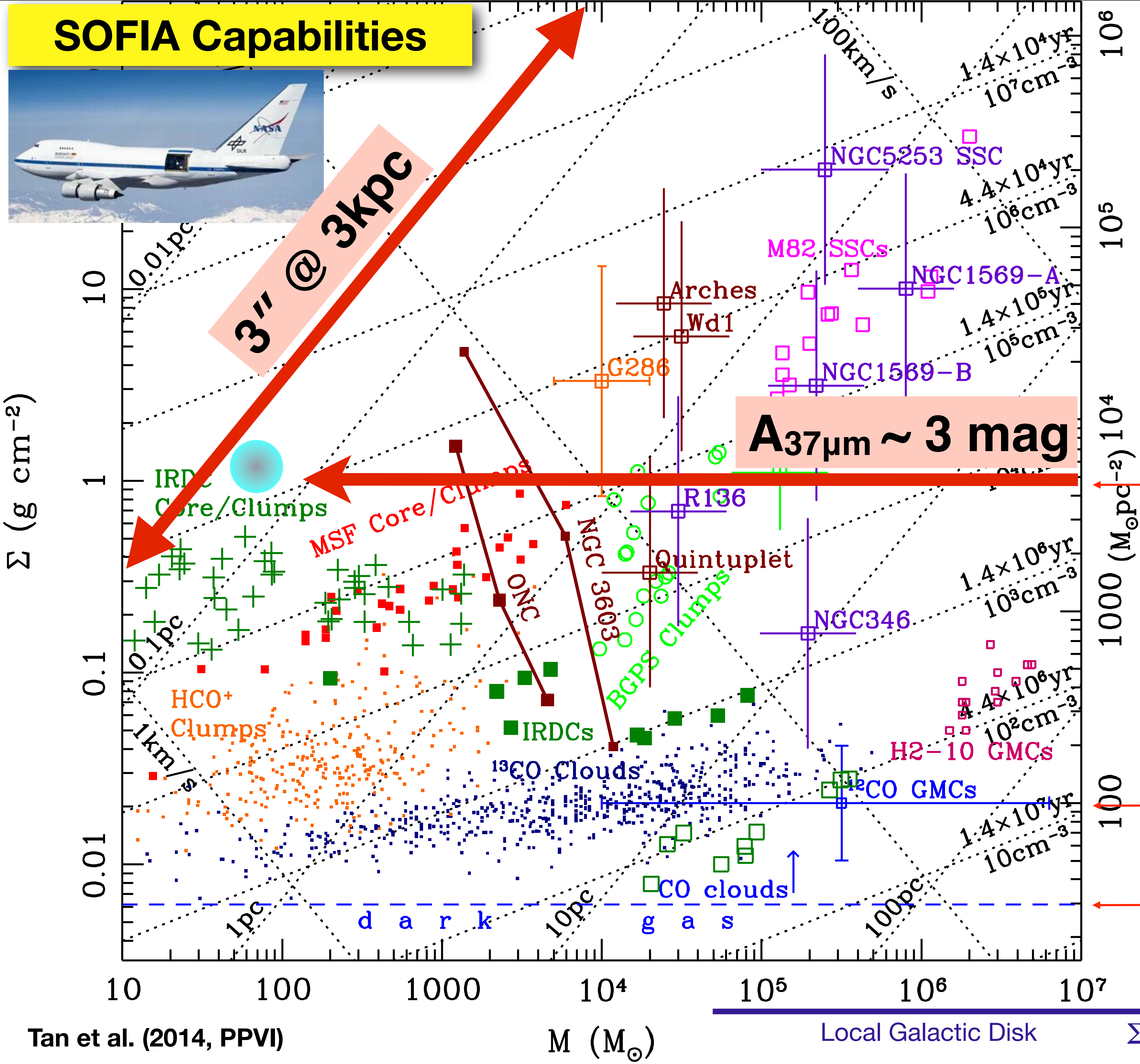


**Σ - M Diagram**

Physical Properties of Star-Forming Regions

$$\Sigma \equiv \frac{M}{\pi R^2}$$

$$\bar{P} \simeq G\Sigma^2$$

$$\bar{P}/k = 4.3 \times 10^8 \Sigma^2\, K\, cm^{-3}$$

$$t_{ff} = \left(\frac{3\pi}{32G\rho}\right)^{1/2}$$

$A_V$=230
$A_{8\mu m}$=8.1
$N_H$=4.2x10$^{23}$cm$^{-2}$
Σ=4800 M$_\odot$ pc$^{-2}$

$A_V$=7.5
$A_{8\mu m}$=0.30
$N_H$=1.6x10$^{22}$cm$^{-2}$
Σ=180 M$_\odot$ pc$^{-2}$

$A_V$=1.4
$N_H$=3.0x10$^{21}$cm$^{-2}$
Σ=34 M$_\odot$ pc$^{-2}$

Σ~10 M$_\odot$ pc$^{-2}$

Tan et al. (2014, PPVI)

# Comparison to Turbulent Core Model

Tan, Kong et al. (2013)

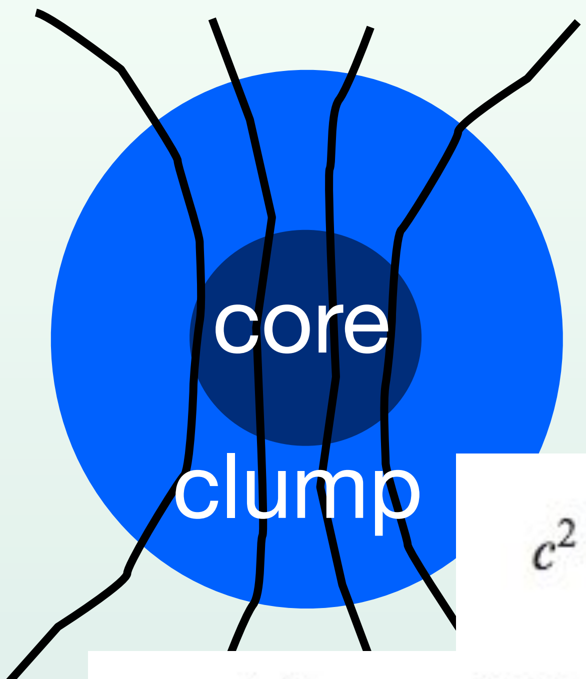


$$c^2 = \sigma^2 + \frac{B^2}{8\pi\rho} + \frac{\delta B^2}{24\pi\rho}$$

$$\phi_B \equiv \frac{\langle c^2 \rangle}{\langle \sigma^2 \rangle} = 1 + \frac{3}{2}\frac{E_B}{E_K} + \frac{E_{\delta B}}{2E_K} = 1.3 + \frac{3}{2m_A^2}$$

$$\sigma_{c,\mathrm{vir}} \to 1.09 \left(\frac{M_c}{60 M_\odot}\right)^{1/4} \left(\frac{\Sigma_{\mathrm{cl}}}{1\ \mathrm{g\ cm^{-2}}}\right)^{1/4} \mathrm{km\ s^{-1}}$$

Core masses inside 3σ $N_2D^+$ contour:

**$\Sigma_{cl} = 0.36$ g cm$^{-2}$**

**$M_{c,MIREX} = 55.2 \pm 25\ M_\odot$**

**$M_{c,mm} = 62.5^{129}_{26.9}\ M_\odot$**

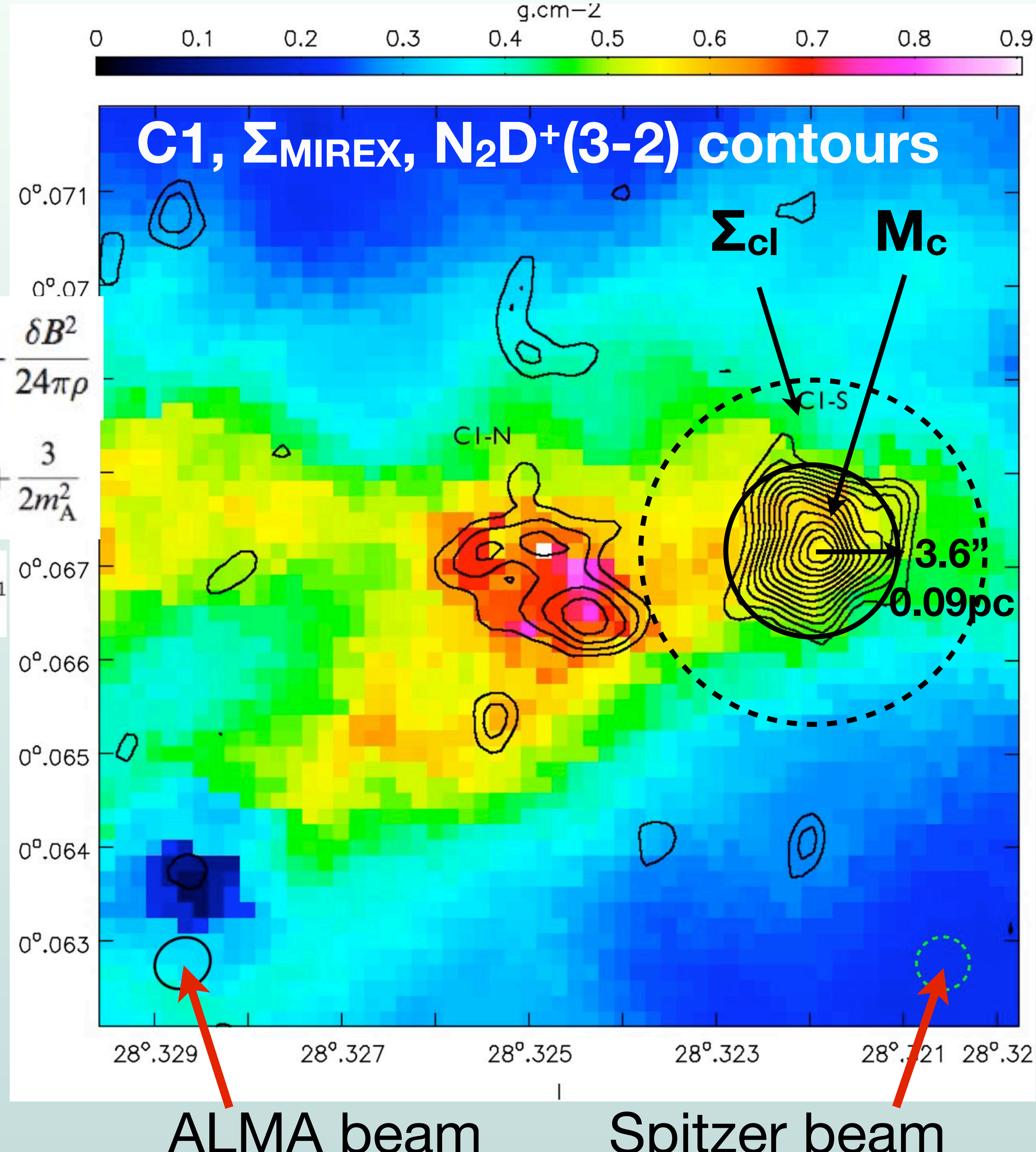

# Predictions from Virial Equilibrium

Tan, Kong et al. (2013)

- 1D velocity dispersion if virialized: $\sigma_{c,vir} \rightarrow 1.09 \left(\frac{M_c}{60 M_\odot}\right)^{1/4} \left(\frac{\Sigma_{cl}}{1\ \mathrm{g\ cm^{-2}}}\right)^{1/4} \mathrm{km\ s^{-1}}$

( $m_A = \sqrt{3}\sigma_c/v_A$ = 1)

| Core | C1-N | C1-S | F1 | F2 | G2-N | G2-S |
|---|---|---|---|---|---|---|
| $\Sigma_{cl}$ (g cm$^{-2}$) | 0.48 | 0.40 | 0.22 | 0.32 | 0.21 | 0.19 |
| $M_c$ ($M_\odot$) | 16 | 63 | 6.5 | 4.7 | 2.4 | 0.83 |
| $\sigma_{vir}$ (km/s) | 0.66±0.22 | 0.88±0.30 | 0.43±0.15 | 0.44±0.15 | 0.33±0.11 | 0.25±0.09 |
| $\sigma_{obs}$ (km/s) | 0.41±0.03 | 0.41±0.02 | 0.25±0.02 | 0.42±0.04 | 0.34±0.02 | 0.30±0.02 |

**$< \sigma_{obs}/\sigma_{vir} > = 0.81 \pm 0.13$**

$m_{A,vir} = 0.28$ -> $B_{vir}$=0.9mG

$B_{med} \simeq 0.12 n_H^{0.65}\ \mu\mathrm{G}$ (for $n_H > 300\ \mathrm{cm^{-3}}$) (Crutcher et al. 2010)

$n_{H,c}$=6.4x10$^5$cm$^{-3}$ -> $B_{med}$ = 0.7mG

**Tentative Conclusion:** Cores appear to be near virial equilibrium, after accounting for clump envelope. Possibly slightly sub-virial; or have stronger B-fields (see also - Kauffmann, Pillai & Goldsmith 2013).

# Massive Pre-Stellar Core
# C1-S High Resolution (0.2″, 0.005pc @ 5kpc)

| Core property (% error) | C1-S inner | C1-S outer |
|---|---|---|
| $\theta_c$ ($''$) | 1.10 | 1.85 |
| $d$ (kpc) (20%) | 5.0 | 5.0 |
| $R_c$ (0.01 pc) (20%) | 2.67 | 4.48 |
| $M_{c,mm}$ ($M_\odot$) | $16.2^{42.8}_{4.25}$ | $47.9^{110}_{18.6}$ |
| $n_{H,c,mm}$ ($10^6 cm^{-3}$) | $5.90^{15.4}_{1.94}$ | $3.67^{8.26}_{1.74}$ |

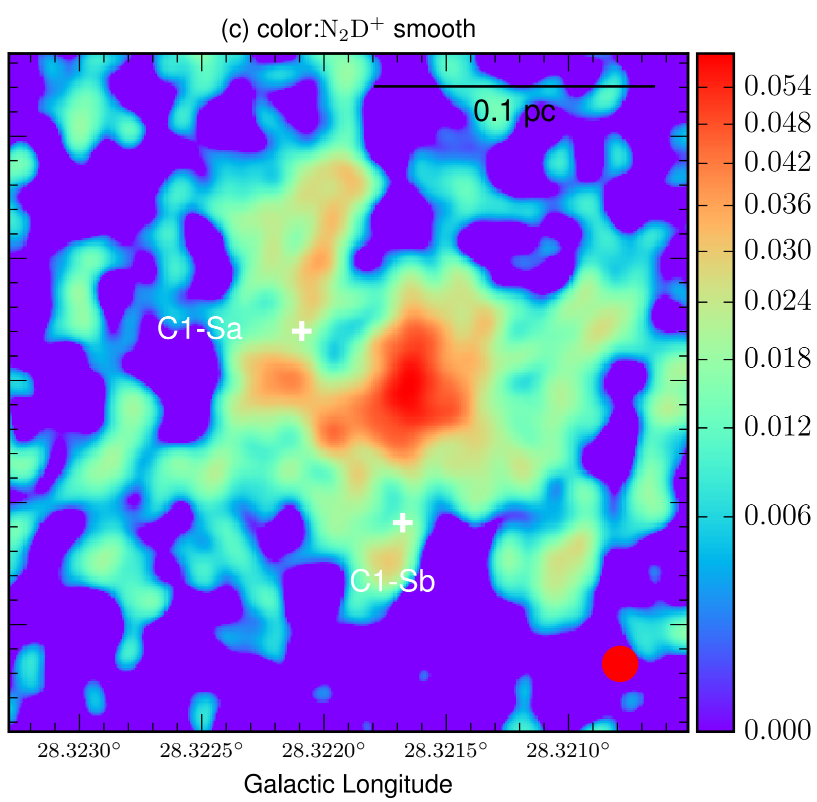


**CO depletion factor: $f_D$>600**

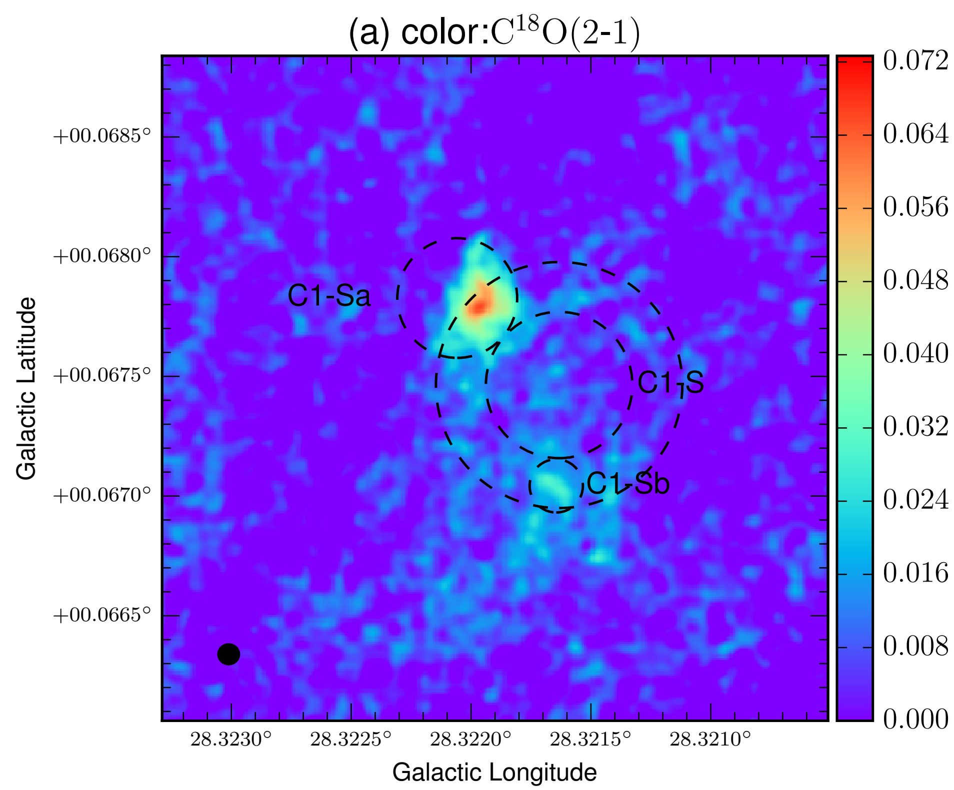


**$DCO^+$ Envelope**

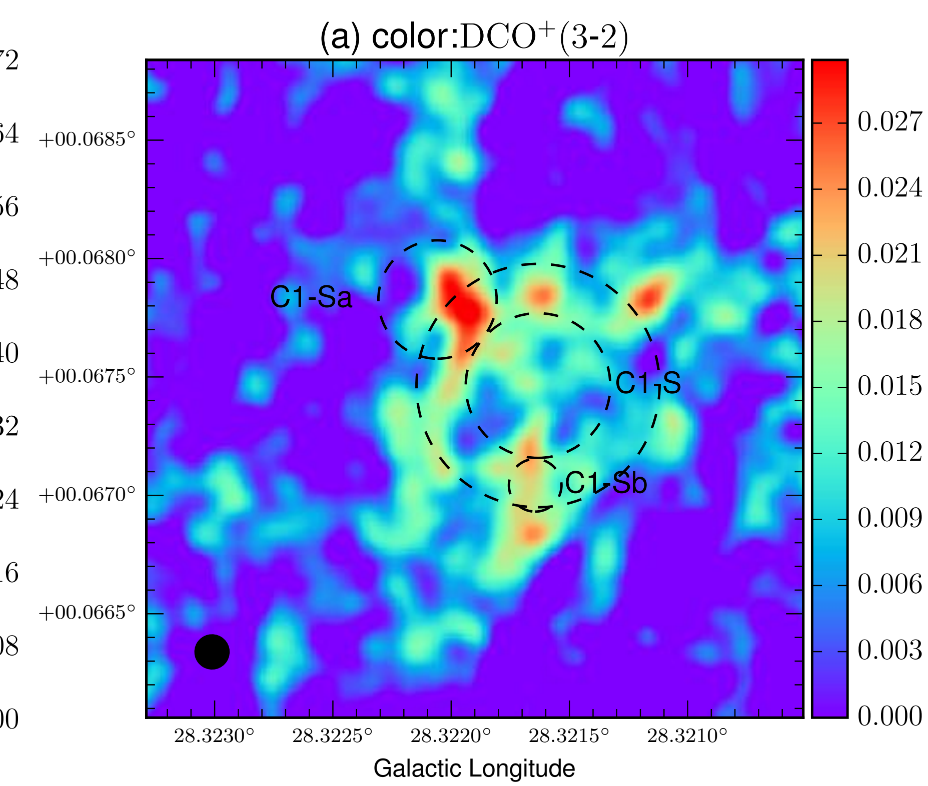


**Kong, Tan et al. (2017b, submitted)**

# Constraints for Initial Conditions of Numerical Simulations

Peters et al. (2011)
M = 100M$_\odot$, R=0.5pc,
$n_H$ = 5400cm$^{-3}$, B=10μG

Seifried et al. (2012)
M = 100M$_\odot$, R=0.25pc,
$n_H$ = 4.4x10$^4$cm$^{-3}$, B~1mG

Myers et al. (2013)
M = 300M$_\odot$, R=0.1pc,
$n_H$ = 2.4x10$^6$cm$^{-3}$, B>~1mG

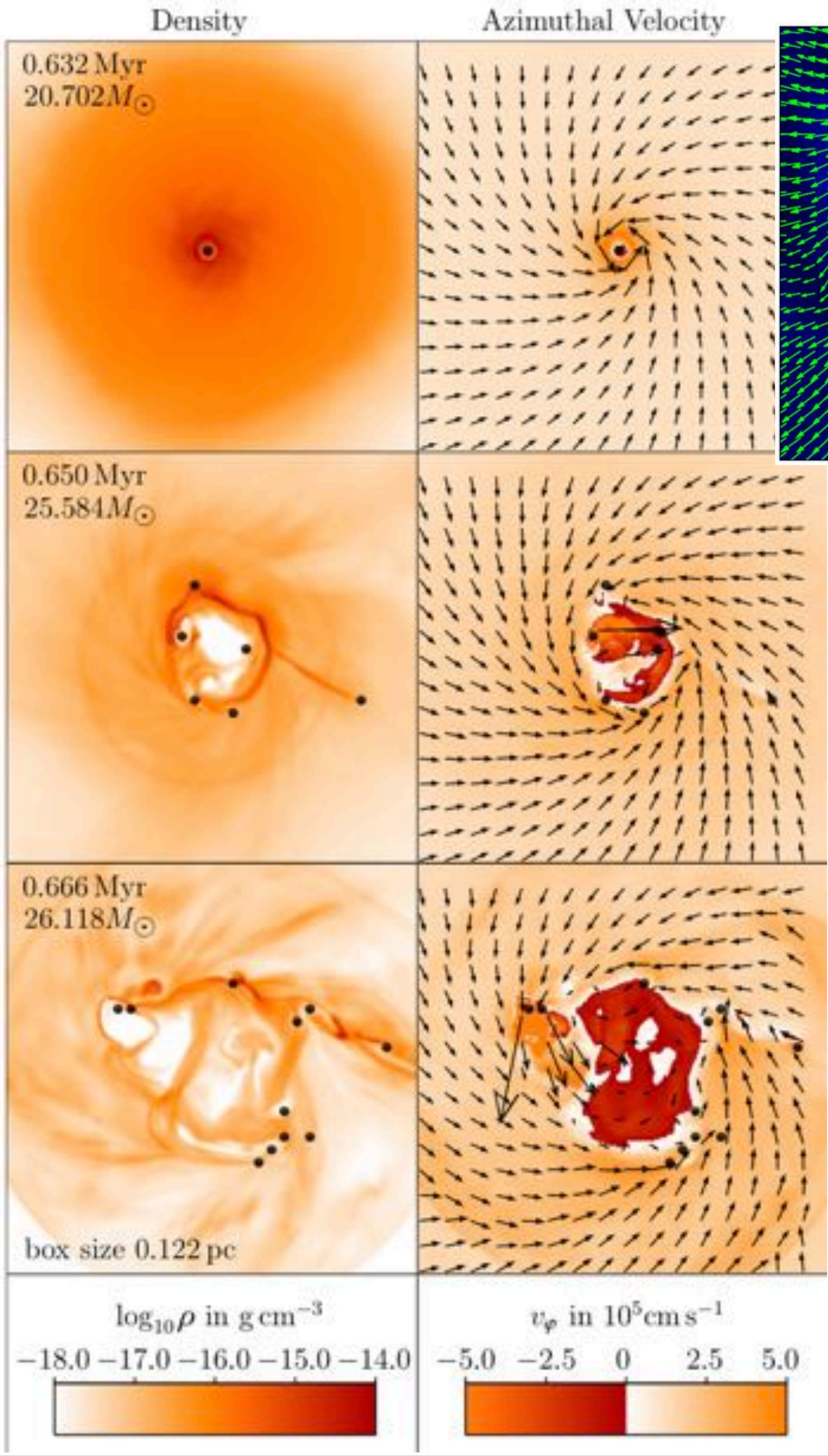


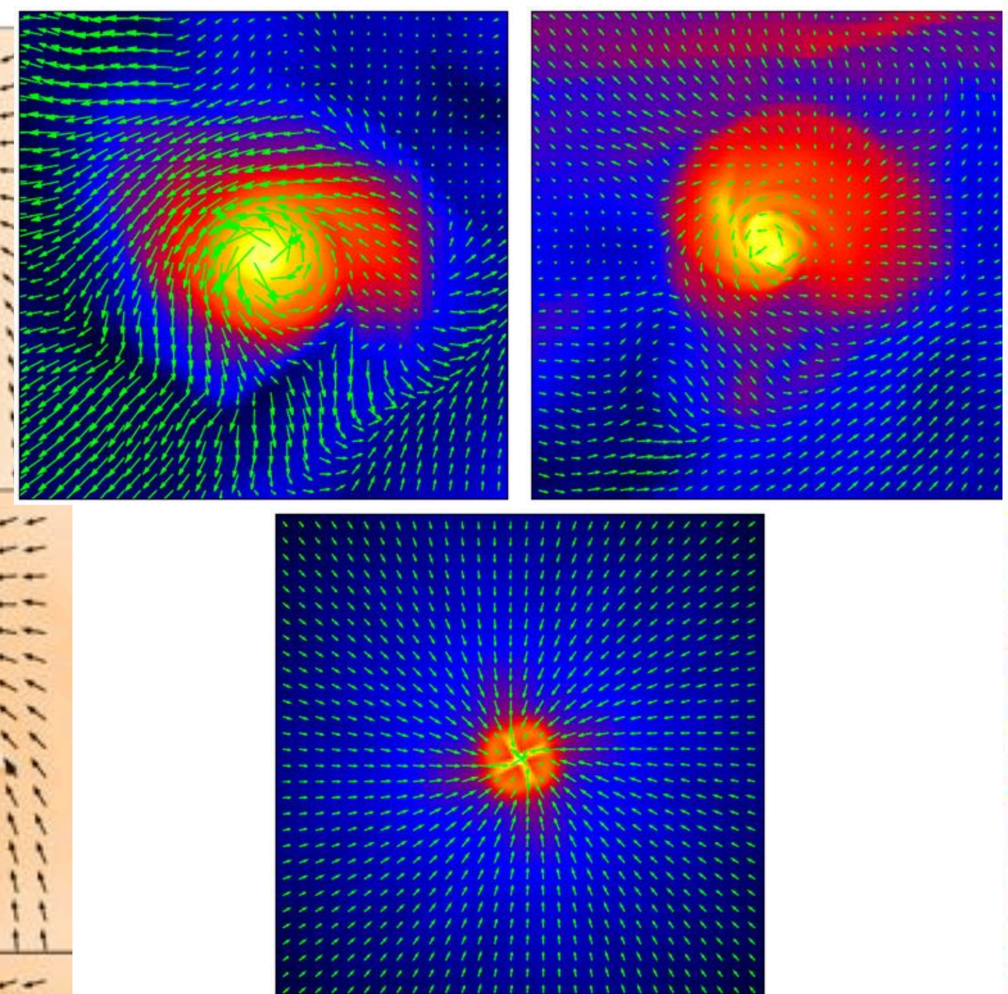

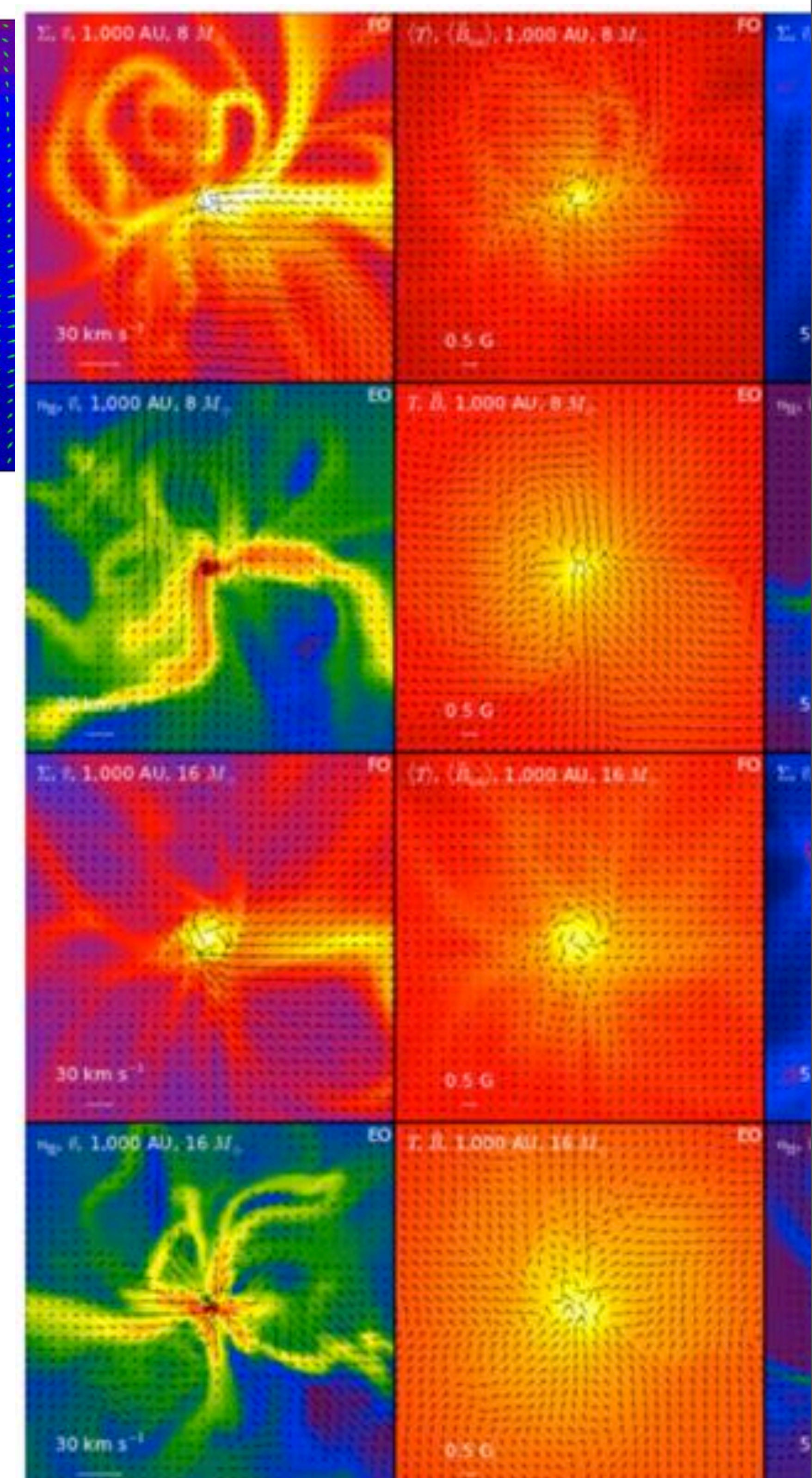

Observations:

# Evidence for strong magnetic fields in some massive star-forming cores

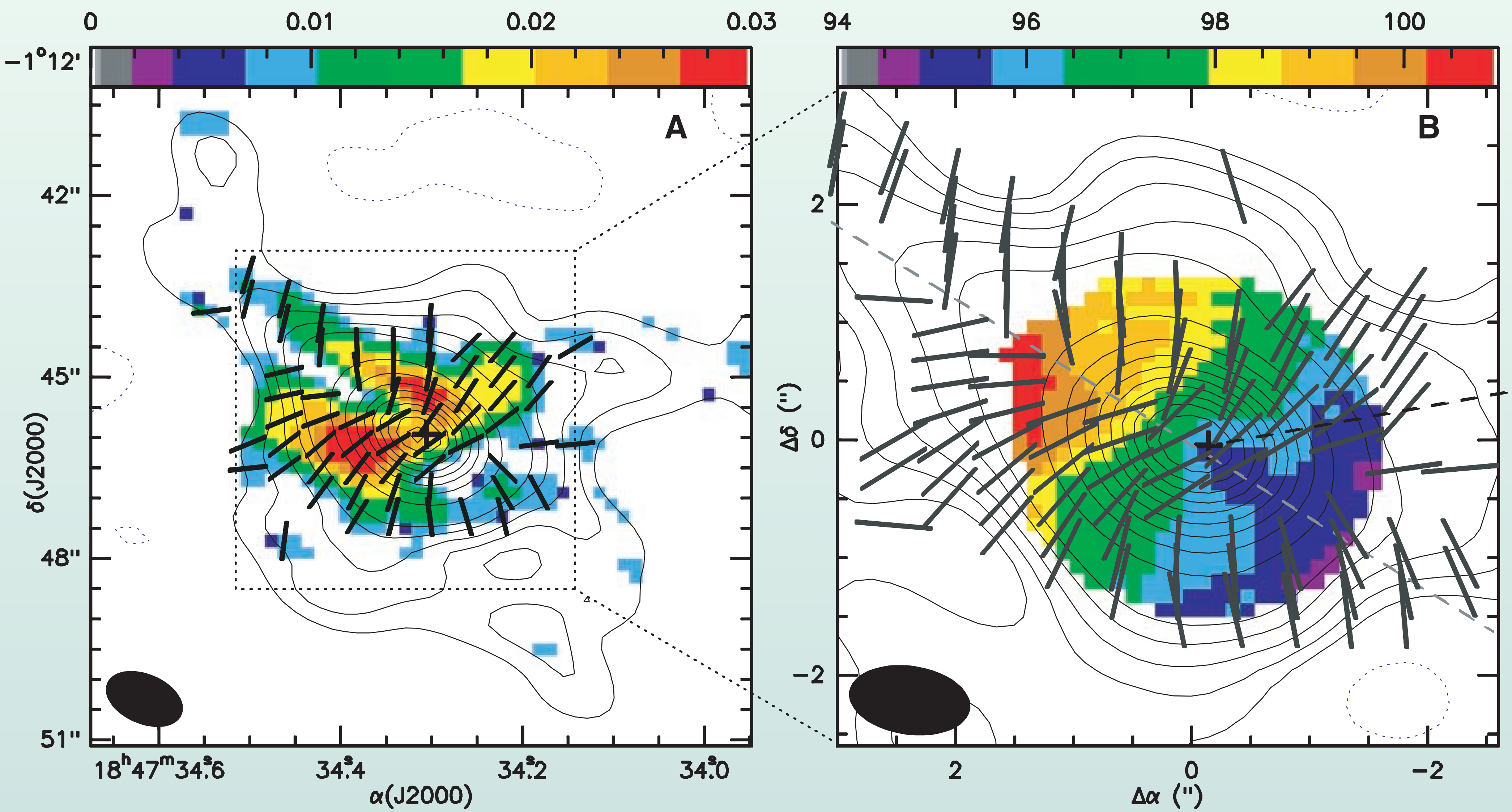


Girart+ (2009)
see also Q. Zhang+ (2015)

Evidence for nonthermal support

# Do massive protostars have morphologies similar to low-mass protostars? What sets the star formation efficiency from the core? CMF -> IMF?

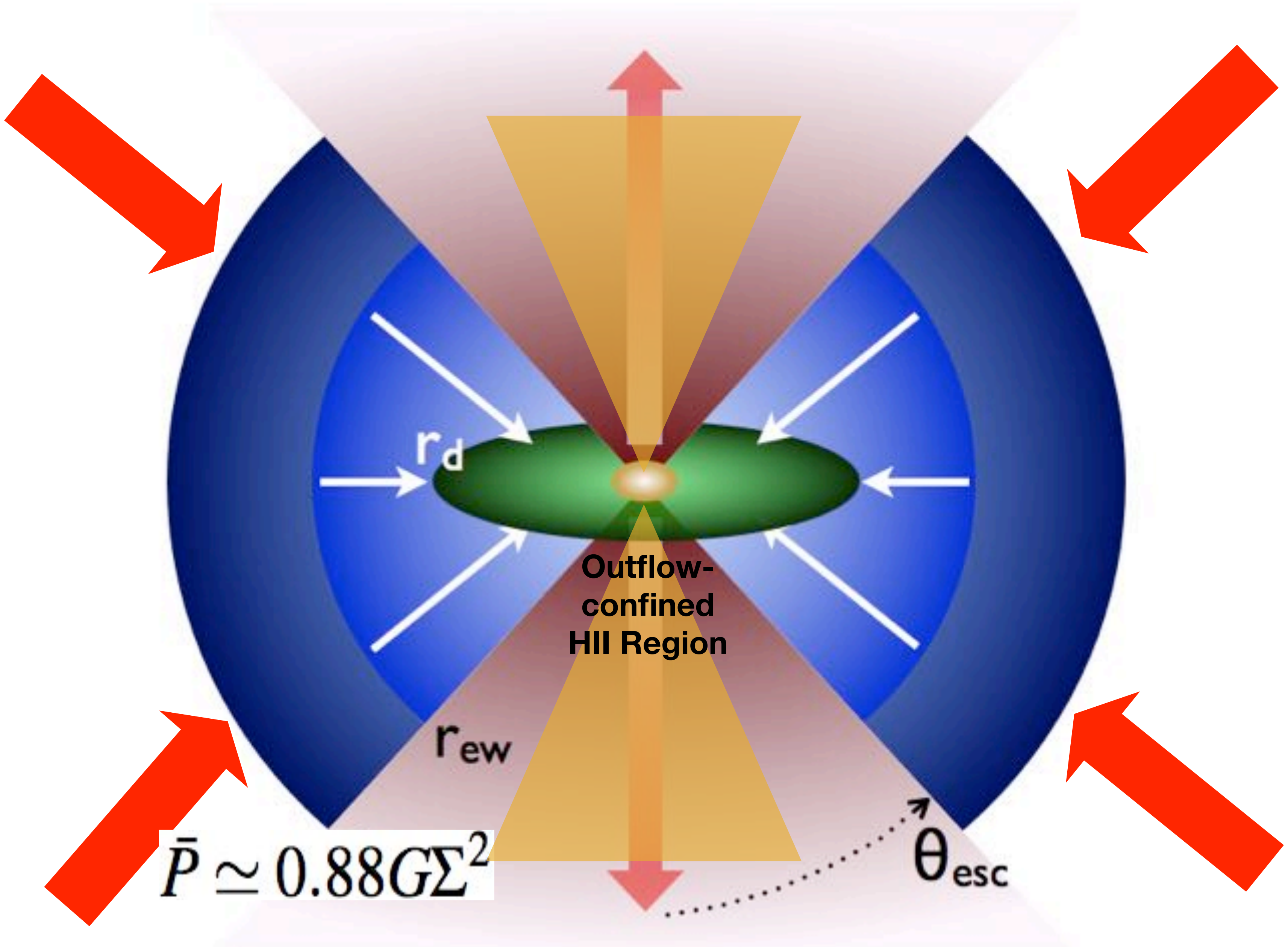

# Protostellar Evolution

Zhang, Tan, Hosokawa (2014)

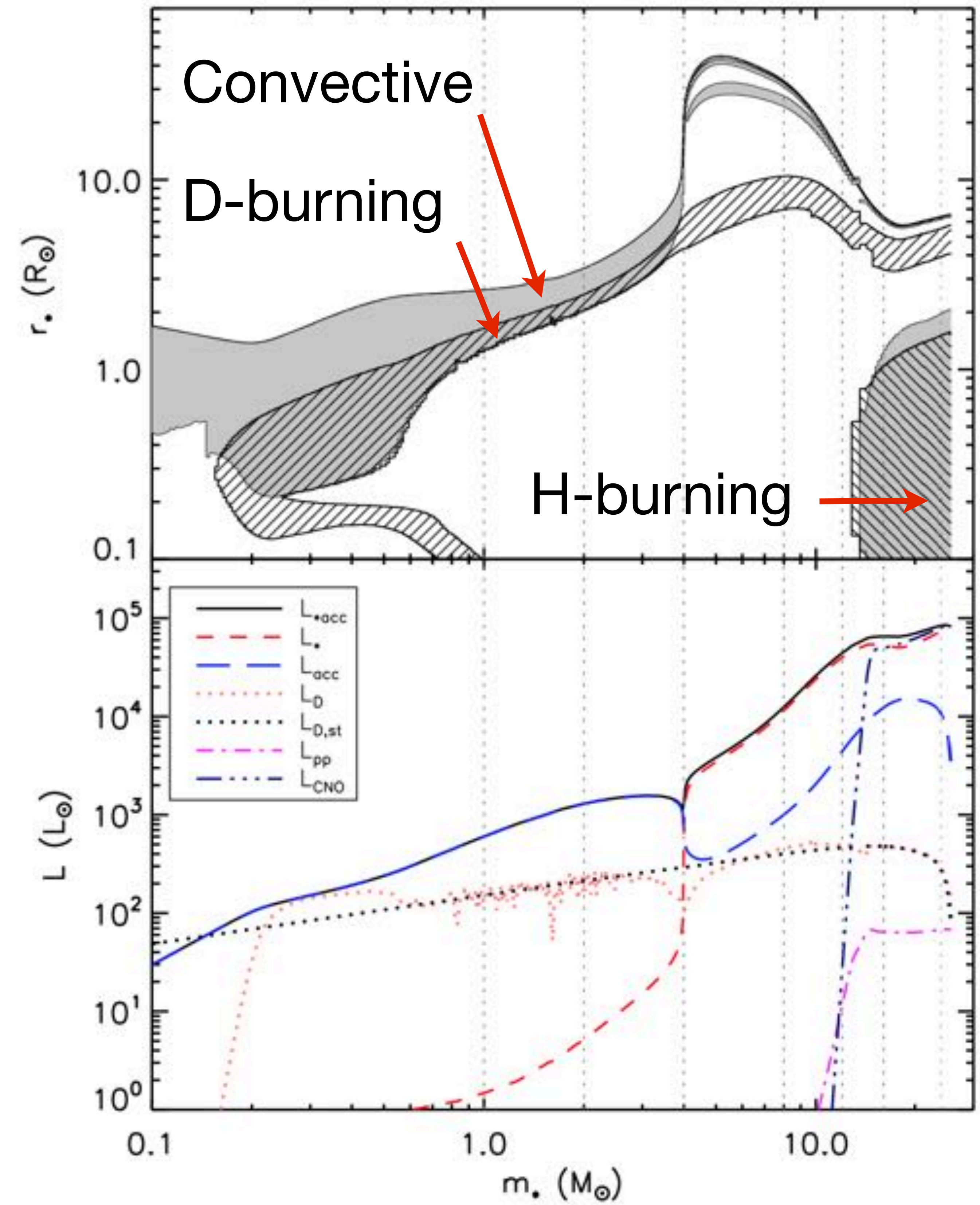


see also Palla & Stahler 1993; Hosokawa et al. (2010)

# Protostellar Evolution

Zhang, Tan, Hosokawa (2014)

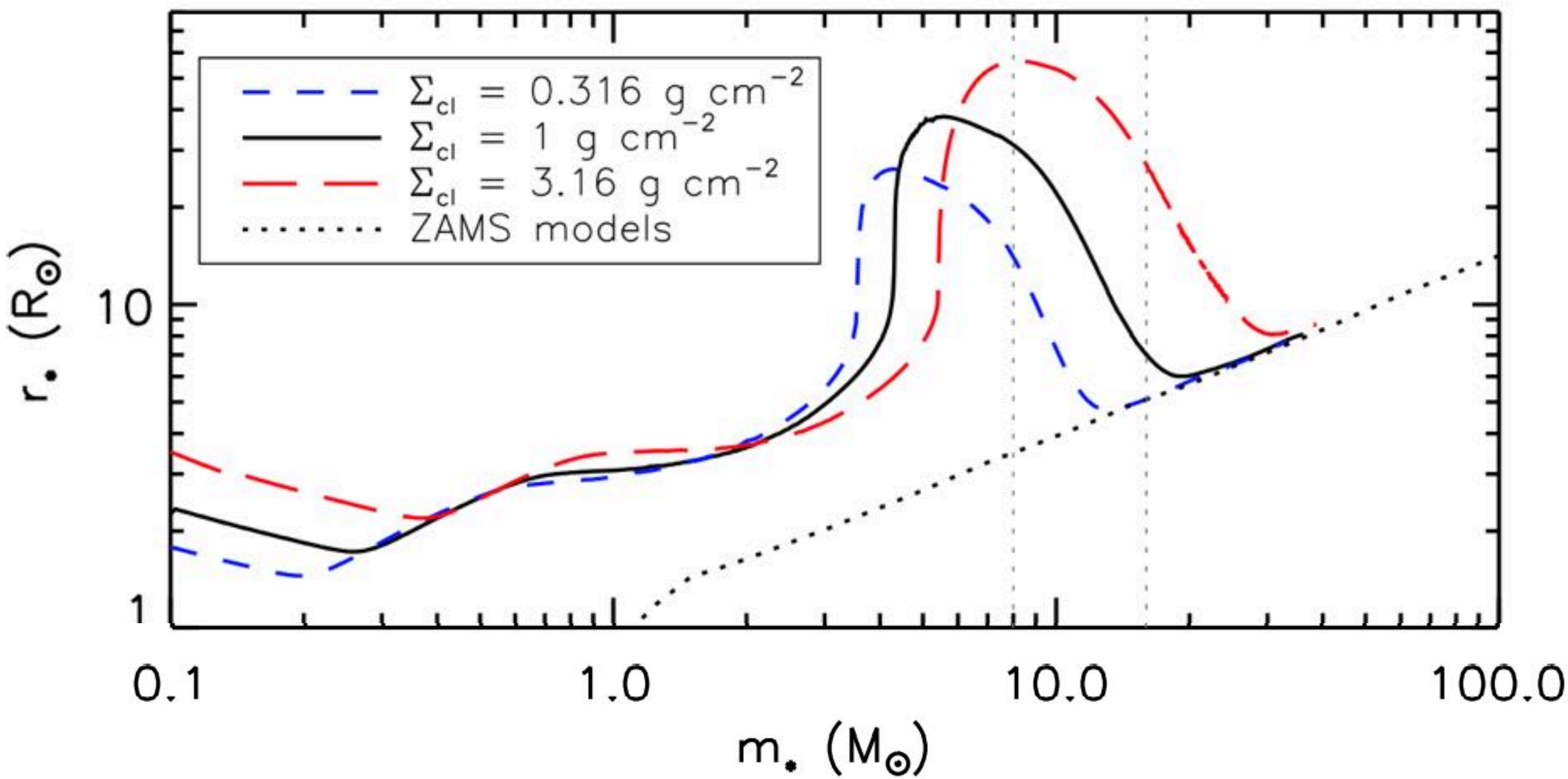


see also Palla & Stahler 1993; Hosokawa et al. (2010)

# Diagnostics of the Turbulent Core Model

Zhang & Tan (2011), Zhang, Tan & McKee (2013), Zhang, Tan & Hosokawa (2014), Tanaka, Tan & Zhang (2016)

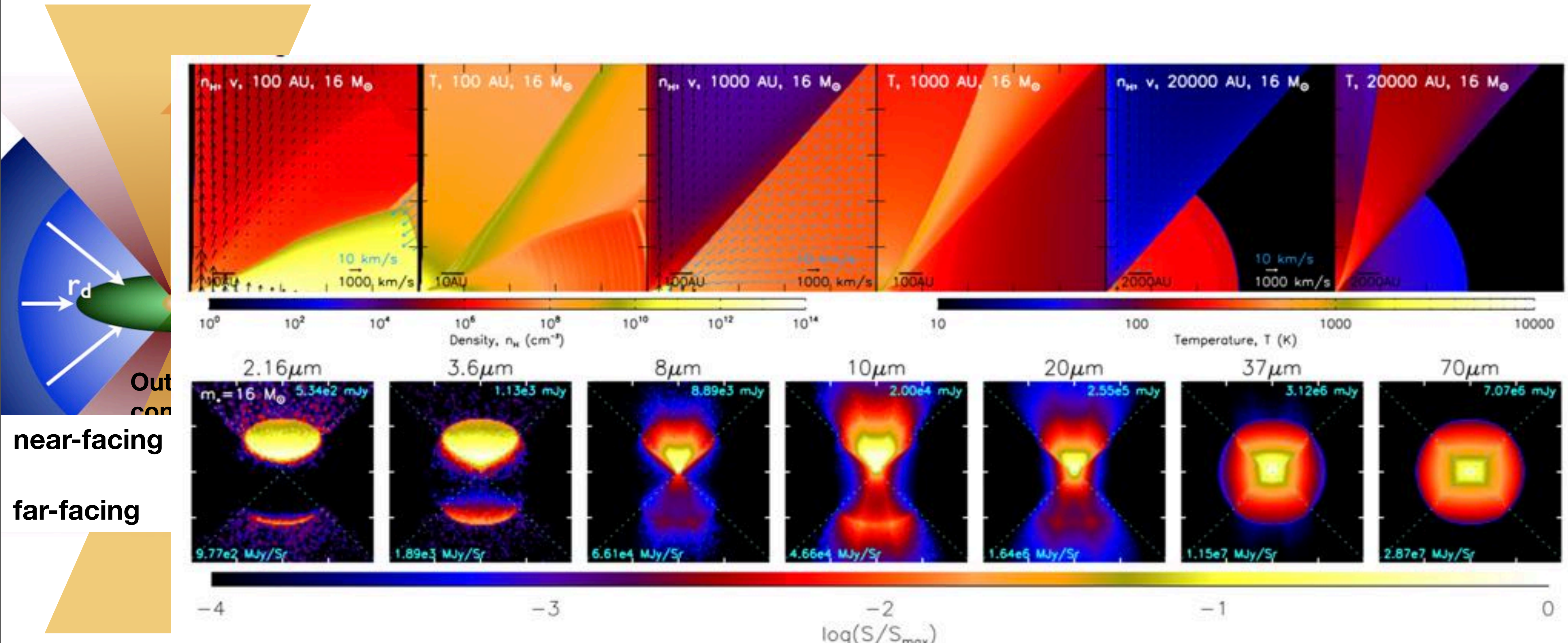


**Prediction: increasing symmetry from MIR-FIR**

The Astrophysical Journal, 788:166 (35pp), 2014 June 20 Zhang, Tan, & Hosokawa

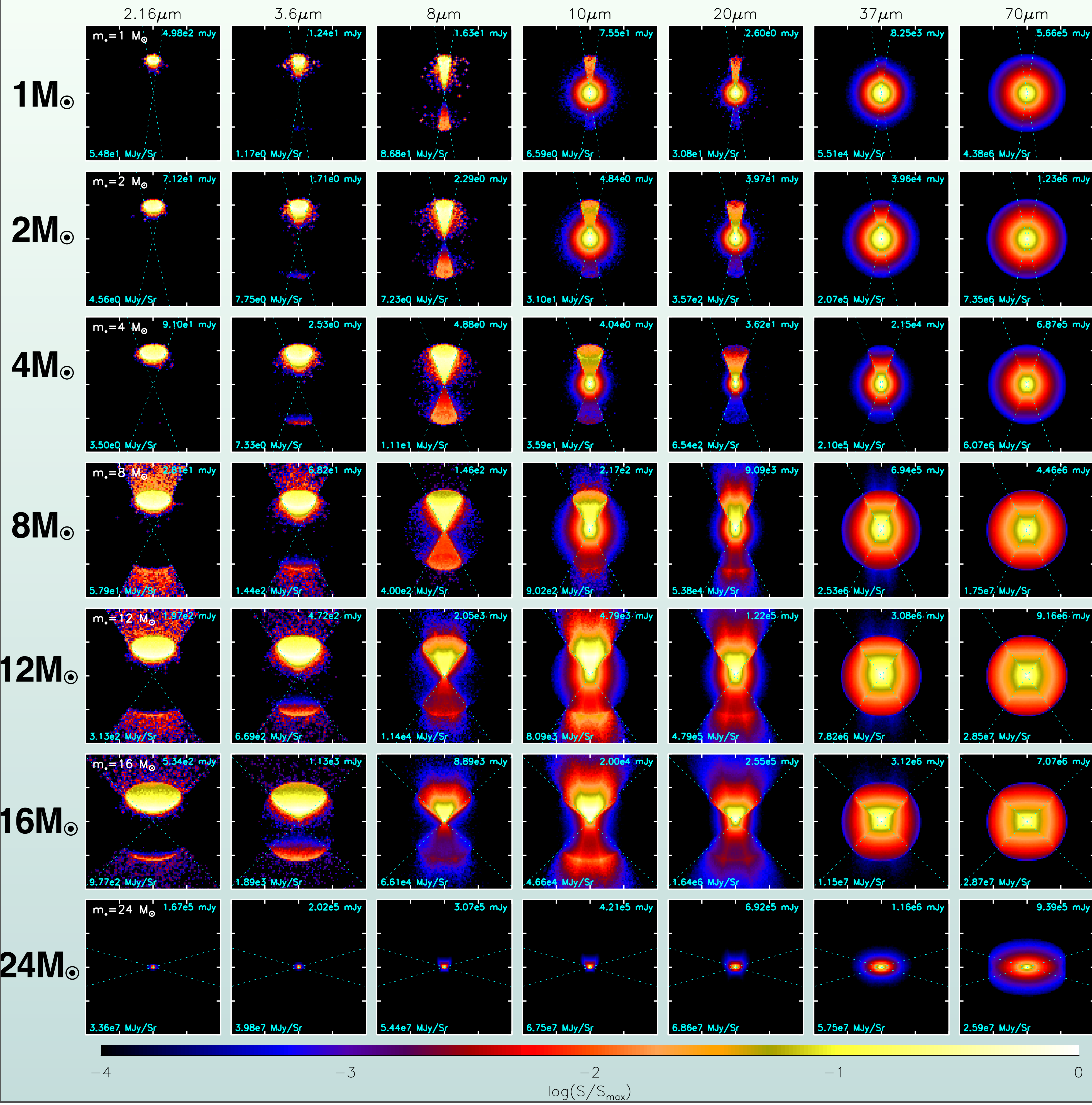


# NIR to FIR morphologies

Rotation and outflow axis inclined at 60° to line of sight.

# Massive Protostar G35.2N: d=2.2kpc; L~$10^5 L_\odot$



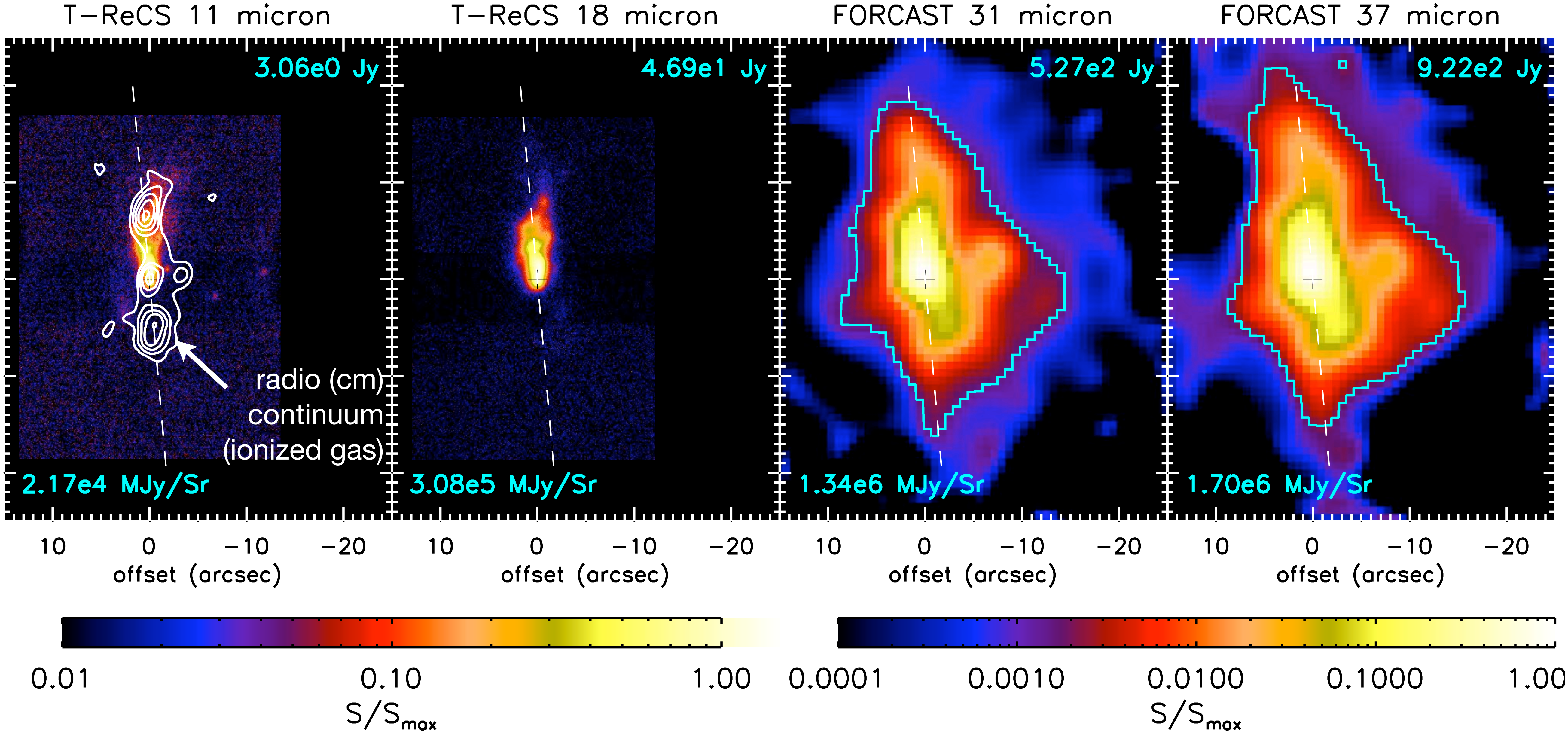


De Buizer (2006)

Zhang, Tan, De Buizer et al. (2013)

# Spectral energy distribution

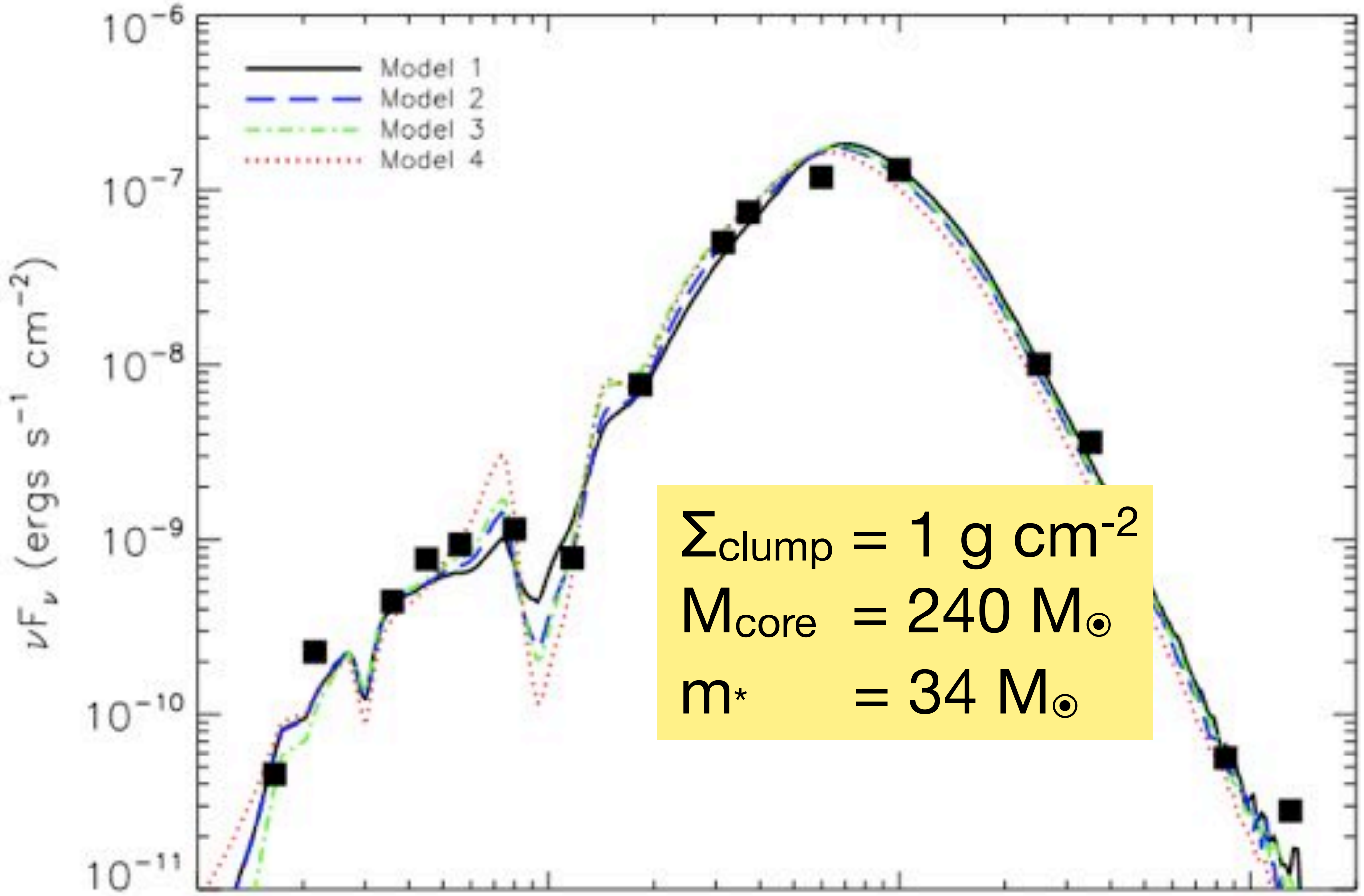


$\Sigma_{clump} = 1\ g\ cm^{-2}$
$M_{core} = 240\ M_\odot$
$m_* = 34\ M_\odot$

MIR SED requires high Σ core/clump

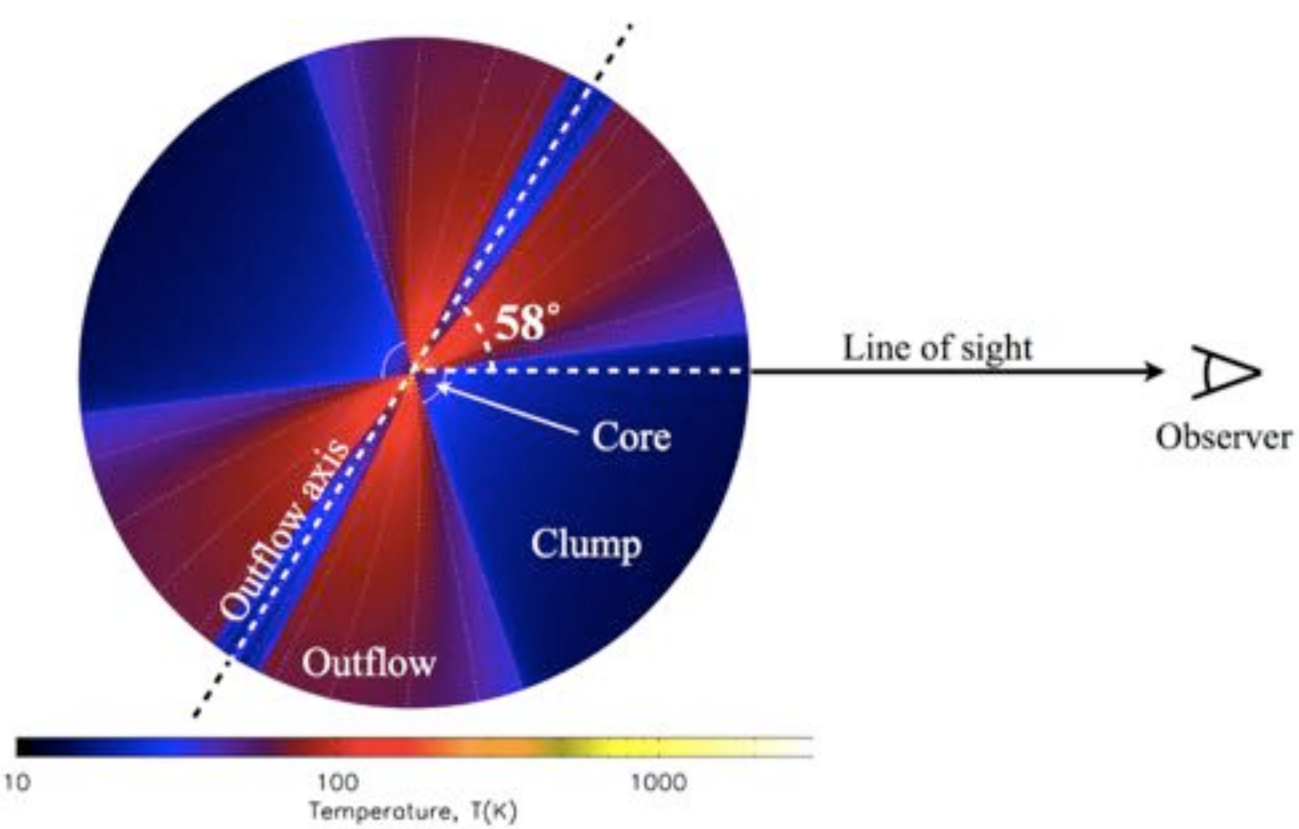


# Flux profiles along outflow cavity axis

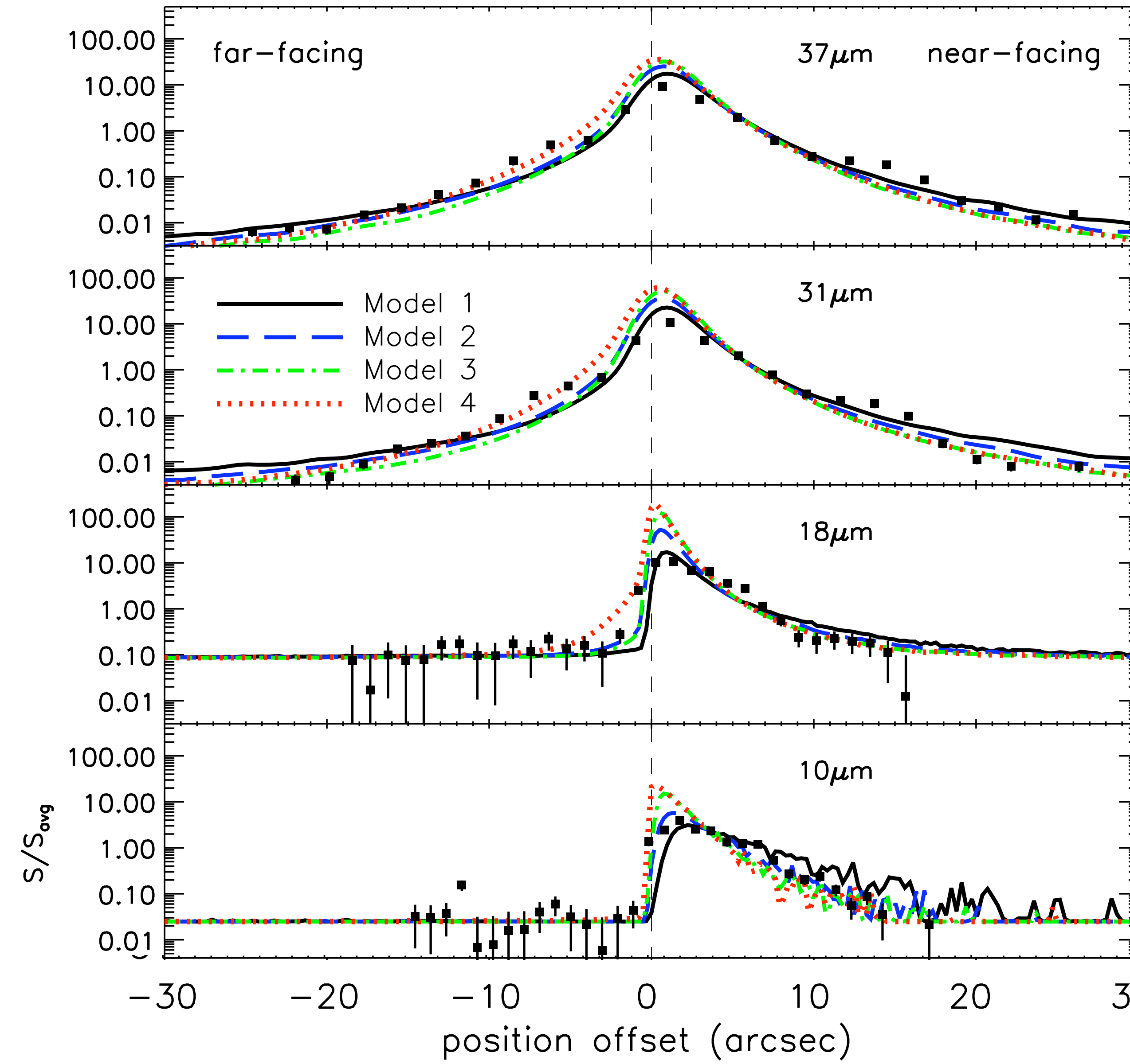


$L_{bol} \sim (0.66 - 2.2)\times10^5 L_\odot$
$M_{core} \sim 240 M_\odot$
$\Sigma_{cl} \sim 0.4 - 1\ g/cm^2$
$\theta_w \sim 35 - 51^\circ$
$\theta_{view} \sim 43 - 58^\circ$
**$m_* \sim 20 - 34\ M_\odot$**

# Spectral energy distribution

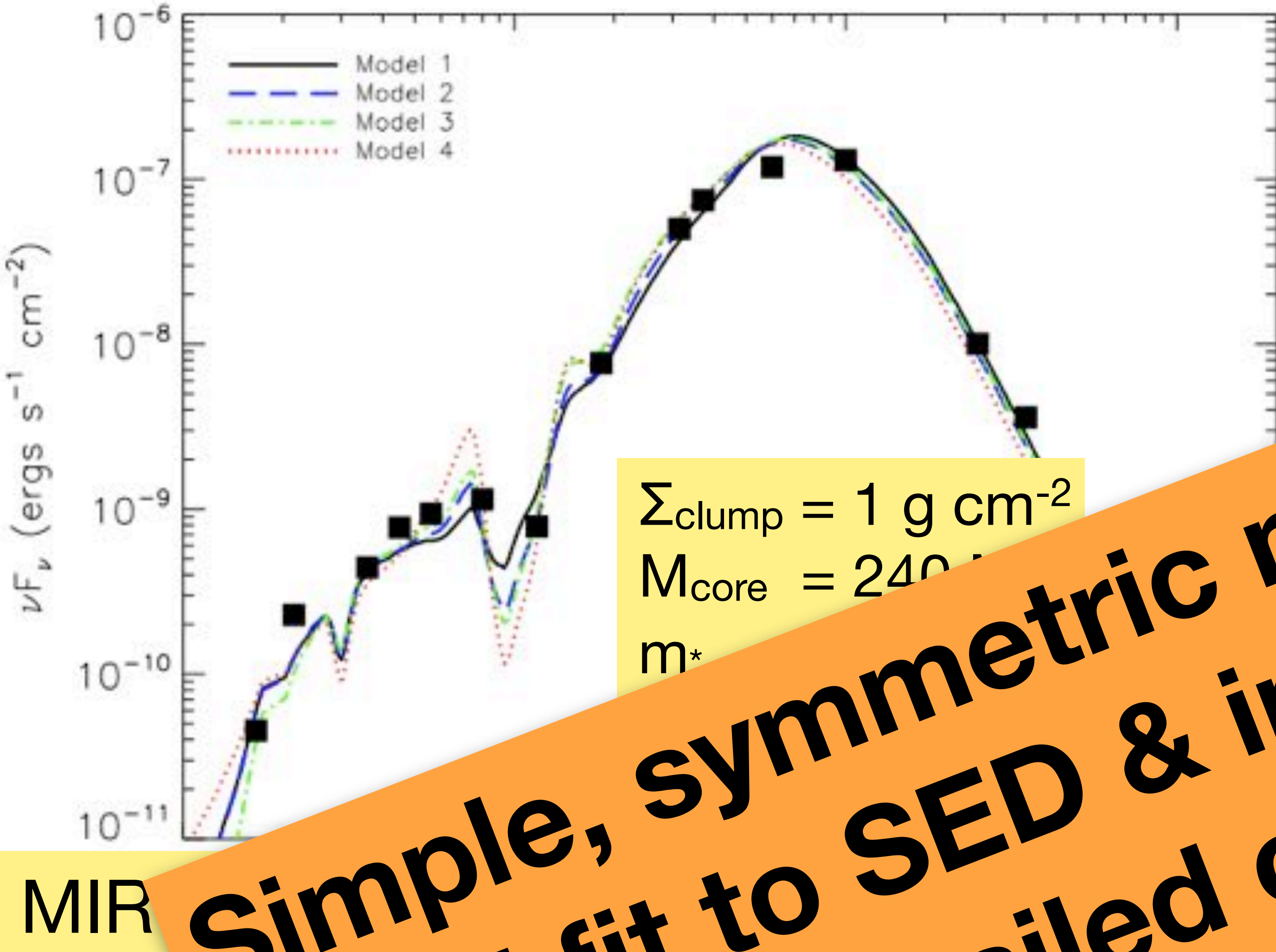


# Flux profiles along outflow cavity axis

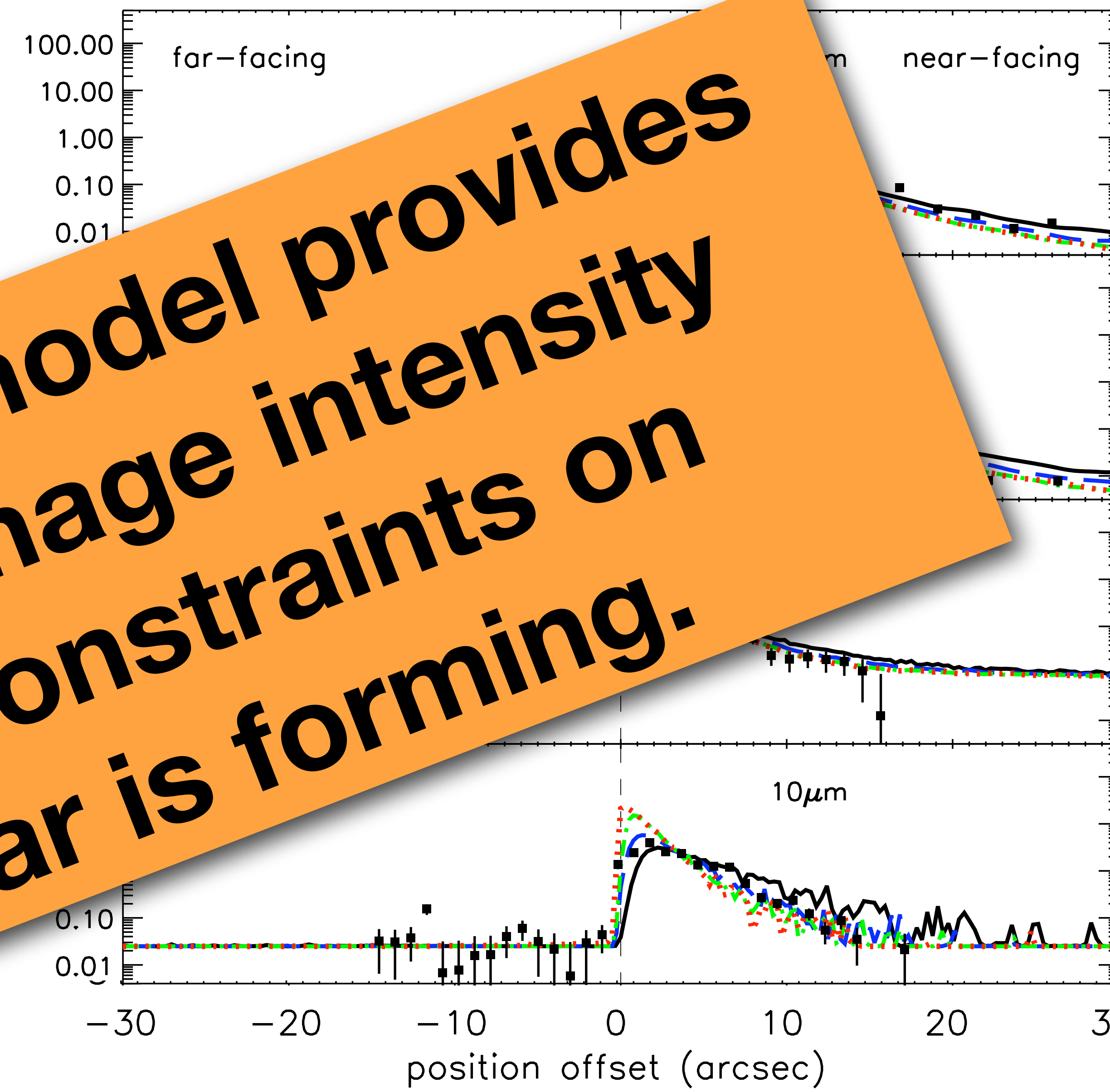


**Simple, symmetric model provides good fit to SED & image intensity profiles: detailed constraints on how a massive star is forming.**

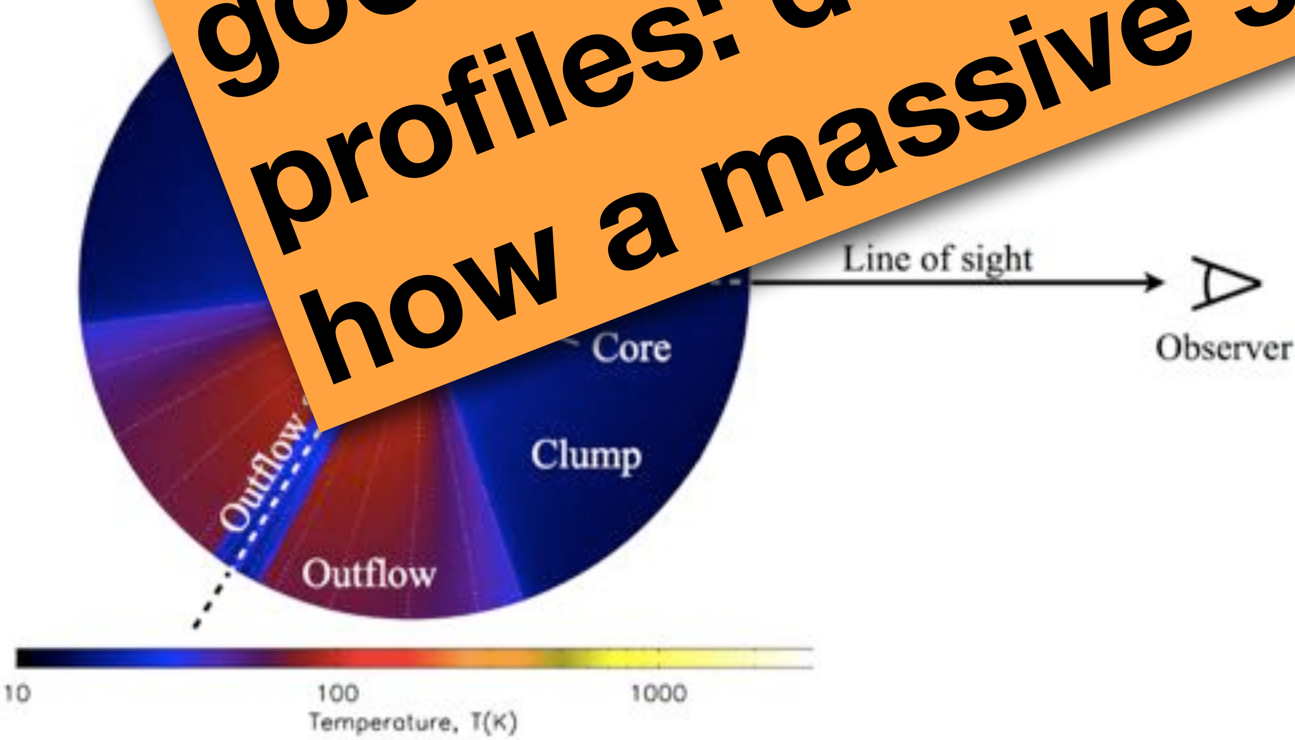


$L_{bol} \sim (0.66 - 2.2)\times10^5 L_\odot$
$M_{core} \sim 240 M_\odot$
$\Sigma_{cl} \sim 0.4 - 1$ g/cm$^2$
$\theta_w \sim 35 - 51^\circ$
$\theta_{view} \sim 43 - 58^\circ$
**$m_* \sim 20 - 34\ M_\odot$**

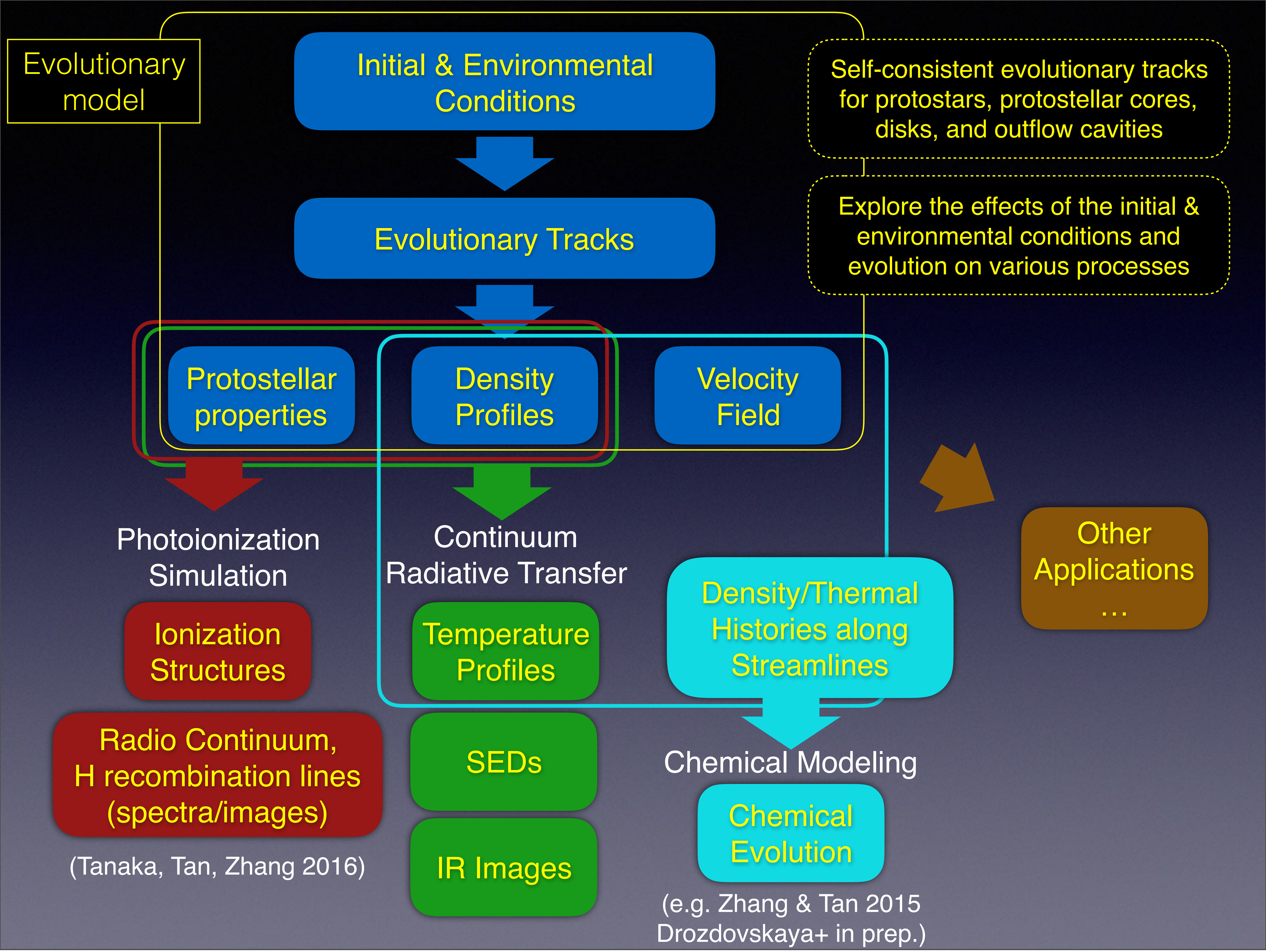
Evolutionary model
Initial & Environmental Conditions
Evolutionary Tracks
Protostellar properties
Density Profiles
Velocity Field
Self-consistent evolutionary tracks for protostars, protostellar cores, disks, and outflow cavities
Explore the effects of the initial & environmental conditions and evolution on various processes
Photoionization Simulation
Ionization Structures
Radio Continuum, H recombination lines (spectra/images)
(Tanaka, Tan, Zhang 2016)
Continuum Radiative Transfer
Temperature Profiles
SEDs
IR Images
Density/Thermal Histories along Streamlines
Chemical Modeling
Chemical Evolution
(e.g. Zhang & Tan 2015 Drozdovskaya+ in prep.)
Other Applications …

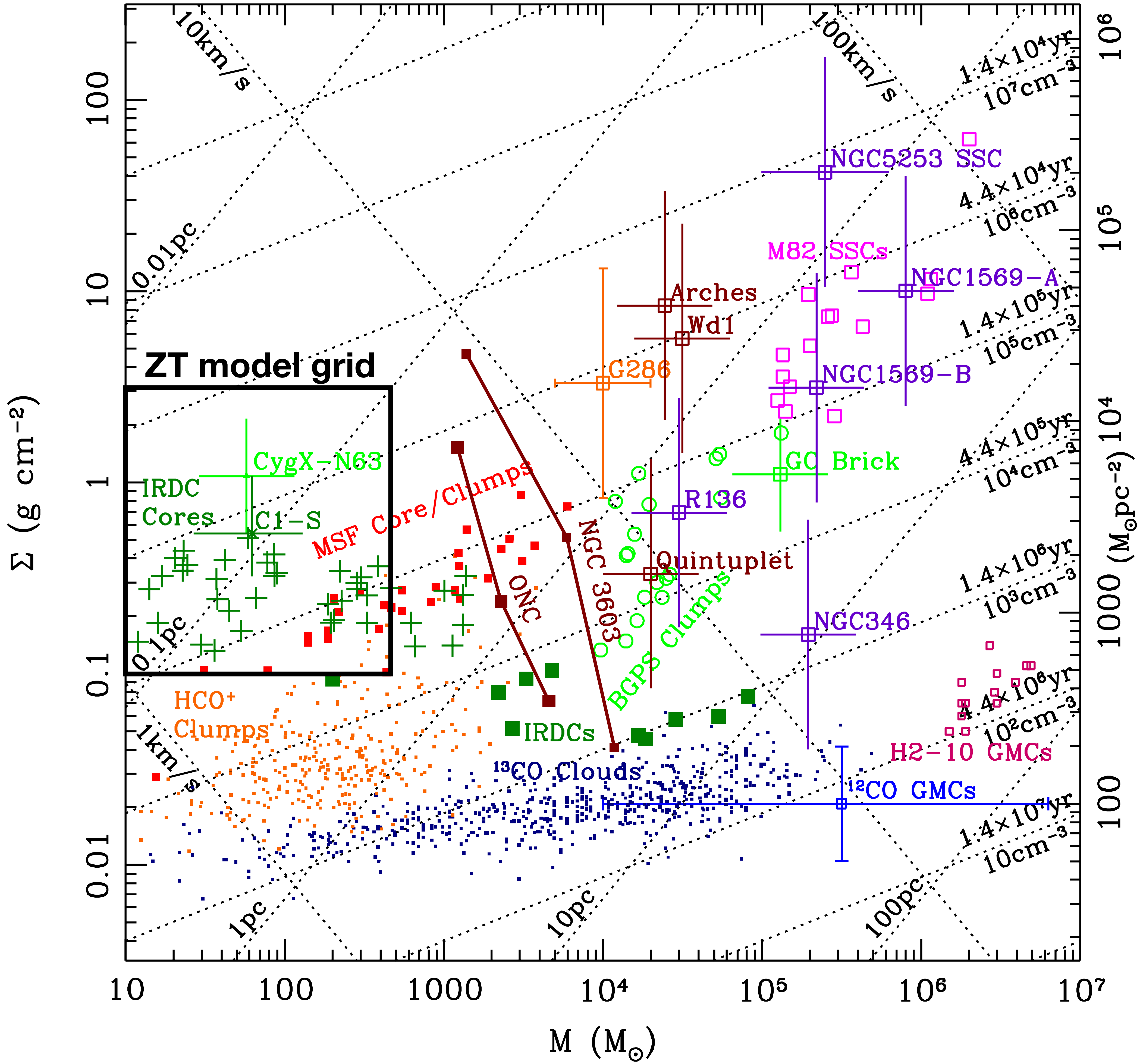

ZT model grid
IRDC Cores
CygX-N63
C1-S
MSF Core/Clumps
HCO+ Clumps
IRDCs
13CO Clouds
ONC
NGC 3603
BGPS Clumps
G286
Arches
Wd1
Quintuplet
R136
GC Brick
NGC5253 SSC
M82 SSCs
NGC1569-A
NGC1569-B
NGC346
H2-10 GMCs
12CO GMCs
10km/s
100km/s
1km/s
0.01pc
0.1pc
1pc
10pc
100pc
1.4×10^4yr
10^7cm^-3
4.4×10^4yr
10^6cm^-3
1.4×10^5yr
10^5cm^-3
4.4×10^5yr
10^4cm^-3
1.4×10^6yr
10^3cm^-3
4.4×10^6yr
10^2cm^-3
1.4×10^7yr
10cm^-3
Σ (g cm^-2)
(M⊙pc^-2)
M (M⊙)

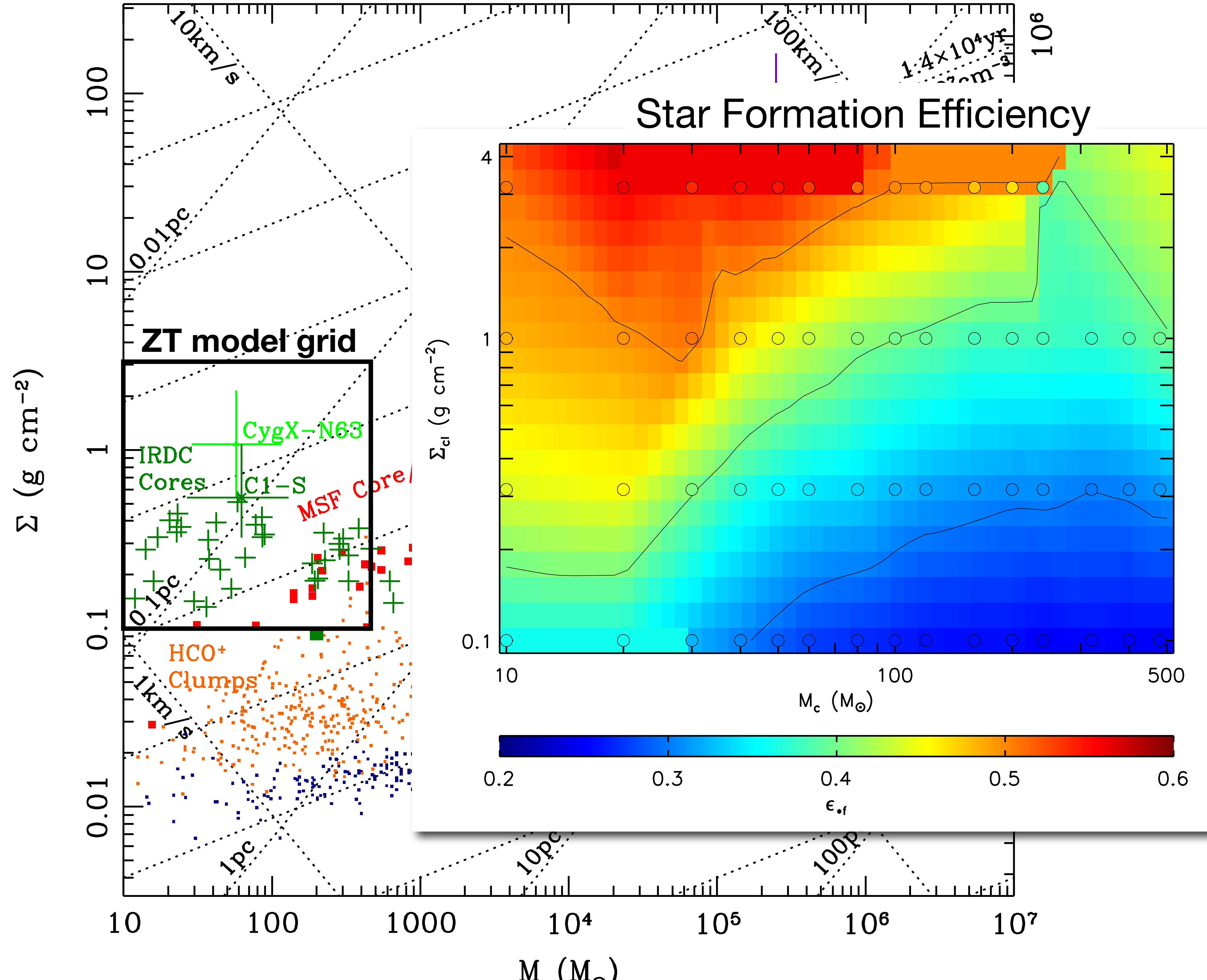
Star Formation Efficiency
ZT model grid
IRDC Cores
CygX-N63
C1-S
MSF Core
HCO+ Clumps
10km/s
100km/s
1km/s
0.01pc
0.1pc
1pc
10pc
100pc
1.4×10⁴yr
Σ (g cm⁻²)
M (M☉)
Σcl (g cm⁻²)
Mc (M☉)
ε*f

Initial & Environmental Conditions

Evolutionary Tracks

Density/velocity Profiles

Continuum Radiative Transfer

(Code: Whitney+ 03, 12; also see Robitaille+ 11)

Temperature Profiles

SEDs

IR Images

$M_c = 60\ M_\odot$, $\Sigma_{cl} = 1\ g/cm^2$, $\beta_c = 0.02$ $\quad$ $M_c = 60\ M_\odot$, $\Sigma_{cl} = 0.3\ g/cm^2$, $\beta_c = 0.02$

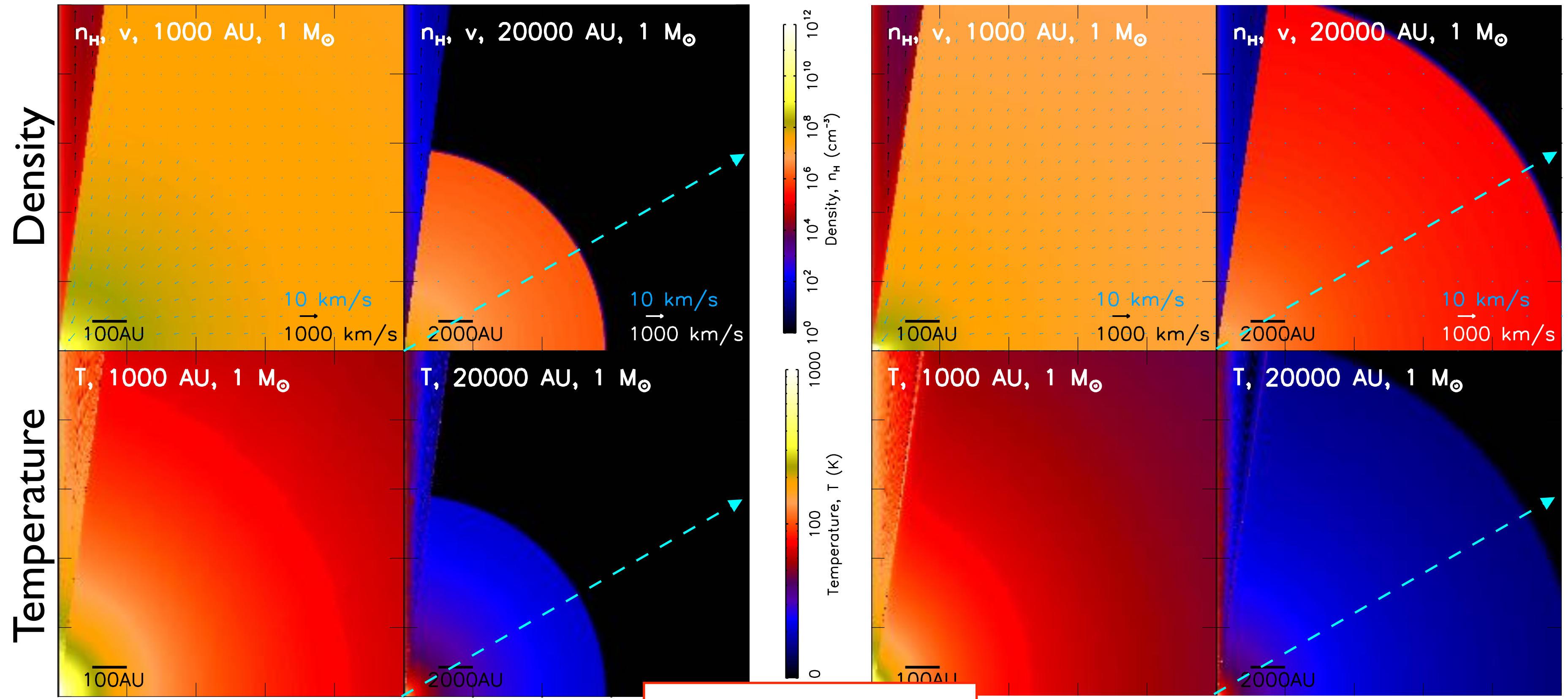


$m_* = 1 M_\odot$

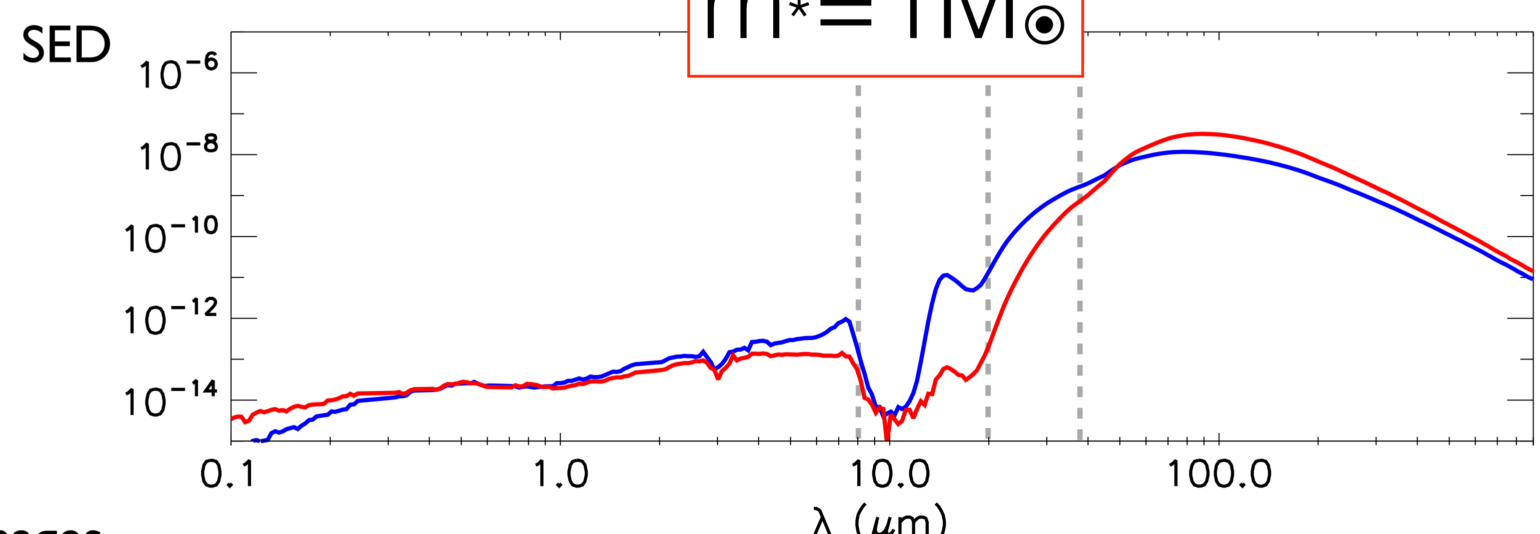


Images

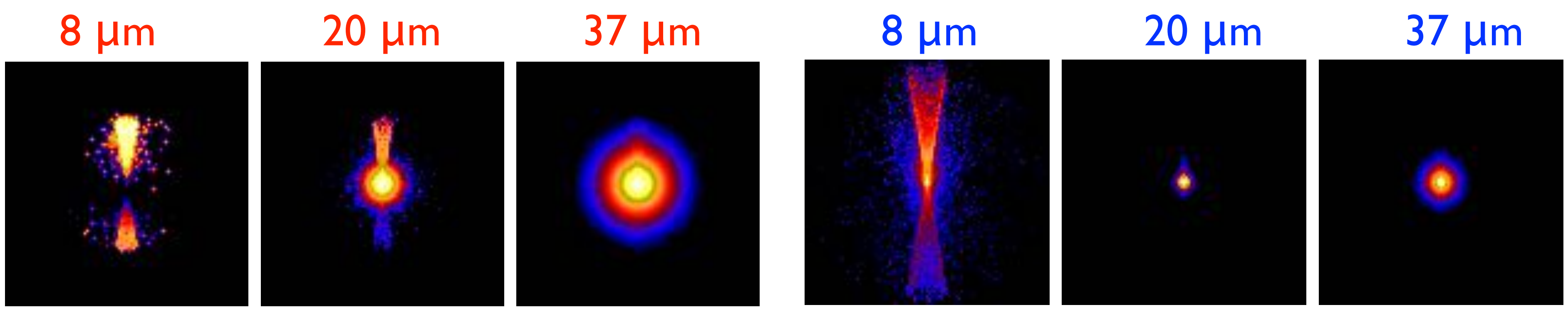

Initial & Environmental Conditions

Evolutionary Tracks

Density/velocity Profiles

Continuum Radiative Transfer

(Code: Whitney+ 03, 12; also see Robitaille+ 11)

Temperature Profiles

SEDs

IR Images

$M_c = 60\ M_\odot$, $\Sigma_{cl} = 1\ g/cm^2$, $\beta_c = 0.02$

$M_c = 60\ M_\odot$, $\Sigma_{cl} = 0.3\ g/cm^2$, $\beta_c = 0.02$

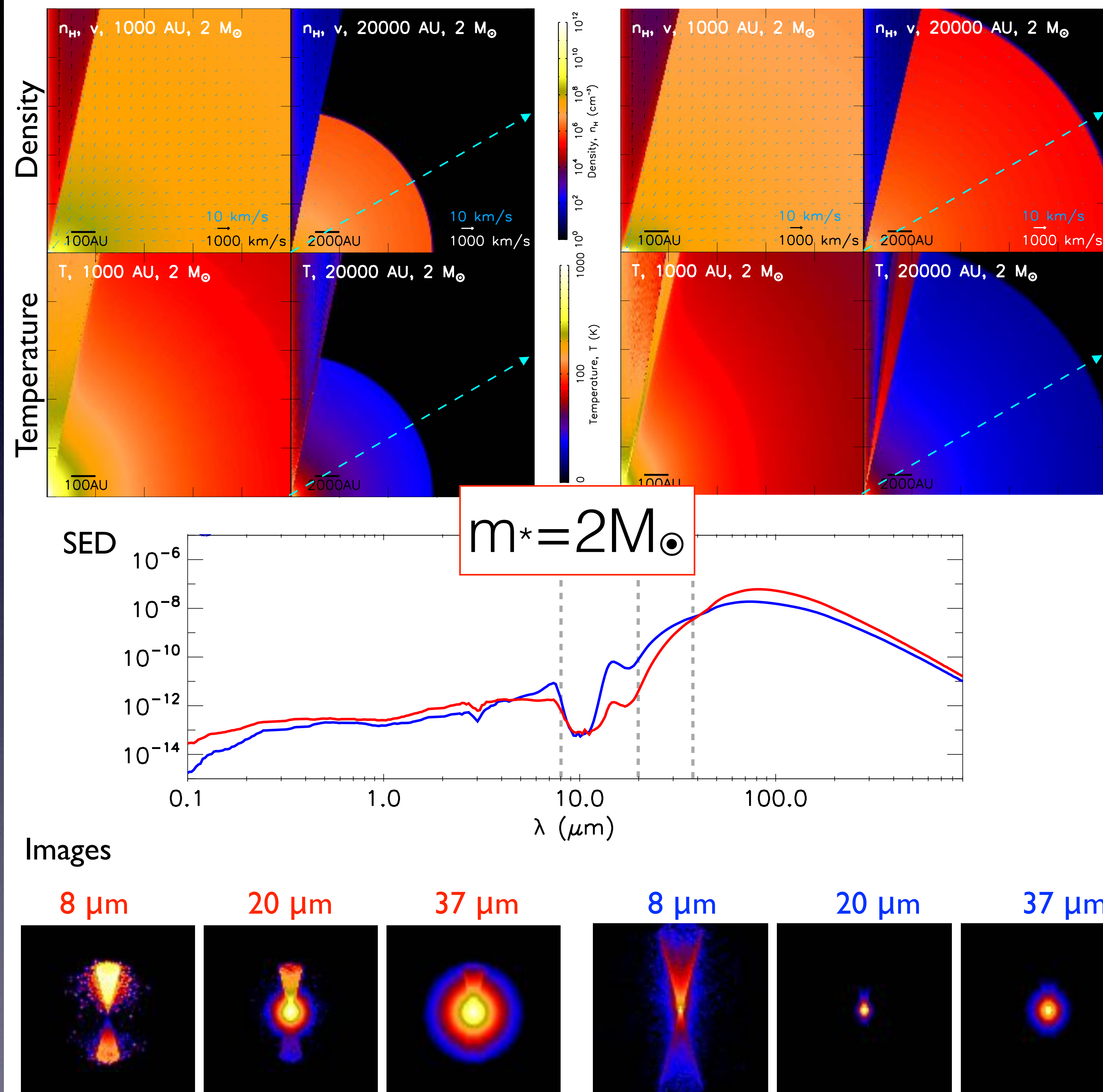

Initial & Environmental Conditions

Evolutionary Tracks

Density/velocity Profiles

Continuum Radiative Transfer

(Code: Whitney+ 03, 12; also see Robitaille+ 11)

Temperature Profiles

SEDs

IR Images

$M_c = 60\ M_\odot$, $\Sigma_{cl} = 1\ g/cm^2$, $\beta_c = 0.02$ $M_c = 60\ M_\odot$, $\Sigma_{cl} = 0.3\ g/cm^2$, $\beta_c = 0.02$

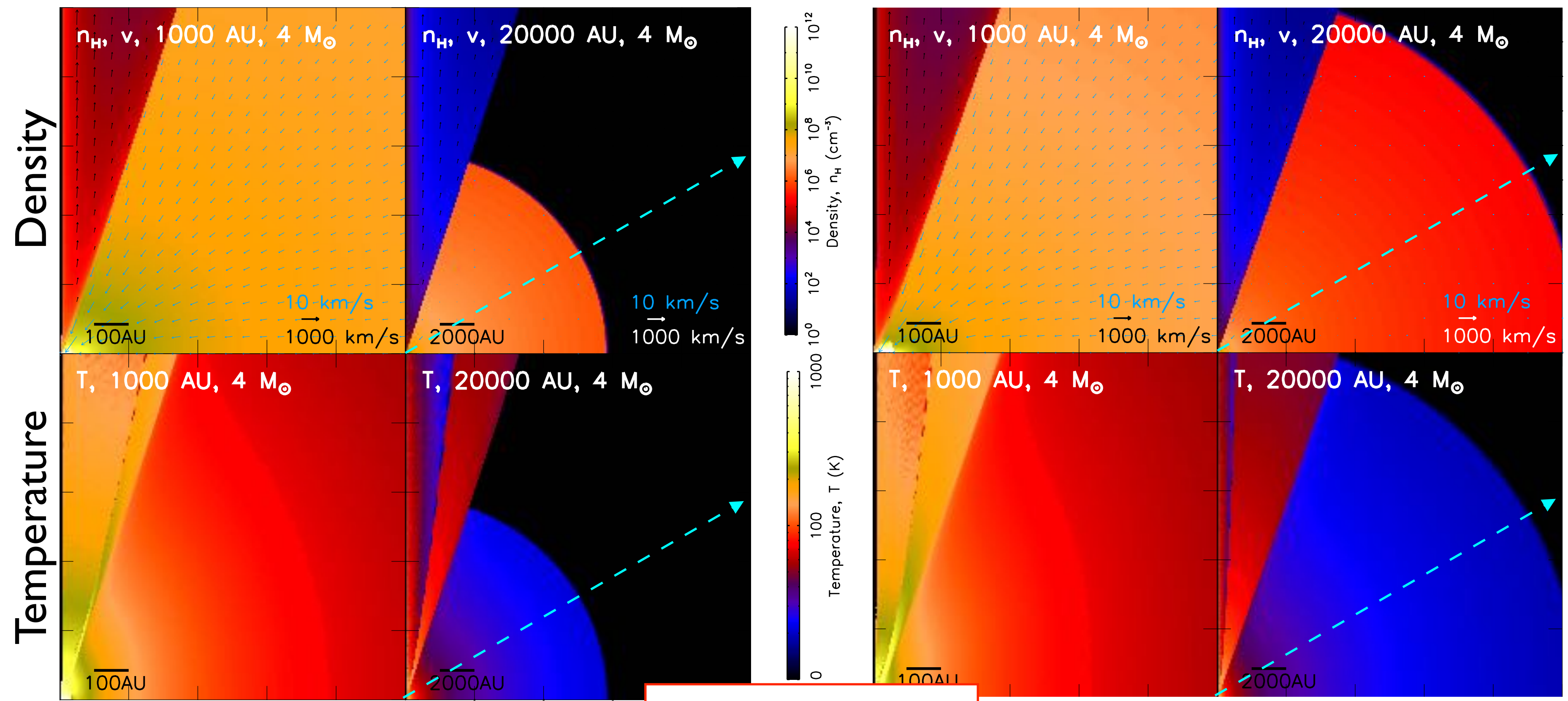


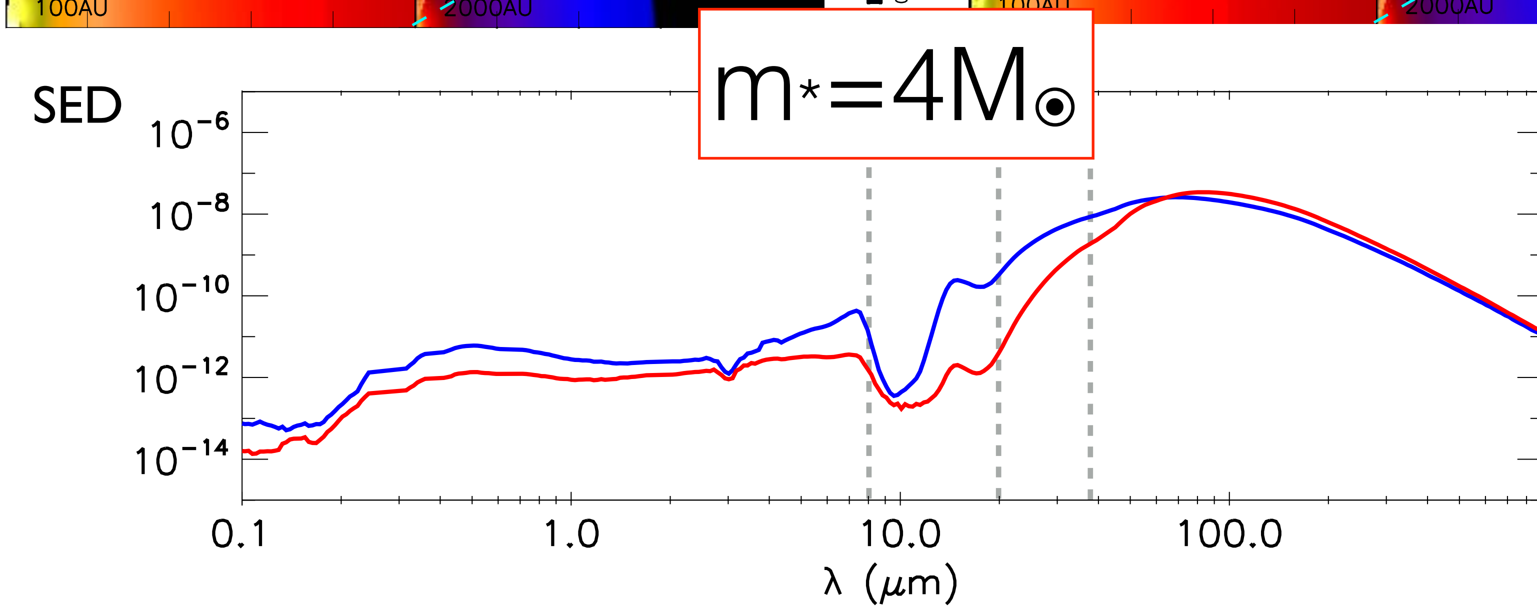


Images

8 μm 20 μm 37 μm 8 μm 20 μm 37 μm

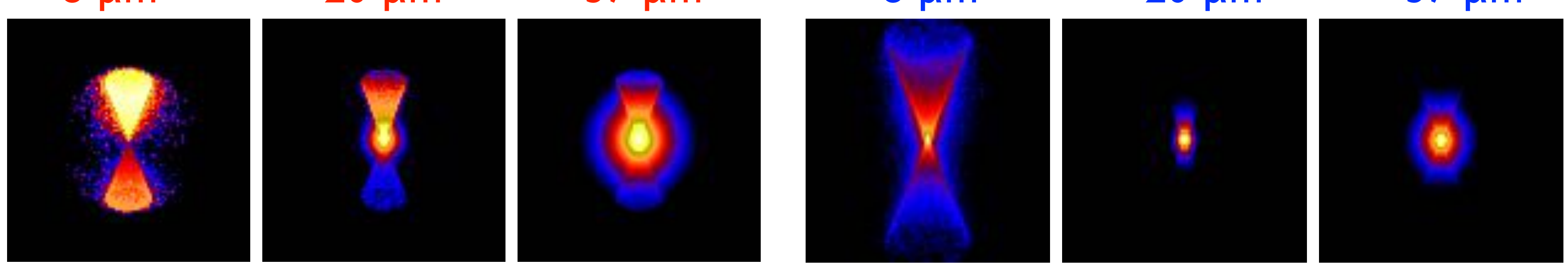

Initial & Environmental Conditions

Evolutionary Tracks

Density/velocity Profiles

Continuum Radiative Transfer
(Code: Whitney+ 03, 12; also see Robitaille+ 11)

Temperature Profiles

SEDs

IR Images

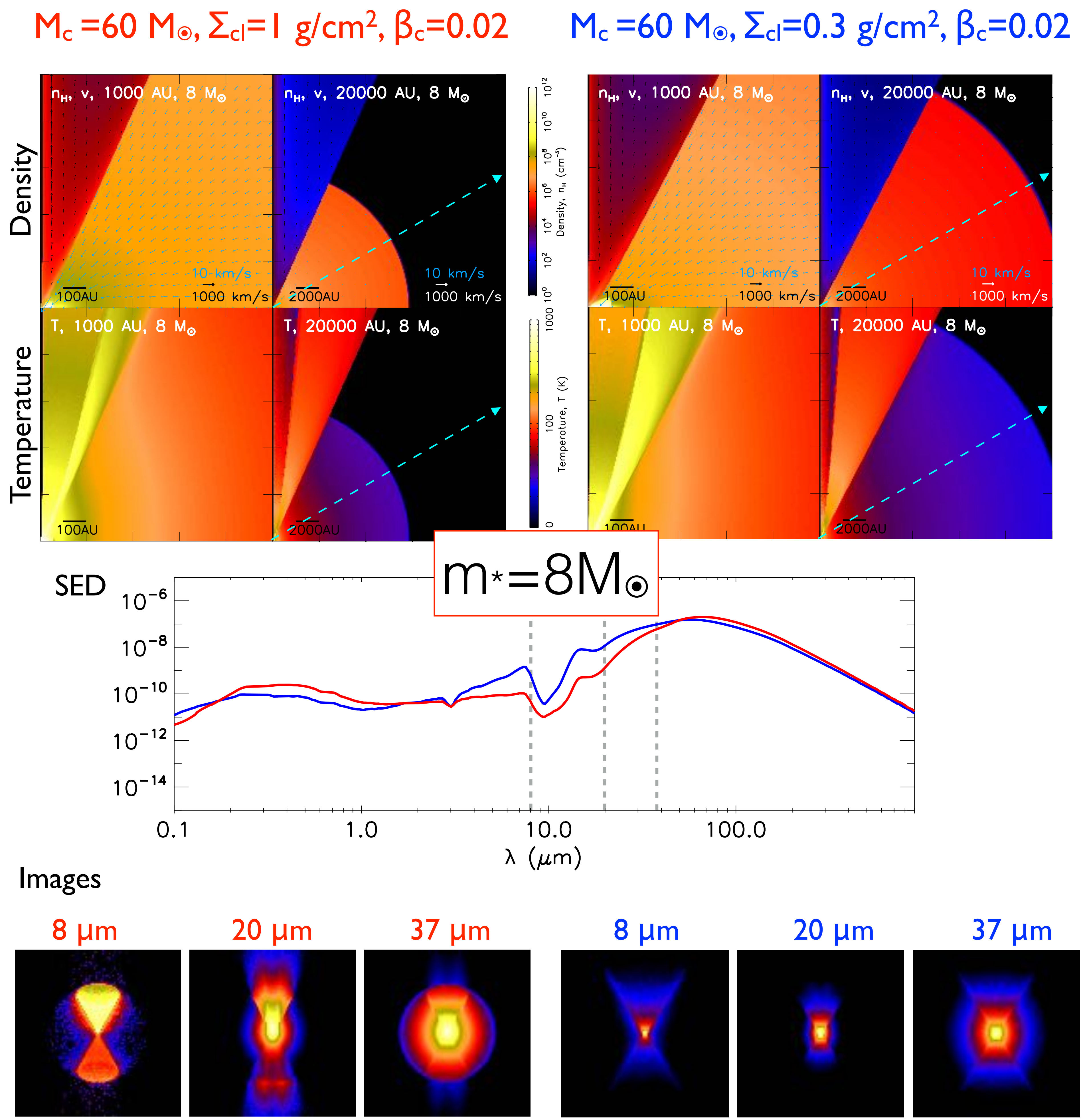

Initial & Environmental Conditions

Evolutionary Tracks

Density/velocity Profiles

Continuum Radiative Transfer

(Code: Whitney+ 03, 12; also see Robitaille+ 11)

Temperature Profiles

SEDs

IR Images

$M_c = 60\ M_\odot$, $\Sigma_{cl} = 1\ g/cm^2$, $\beta_c = 0.02$

$M_c = 60\ M_\odot$, $\Sigma_{cl} = 0.3\ g/cm^2$, $\beta_c = 0.02$

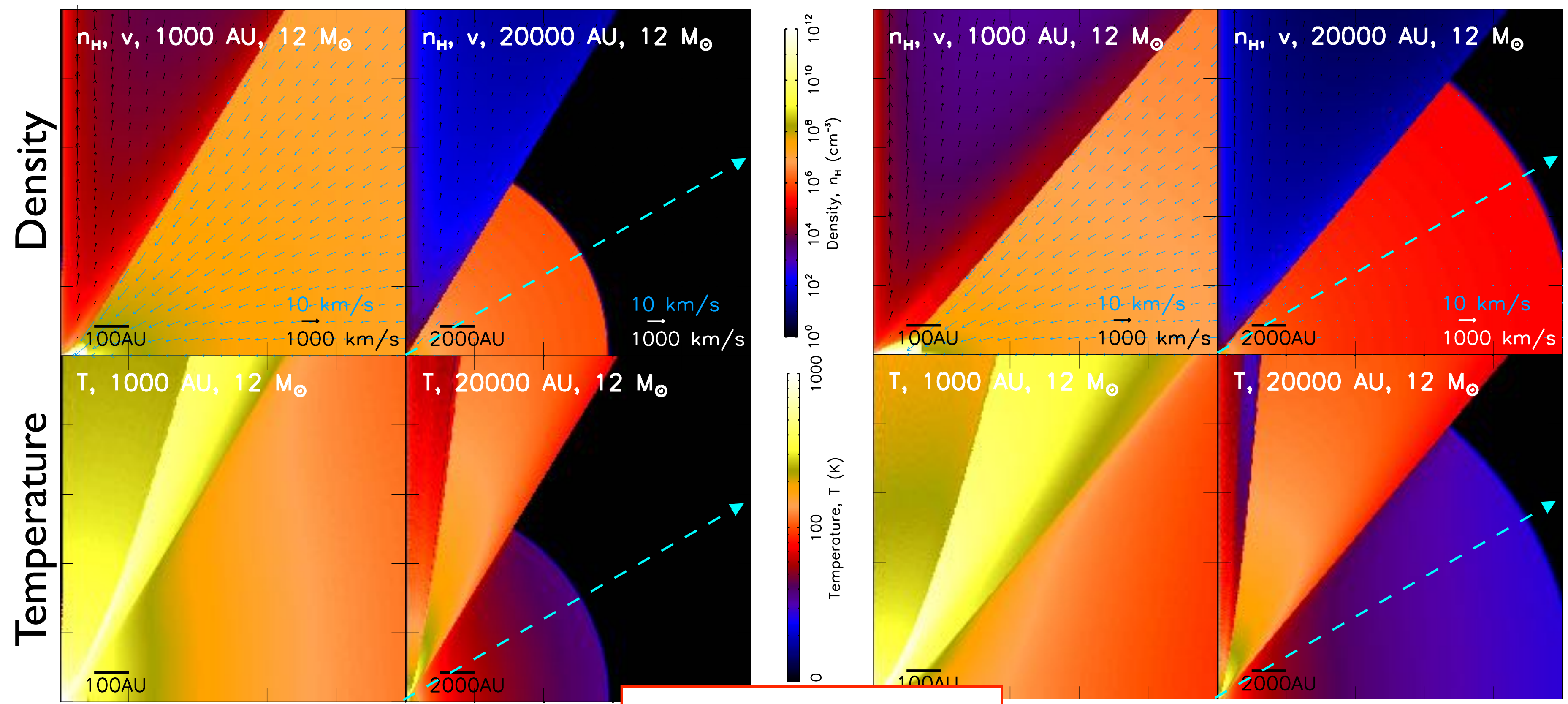


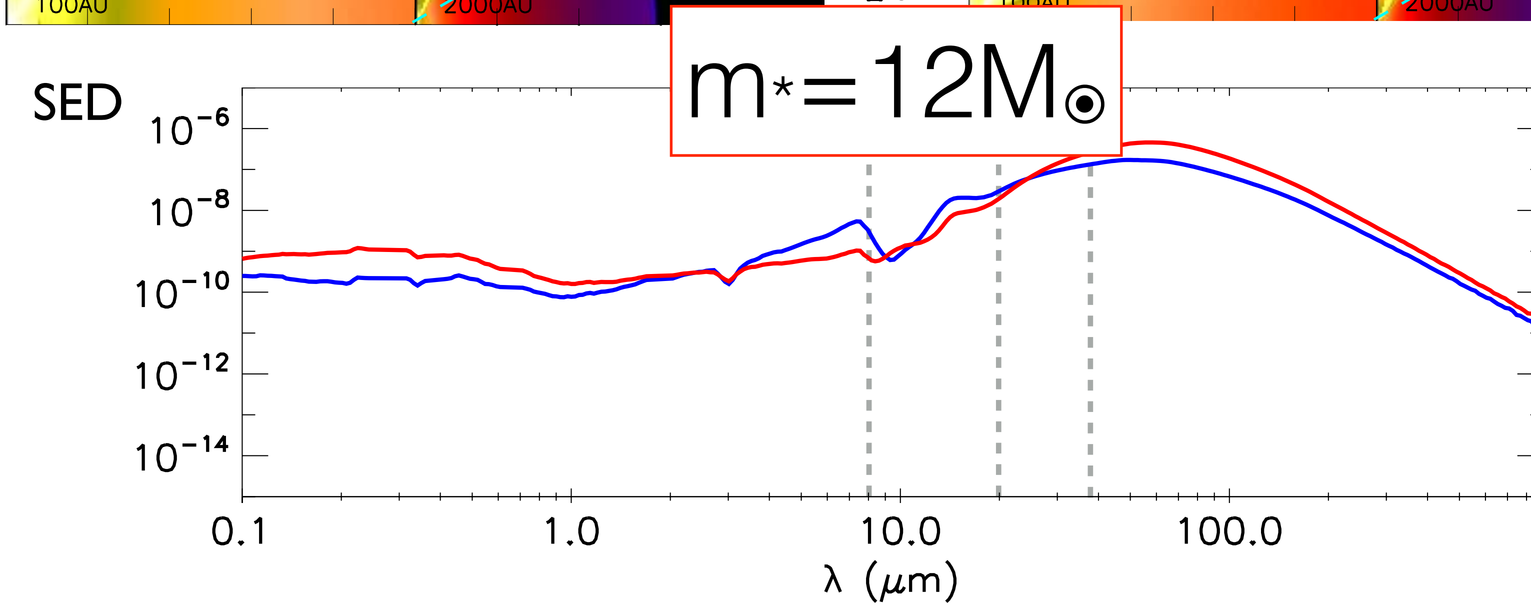


Images

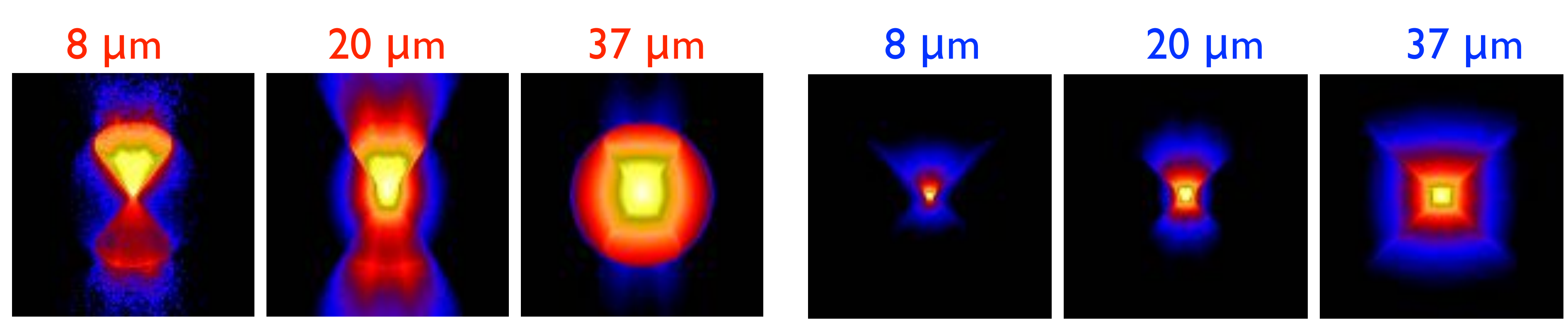

Initial & Environmental Conditions

↓

Evolutionary Tracks

↓

Density/velocity Profiles

↓

Continuum Radiative Transfer
(Code: Whitney+ 03, 12; also see Robitaille+ 11)

Temperature Profiles

SEDs

IR Images

$M_c = 60\ M_\odot$, $\Sigma_{cl} = 1\ g/cm^2$, $\beta_c = 0.02$ $M_c = 60\ M_\odot$, $\Sigma_{cl} = 0.3\ g/cm^2$, $\beta_c = 0.02$

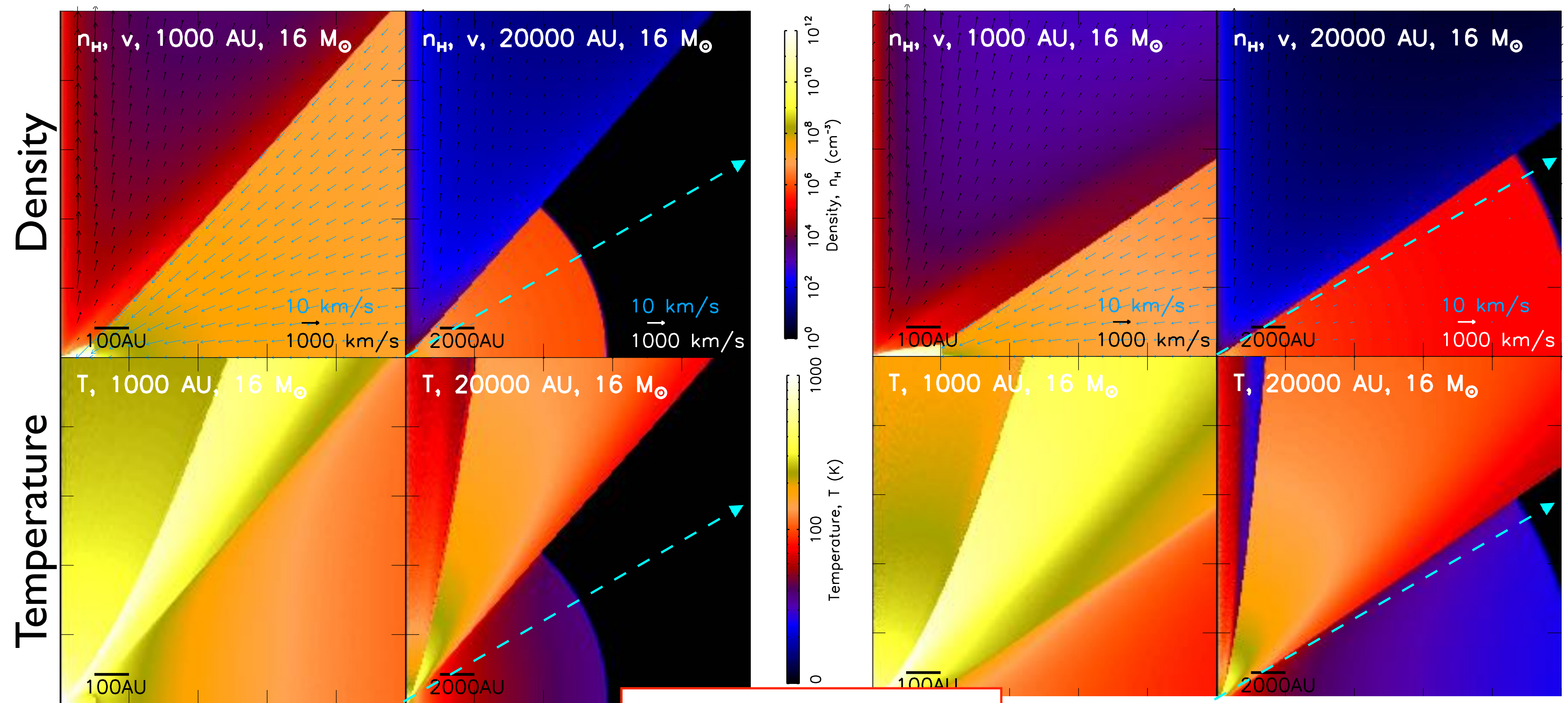


$m_* = 16 M_\odot$

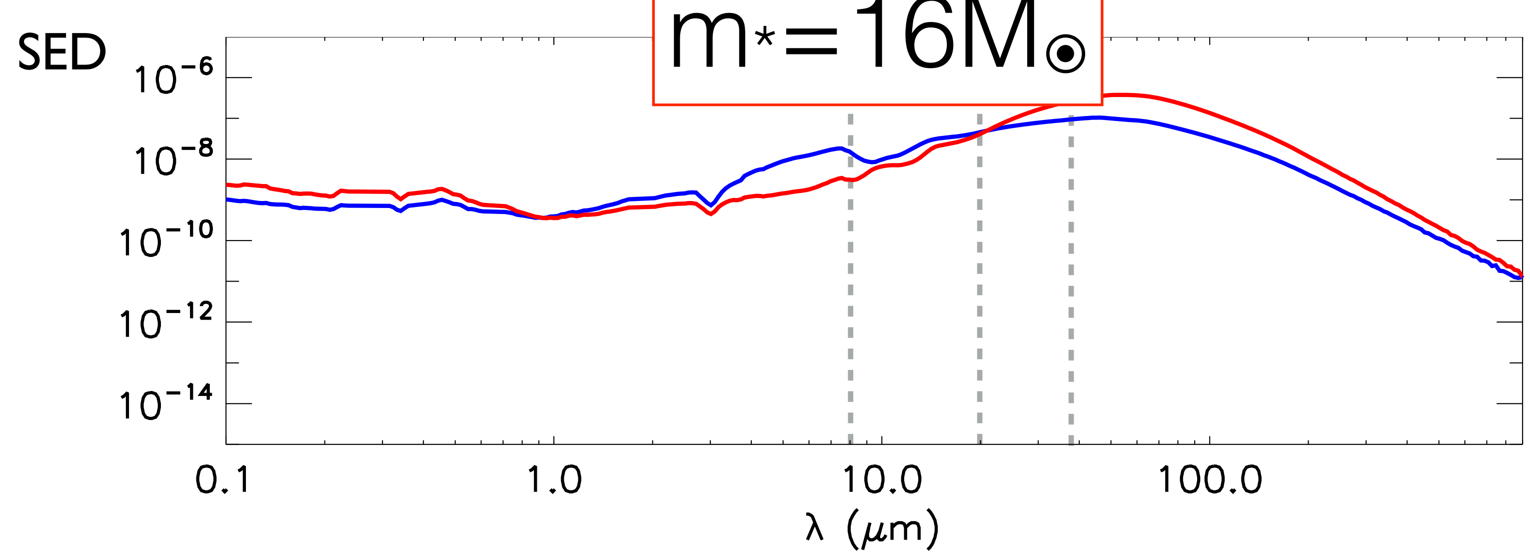


Images

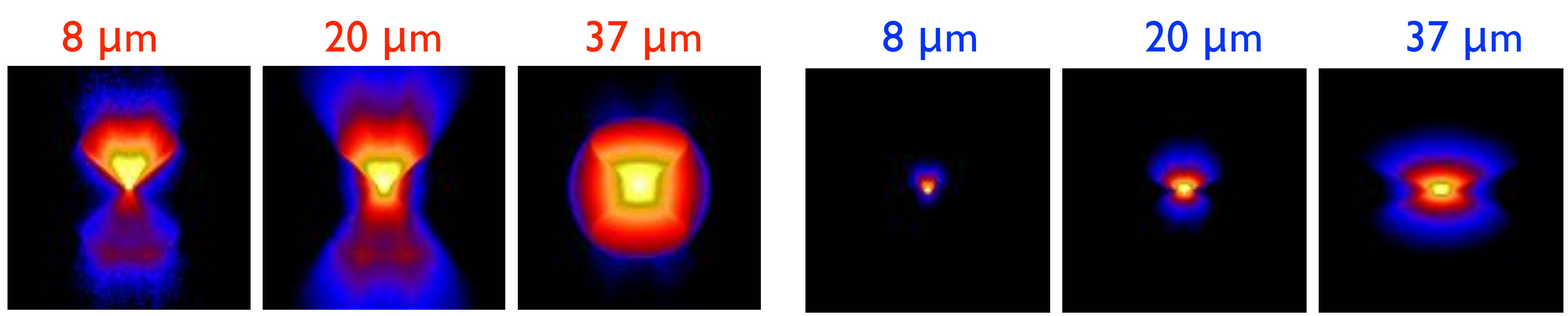

# Model grid

3+3 parameters:

$\Sigma_{cl}$, $M_c$, $m_{star}$, d, inc., $A_V$

Determine the evolutionary tracks

Determine how it is viewed

Determine the current stage

$\Sigma_{cl}$ : 0.1 ~ 3 g/cm² (4)

$M_c$ : 10 ~ 500 (15)

$m_{star}$: 0.5 ~ 160 (14)

SEDs: (8640) + (d, $A_V$)

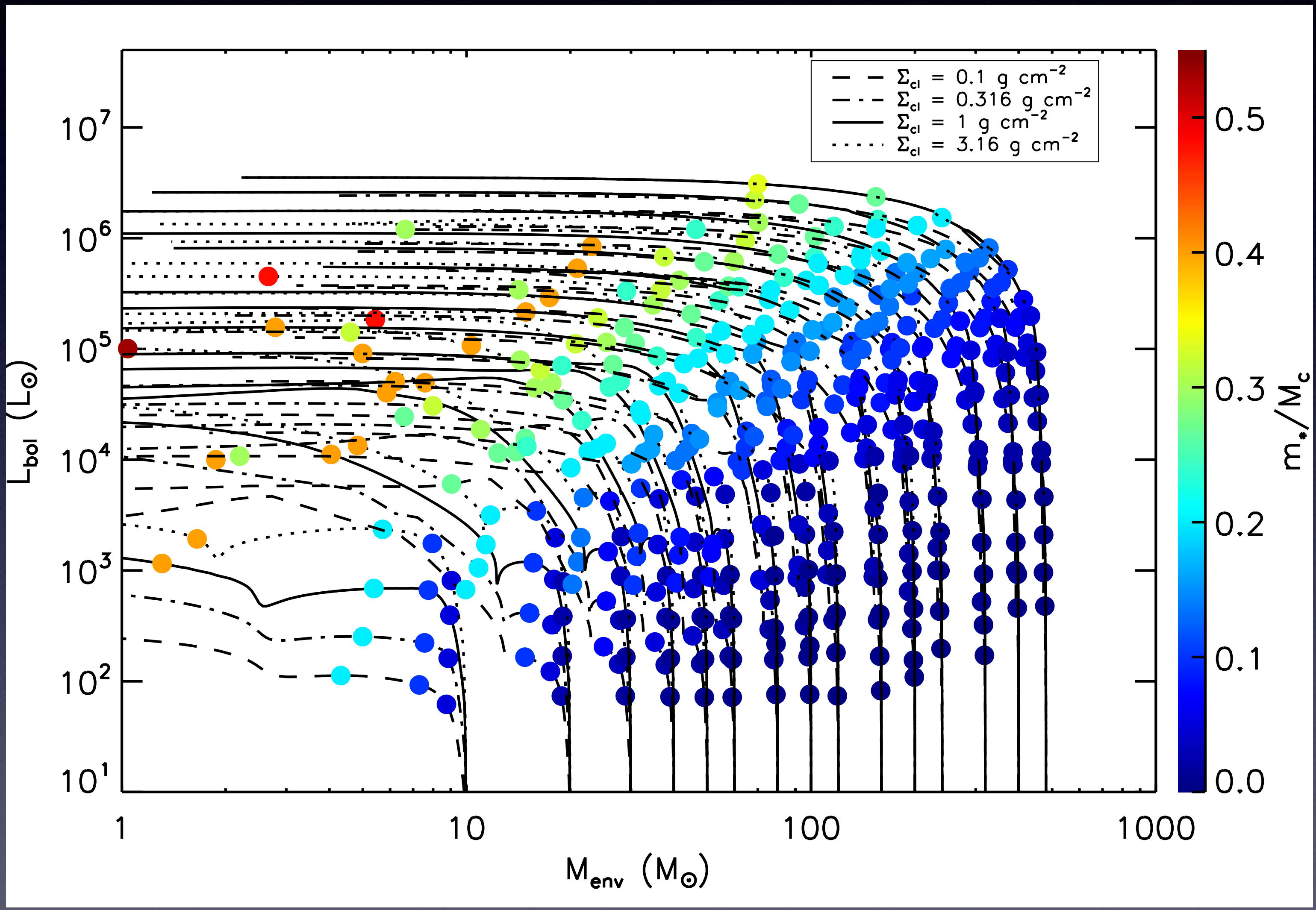

# The SOFIA Massive (SOMA) Star Formation Survey

**Jonathan C. Tan, James M. De Buizer, Mengyao Liu, Yichen Zhang, Jan E. Staff, Maria T. Beltrán, Ralph Shuping, Barbara Whitney**

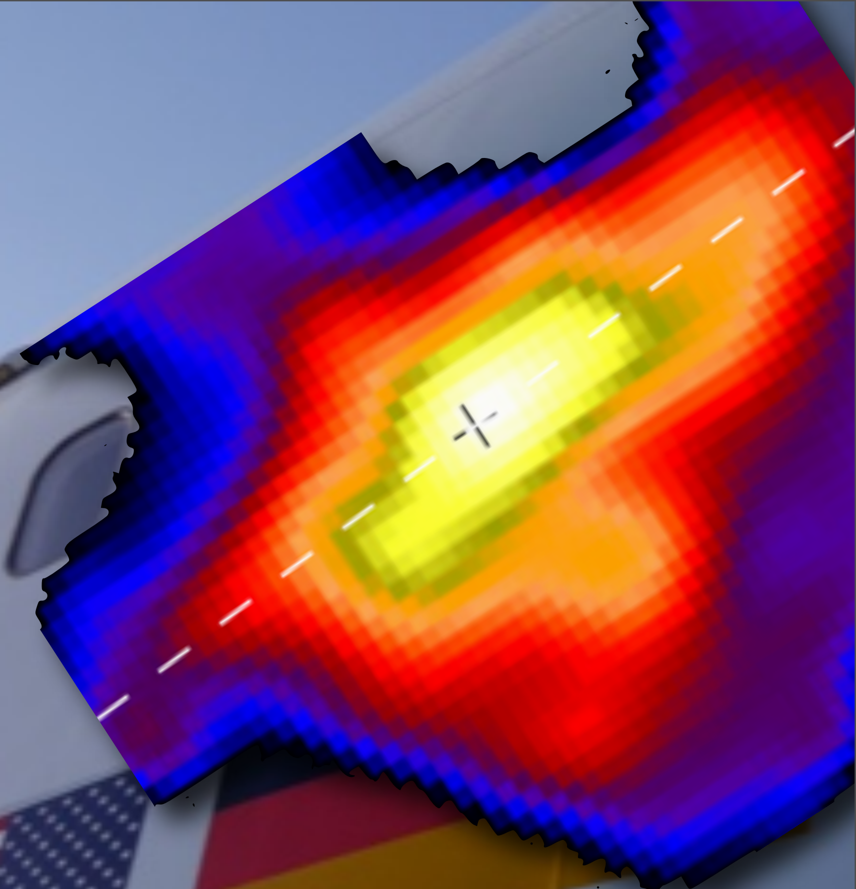

THE SOFIA MASSIVE (SOMA) STAR FORMATION SURVEY: I. OVERVIEW AND FIRST RESULTS

James M. De Buizer[1], Mengyao Liu[2], Jonathan C. Tan[2,3], Yichen Zhang[4,5], Maria T. Beltrán[6], Ralph Shuping[1], Jan E. Staff[2,7], Kei E. I. Tanaka[2], Barbara Whitney[8]

[1]SOFIA-USRA, NASA Ames Research Center, MS 232-12, Moffett Field, CA 94035, USA
[2]Department of Astronomy, University of Florida, Gainesville, FL 32611, USA
[3]Department of Physics, University of Florida, Gainesville, FL 32611, USA
[4]Departamento de Astronomía, Universidad de Chile, Casilla 36-D, Santiago, Chile
[5]The Institute of Physical and Chemical Research (RIKEN), Hirosawa 2-1, Wako-shi, Saitama 351-0198, Japan
[6]INAF-Osservatorio Astrofisico di Arcetri, Largo E. Fermi 5, I-50125 Firenze, Italy
[7]College of Science and Math, University of Virgin Islands, St. Thomas, United States Virgin Islands 00802
[8]Department of Astronomy, University of Wisconsin-Madison, 475 N. Charter St, Madison, WI 53706, USA



ABSTRACT

We present an overview and first results of the *SOFIA* Massive (SOMA) Star Formation Survey, which is using the FORCAST instrument to image massive protostars from $\sim$ 10–40 $\mu$m. These wavelengths trace thermal emission from warm dust, which in Core Accretion models mainly emerges from the inner regions of protostellar outflow cavities. Dust in dense core envelopes also imprints characteristic extinction patterns at these wavelengths causing intensity peaks to shift along the outflow axis and profiles to become more symmetric at longer wavelengths. We present observational results for the first eight protostars in the survey, i.e., multiwavelength images, including some ancillary ground-based MIR observations and archival *Spitzer* and *Herschel* data. These images generally show extended MIR/FIR emission along directions consistent with those of known outflows and with shorter wavelength peak flux positions displaced from the protostar along the blue-shifted, near-facing sides, thus confirming qualitative predictions of Core Accretion models. We then compile spectral energy distributions and use these to derive protostellar properties by fitting theoretical radiative transfer models. Zhang & Tan models, based on the Turbulent Core Model of McKee & Tan, imply the sources have protostellar masses $m_* \sim 10$–$50\,M_\odot$ accreting at $\sim 10^{-4}$–$10^{-3}\,M_\odot\,\mathrm{yr}^{-1}$ inside cores of initial masses $M_c \sim 30$–$500\,M_\odot$ embedded in clumps with mass surface densities $\Sigma_{cl} \sim 0.1$–$3\,\mathrm{g\,cm^{-2}}$. Fitting Robitaille et al. models typically leads to slightly higher protostellar masses, but with disk accretion rates $\sim 100\times$ smaller. We discuss reasons for these differences and overall implications of these first survey results for massive star formation theories.

*Keywords:* ISM: jets and outflows — dust — stars: formation — stars: winds, outflows — stars: early-type — infrared radiation — ISM: individual(AFGL 4029, AFGL 437, IRAS 07299-1651, G35.20-0.74, G45.45+0.05, IRAS 20126+4104, Cepheus A, NGC 7538 IRS9)

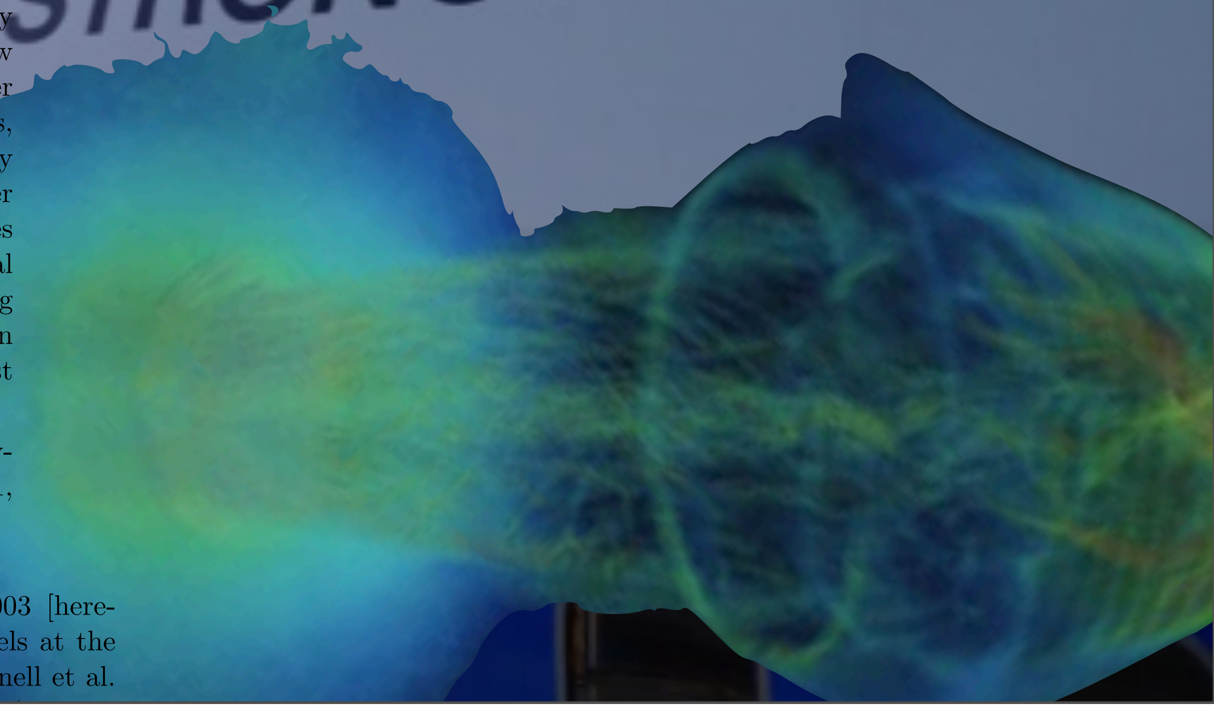

1. INTRODUCTION

The enormous radiative and mechanical luminosities of massive stars impact a vast range of scales and pro-

lent Core Model of McKee & Tan 2002; 2003 [hereafter MT03]), to Competitive Accretion models at the crowded centers of forming star clusters (Bonnell et al.

# The SOMA Survey

**SOFIA-FORCAST observations of a sample of ~50 massive & intermediate-mass protostars (Cycles 0, 1, 2, 3, 4).**

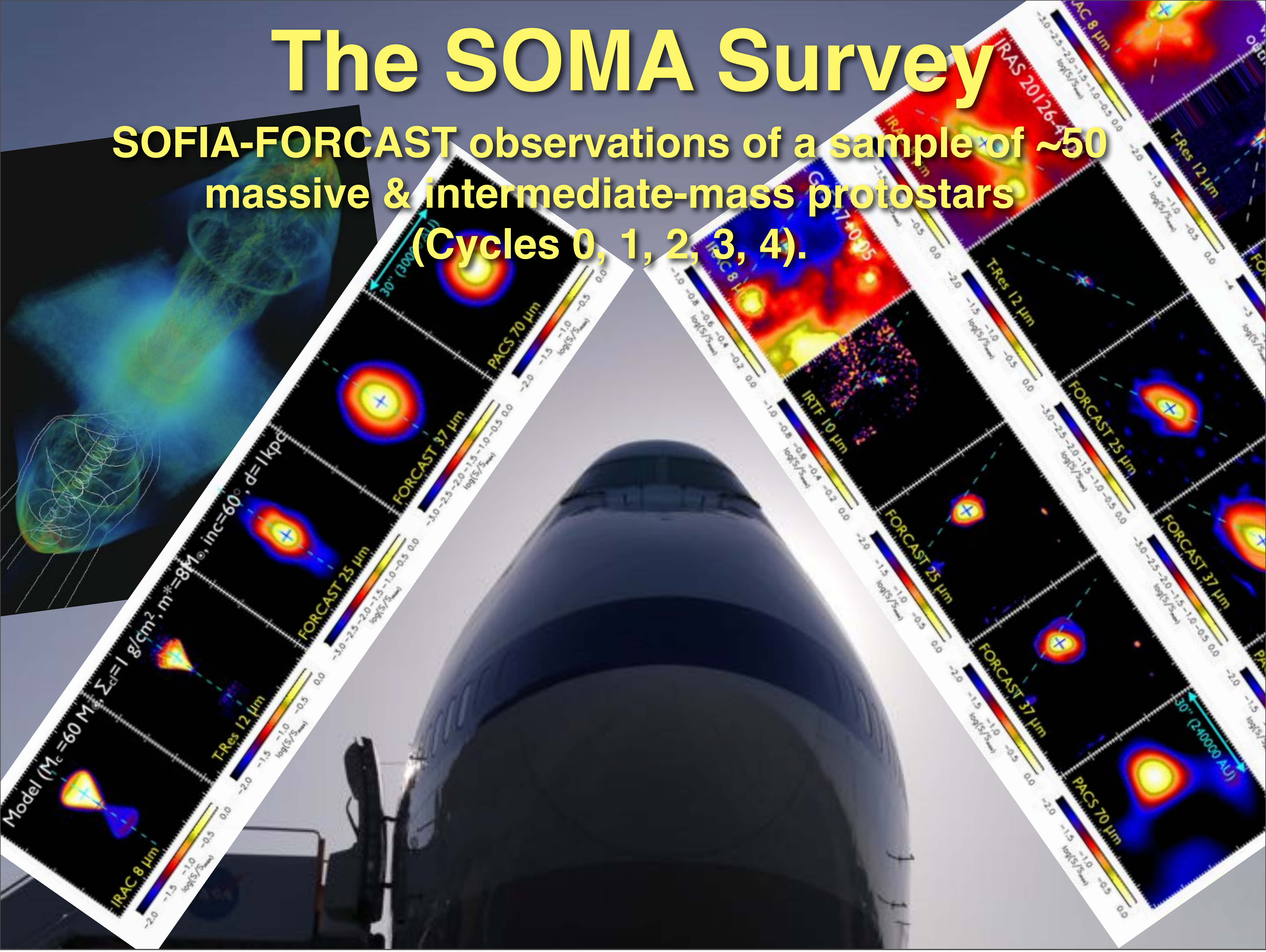

# The SOMA Survey

**SOFIA-FORCAST observations of a sample of ~50 massive & intermediate-mass protostars (Cycles 0, 1, 2, 3, 4).**

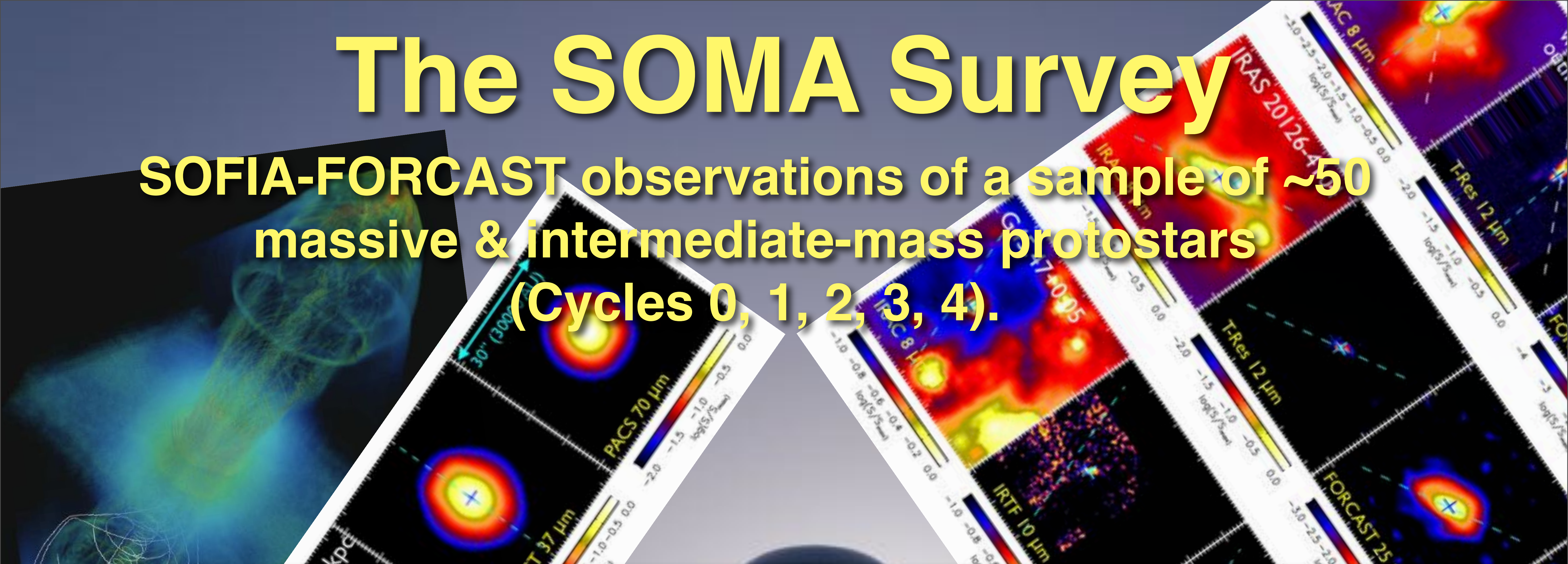


**Type I: MIR sources in IRDCs** - relatively isolated sources in Infrared Dark Clouds, some without detected radio
**Type II: Hyper-compact** - often jet-like, radio sources, where the MIR emission extends beyond the observed radio emission (e.g., G35.2)
**Type III: Ultra-compact** - radio sources where the radio emission is more extended than the MIR emission
**Type IV: Clustered sources** - a MIR source exhibiting radio emission is surrounded by several other MIR sources within ~60”

Also extended to **Intermediate-Mass protostars**.

# First 8 Sources

**Table 1**. *SOFIA* FORCAST Observations: Obs. Dates & Exposure Times (s)

| Source | R.A.(J2000) | Dec.(J2000) | d (kpc) | Obs. Date | 7.7 $\mu$m | 11.1 $\mu$m | 19.7 $\mu$m | 25.3 $\mu$m | 31.5 $\mu$m | 37.1 $\mu$m |
|---|---|---|---|---|---|---|---|---|---|---|
| AFGL 4029 | $03^h01^m31\overset{s}{.}28$ | $+60°29'12\overset{''}{.}87$ | 2.0 | 2014-03-29 | 112 | ... | 158 | ... | 282 | 678 |
| AFGL 437 | $03^h07^m24\overset{s}{.}55$ | $+58°30'52\overset{''}{.}76$ | 2.0 | 2014-06-11 | 217 | ... | 2075 | ... | 2000 | 884 |
| IRAS 07299-1651 | $07^h32^m09\overset{s}{.}74$ | $-16°58'11\overset{''}{.}28$ | 1.68 | 2015-02-06 | 280 | ... | 697 | ... | 449 | 1197 |
| G35.20-0.74 | $18^h58^m13\overset{s}{.}02$ | $+01°40'36\overset{''}{.}2$ | 2.2 | 2011-05-25 | ... | 909 | 959 | ... | 4068 | 4801 |
| G45.47+0.05 | $19^h14^m25\overset{s}{.}67$ | $+11°09'25\overset{''}{.}45$ | 8.4 | 2013-06-26 | ... | 309 | ... | 588 | 316 | 585 |
| IRAS 20126+4104 | $20^h14^m26\overset{s}{.}05$ | $+41°13'32\overset{''}{.}48$ | 1.64 | 2013-09-13 | ... | 484 | ... | 1276 | 487 | 1317 |
| Cepheus A | $22^h56^m17\overset{s}{.}98$ | $+62°01'49\overset{''}{.}39$ | 0.7 | 2014-03-25 | 242 | ... | 214 | ... | 214 | 1321 |
| NGC 7538 IRS9 | $23^h14^m01\overset{s}{.}77$ | $+61°27'19\overset{''}{.}8$ | 2.65 | 2014-06-06 | 215 | ... | 653 | ... | 491 | 923 |

De Buizer, Liu, Tan, Zhang et al. (2017)

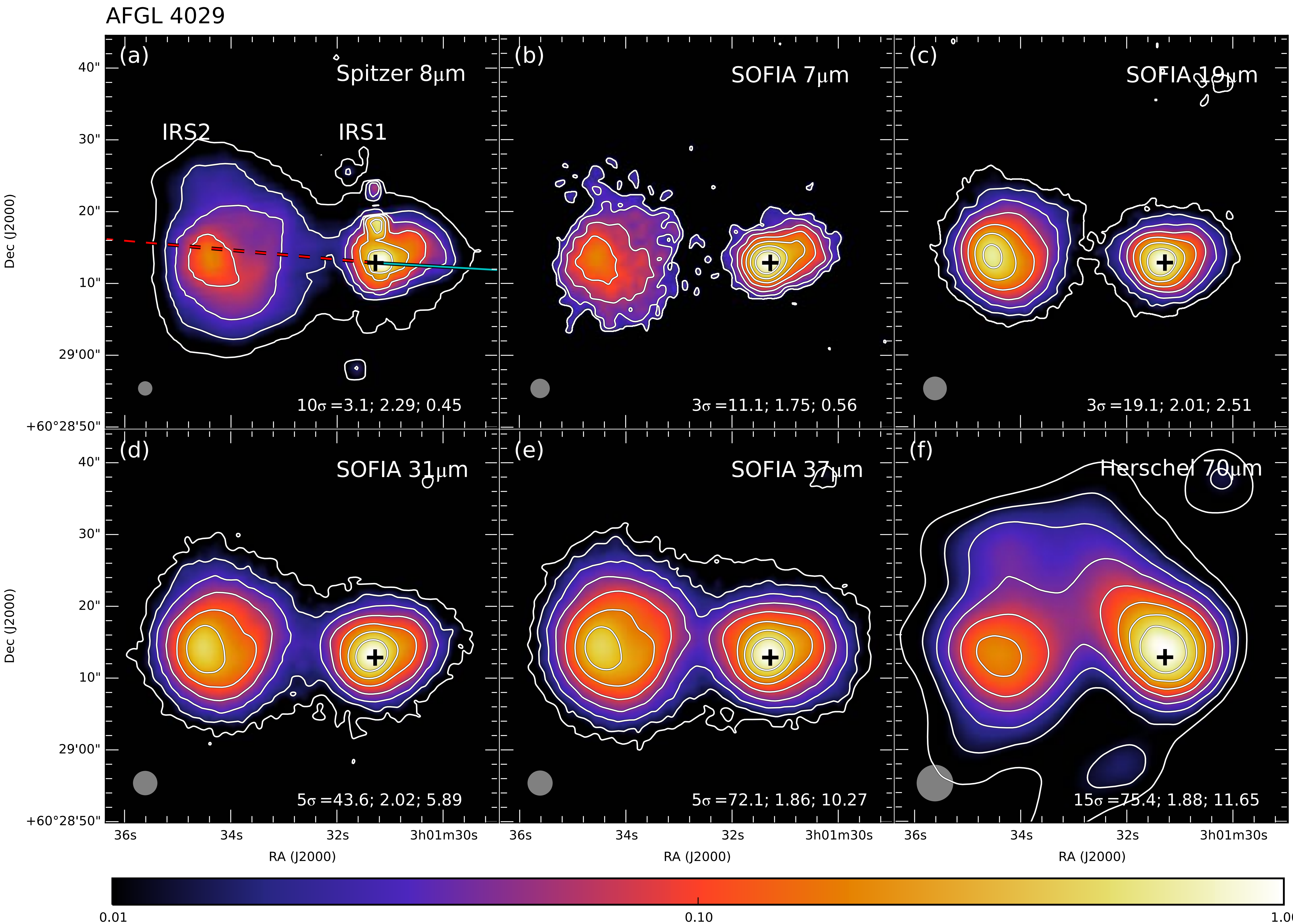

AFGL 4029
(a)
Spitzer 8μm
IRS2
IRS1
10σ =3.1; 2.29; 0.45
(b)
SOFIA 7μm
3σ =11.1; 1.75; 0.56
(c)
SOFIA 19μm
3σ =19.1; 2.01; 2.51
(d)
SOFIA 31μm
5σ =43.6; 2.02; 5.89
(e)
SOFIA 37μm
5σ =72.1; 1.86; 10.27
(f)
Herschel 70μm
15σ =75.4; 1.88; 11.65
Dec (J2000)
40"
30"
20"
10"
29'00"
+60°28'50"
RA (J2000)
36s
34s
32s
3h01m30s
0.01
0.10
1.00

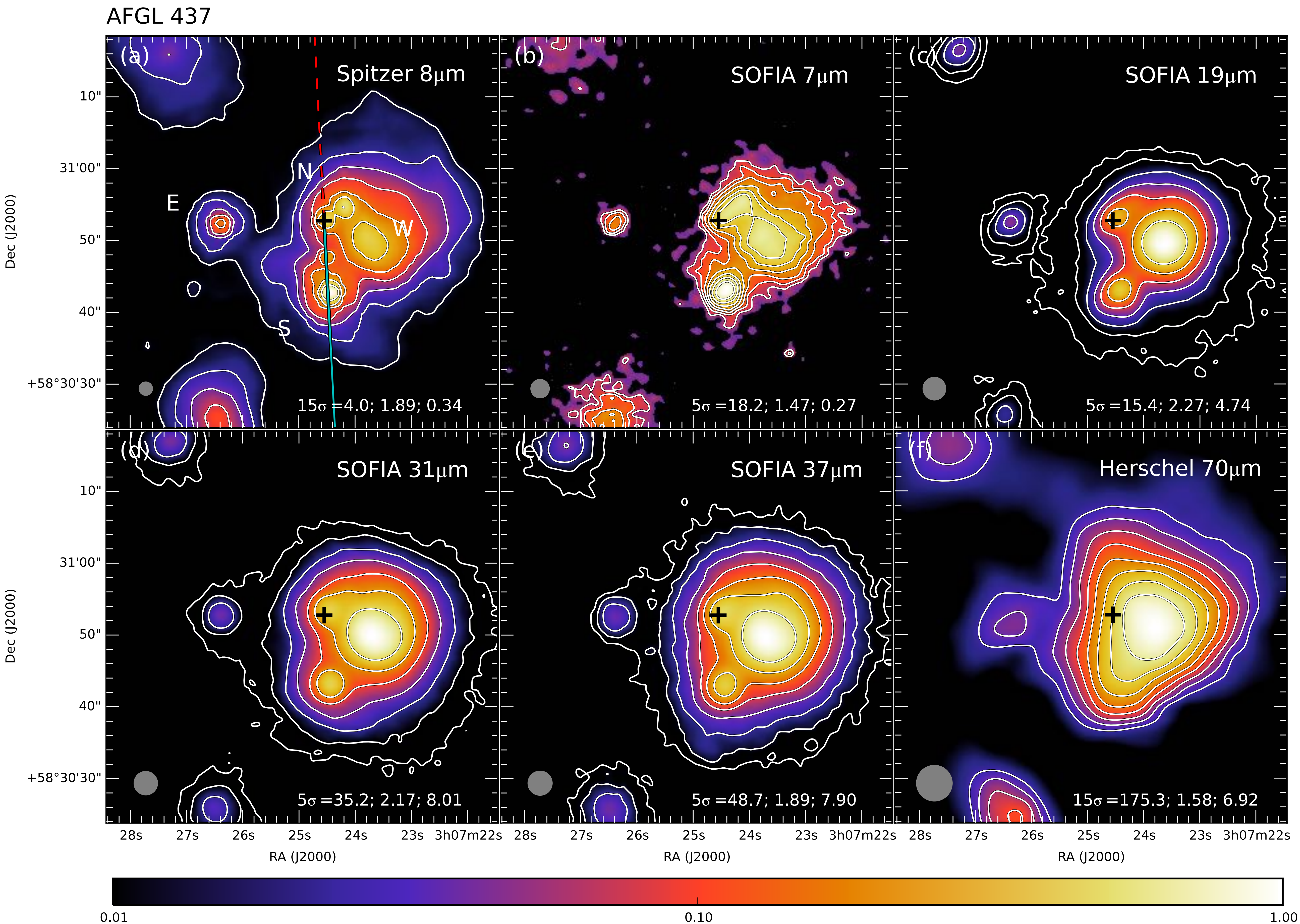
AFGL 437
(a)
Spitzer 8μm
N
E
W
S
15σ =4.0; 1.89; 0.34
(b)
SOFIA 7μm
5σ =18.2; 1.47; 0.27
(c)
SOFIA 19μm
5σ =15.4; 2.27; 4.74
(d)
SOFIA 31μm
5σ =35.2; 2.17; 8.01
(e)
SOFIA 37μm
5σ =48.7; 1.89; 7.90
(f)
Herschel 70μm
15σ =175.3; 1.58; 6.92
Dec (J2000)
10"
31'00"
50"
40"
+58°30'30"
RA (J2000)
28s
27s
26s
25s
24s
23s
3h07m22s
0.01
0.10
1.00

IRAS 07299-1651

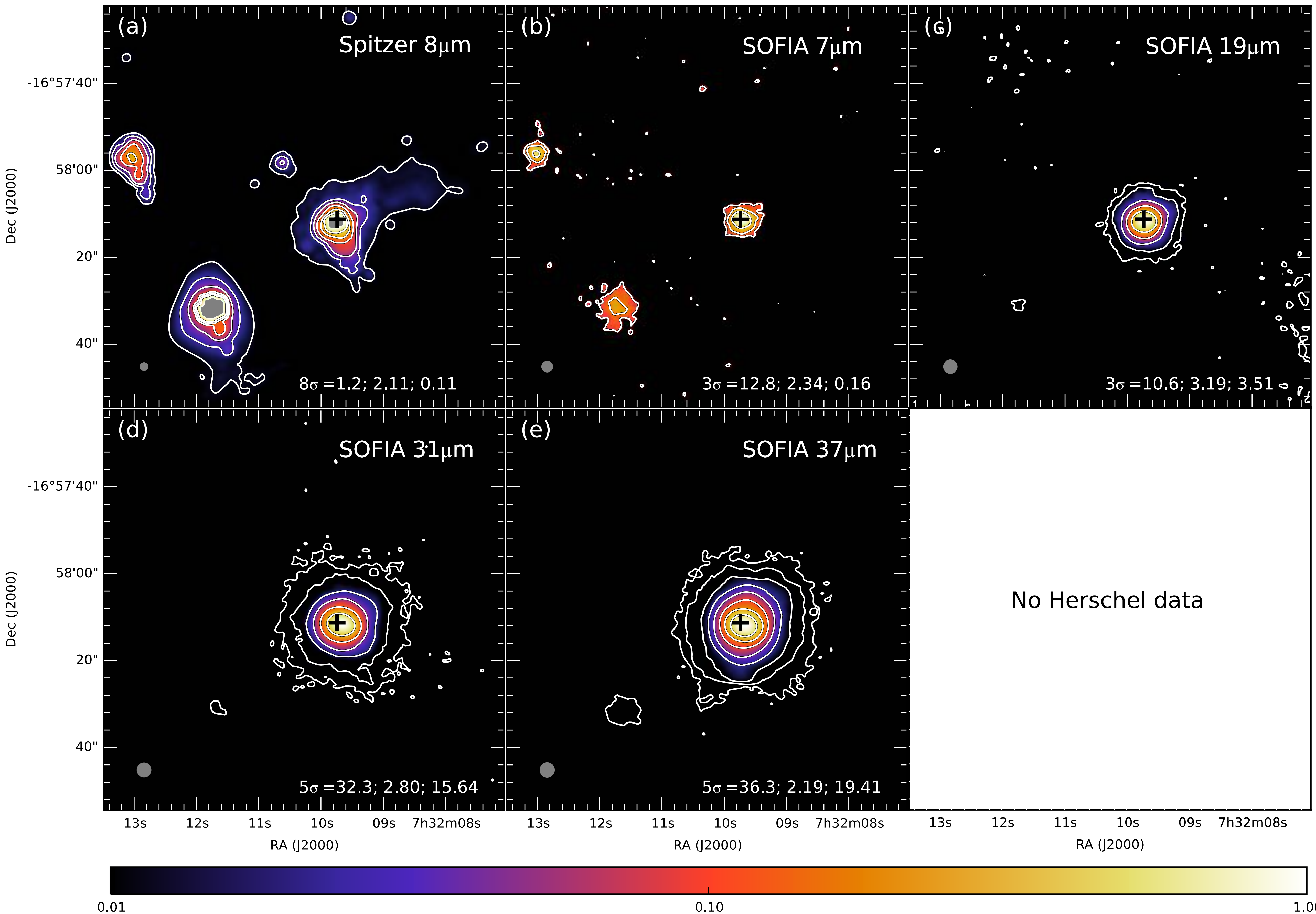

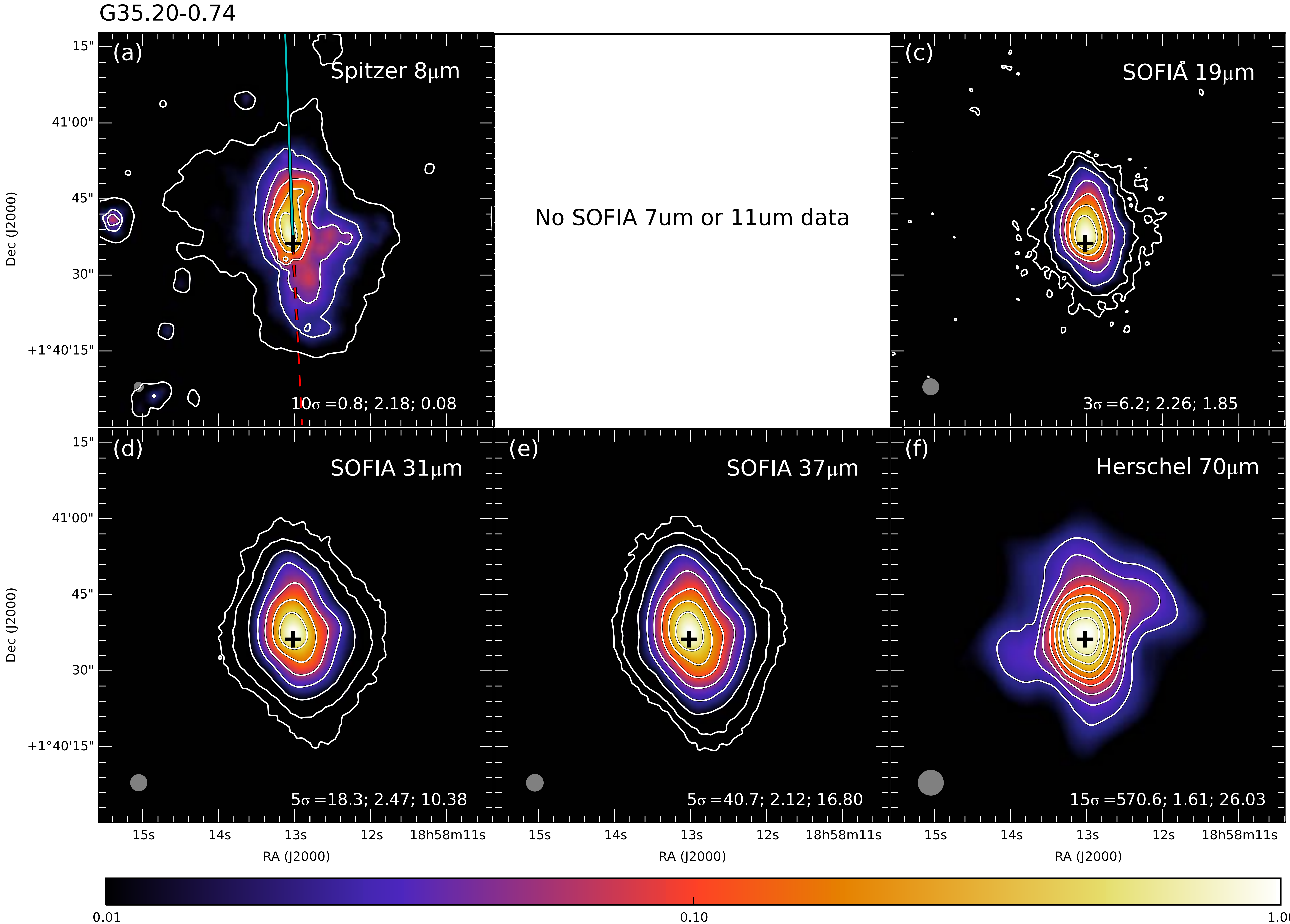

G35.20-0.74
(a)
Spitzer 8μm
10σ =0.8; 2.18; 0.08
No SOFIA 7um or 11um data
(c)
SOFIA 19μm
3σ =6.2; 2.26; 1.85
(d)
SOFIA 31μm
5σ =18.3; 2.47; 10.38
(e)
SOFIA 37μm
5σ =40.7; 2.12; 16.80
(f)
Herschel 70μm
15σ =570.6; 1.61; 26.03
Dec (J2000)
15"
41'00"
45"
30"
+1°40'15"
RA (J2000)
15s
14s
13s
12s
18h58m11s
0.01
0.10
1.00

G45.47+0.05

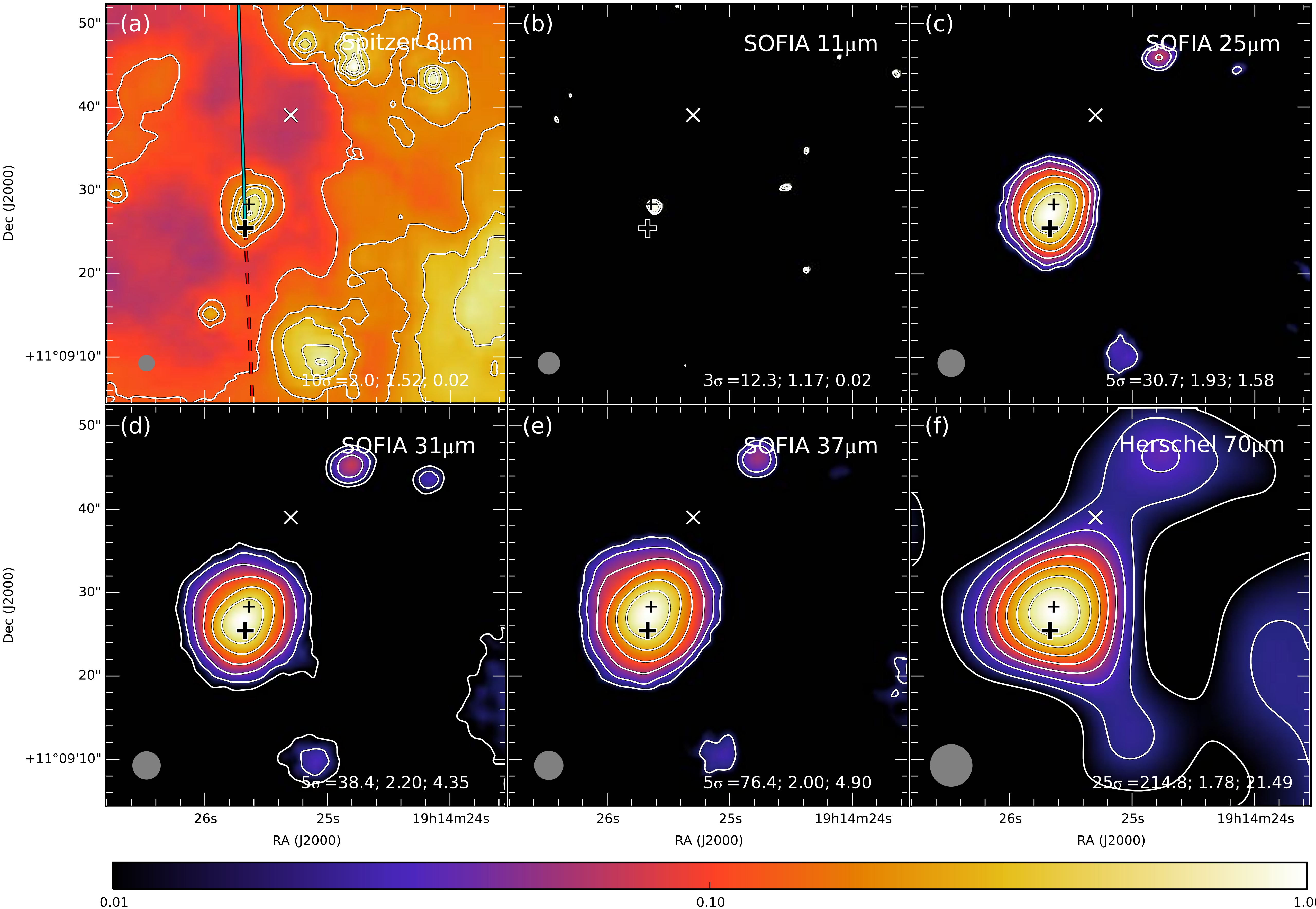

(a)
Spitzer 8μm
10σ =2.0; 1.52; 0.02
(b)
SOFIA 11μm
3σ =12.3; 1.17; 0.02
(c)
SOFIA 25μm
5σ =30.7; 1.93; 1.58
(d)
SOFIA 31μm
5σ =38.4; 2.20; 4.35
(e)
SOFIA 37μm
5σ =76.4; 2.00; 4.90
(f)
Herschel 70μm
25σ =214.8; 1.78; 21.49
50"
40"
30"
20"
+11°09'10"
Dec (J2000)
26s
25s
19h14m24s
RA (J2000)
0.01
0.10
1.00

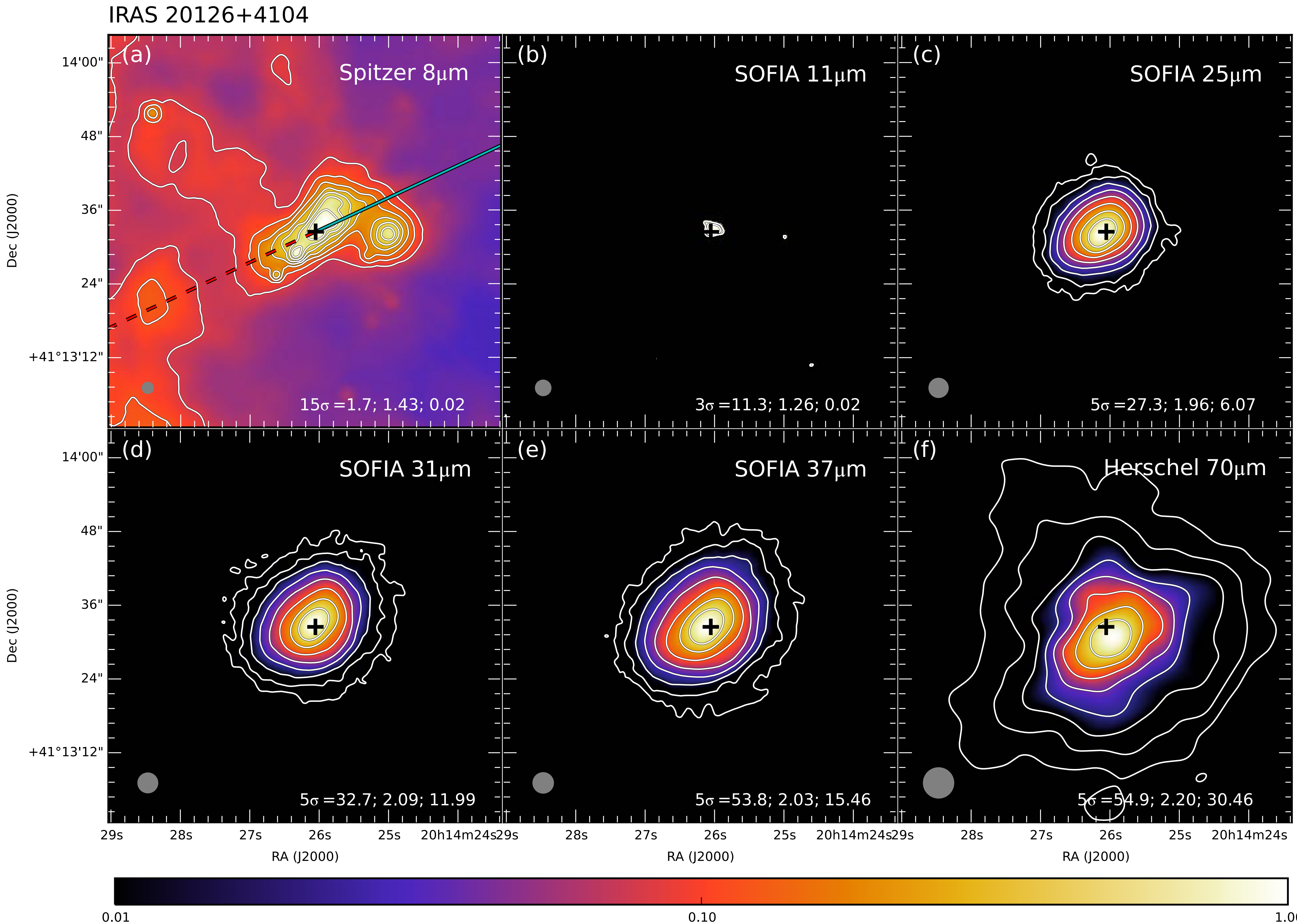
IRAS 20126+4104
(a)
Spitzer 8μm
15σ =1.7; 1.43; 0.02
(b)
SOFIA 11μm
3σ =11.3; 1.26; 0.02
(c)
SOFIA 25μm
5σ =27.3; 1.96; 6.07
(d)
SOFIA 31μm
5σ =32.7; 2.09; 11.99
(e)
SOFIA 37μm
5σ =53.8; 2.03; 15.46
(f)
Herschel 70μm
5σ =54.9; 2.20; 30.46
Dec (J2000)
14'00"
48"
36"
24"
+41°13'12"
RA (J2000)
29s
28s
27s
26s
25s
20h14m24s
0.01
0.10
1.00

Cepheus A

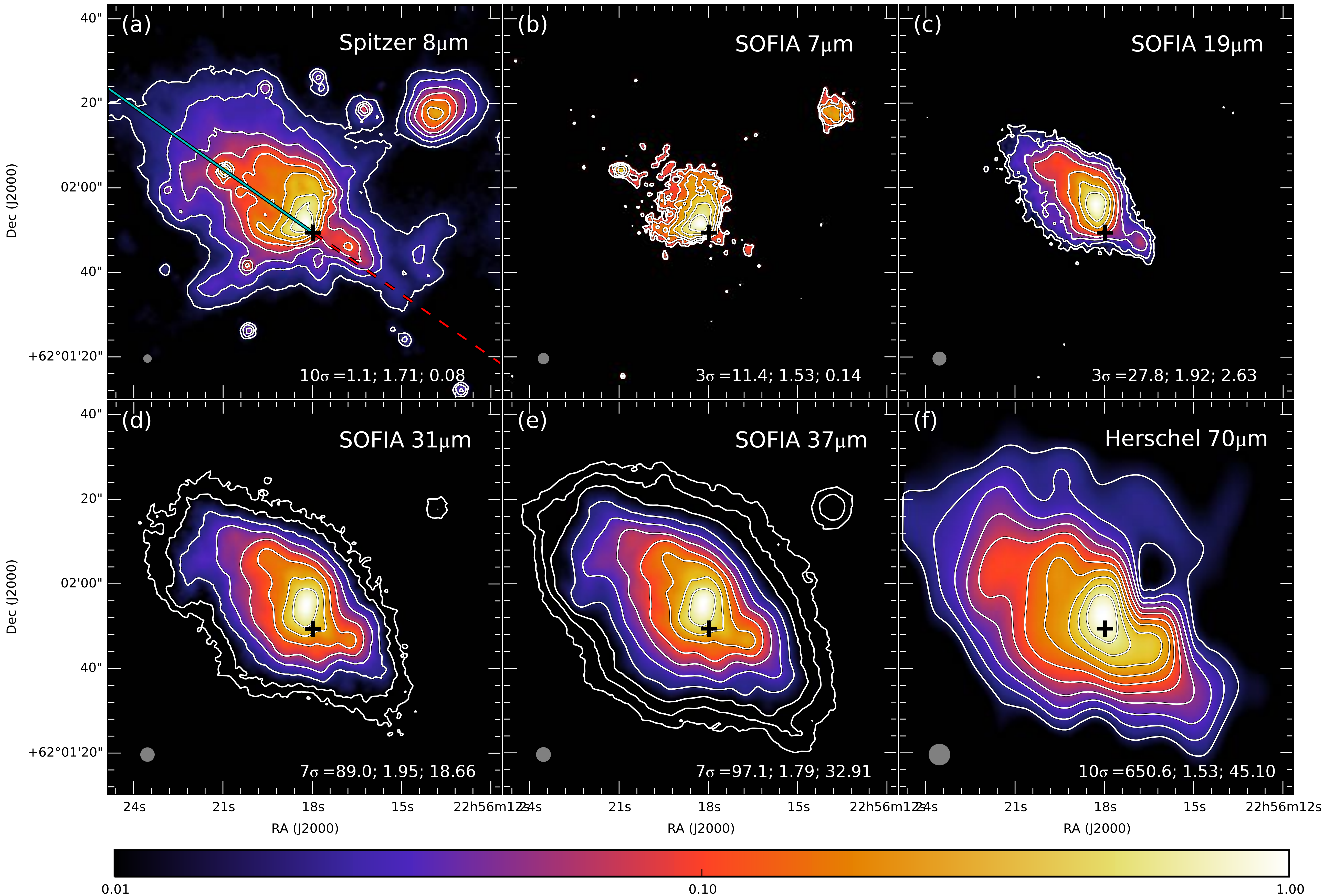
(a)
Spitzer 8μm
10σ =1.1; 1.71; 0.08
(b)
SOFIA 7μm
3σ =11.4; 1.53; 0.14
(c)
SOFIA 19μm
3σ =27.8; 1.92; 2.63
(d)
SOFIA 31μm
7σ =89.0; 1.95; 18.66
(e)
SOFIA 37μm
7σ =97.1; 1.79; 32.91
(f)
Herschel 70μm
10σ =650.6; 1.53; 45.10
40"
20"
02'00"
40"
+62°01'20"
Dec (J2000)
24s
21s
18s
15s
22h56m12s
RA (J2000)
0.01
0.10
1.00

NGC 7538 IRS9

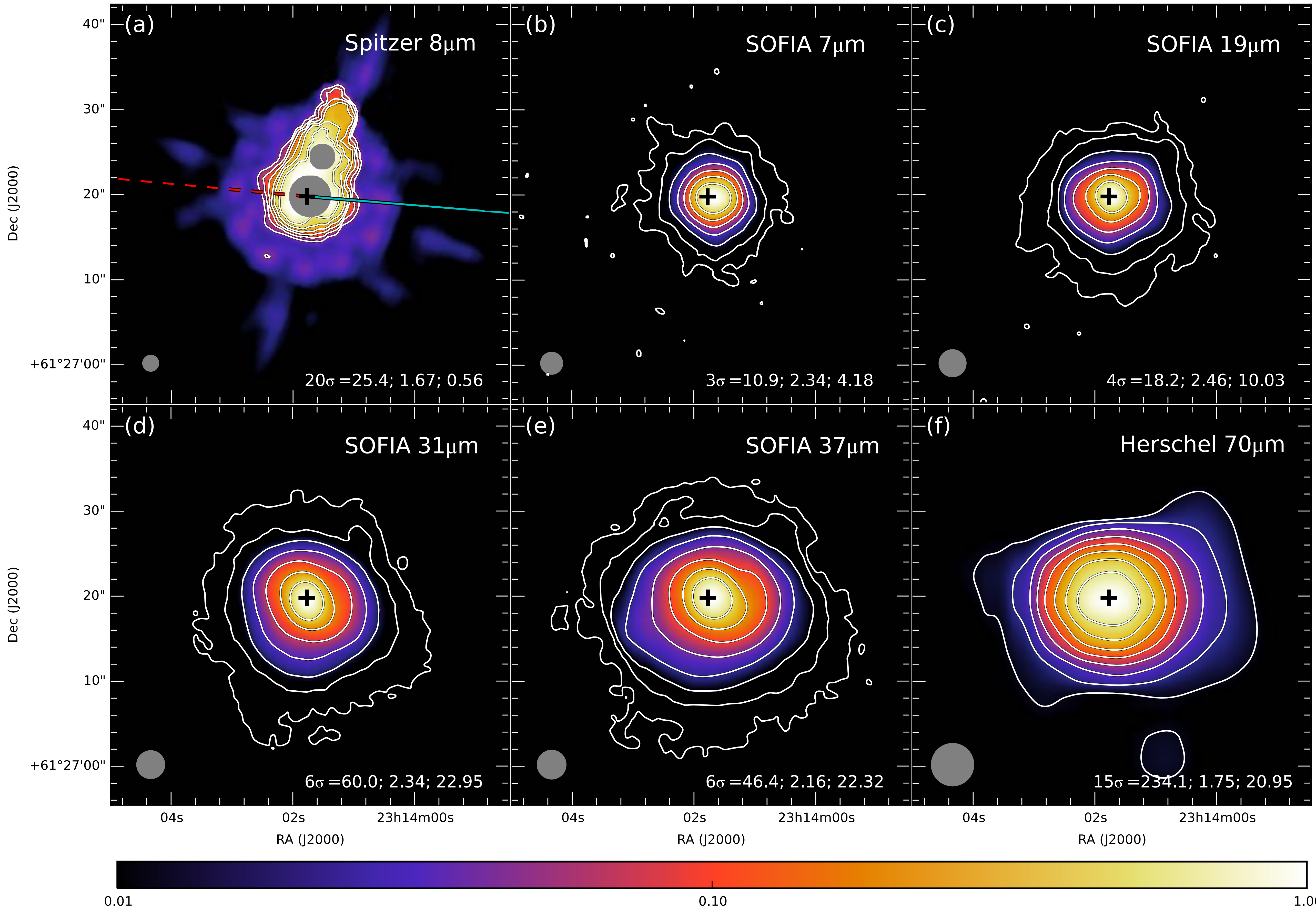

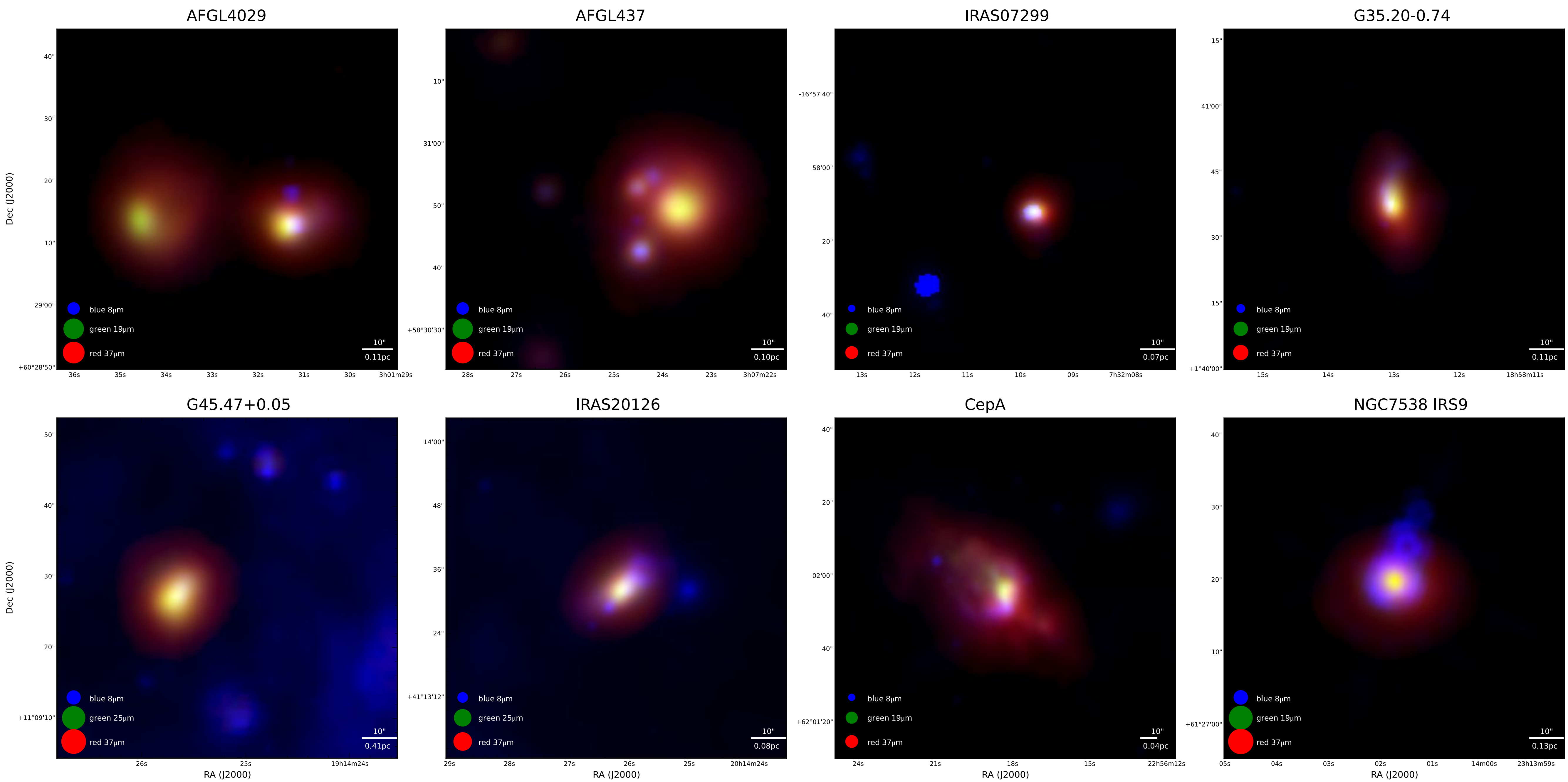

AFGL4029
blue 8μm
green 19μm
red 37μm
10"
0.11pc
AFGL437
blue 8μm
green 19μm
red 37μm
10"
0.10pc
IRAS07299
blue 8μm
green 19μm
red 37μm
10"
0.07pc
G35.20-0.74
blue 8μm
green 19μm
red 37μm
10"
0.11pc
G45.47+0.05
blue 8μm
green 25μm
red 37μm
10"
0.41pc
IRAS20126
blue 8μm
green 25μm
red 37μm
10"
0.08pc
CepA
blue 8μm
green 19μm
red 37μm
10"
0.04pc
NGC7538 IRS9
blue 8μm
green 19μm
red 37μm
10"
0.13pc
Dec (J2000)
RA (J2000)

# SEDs

effect of aperture definition:

fixed

variable

effect of clump envelope subtraction:

total (core+clump)

core (total-clump)

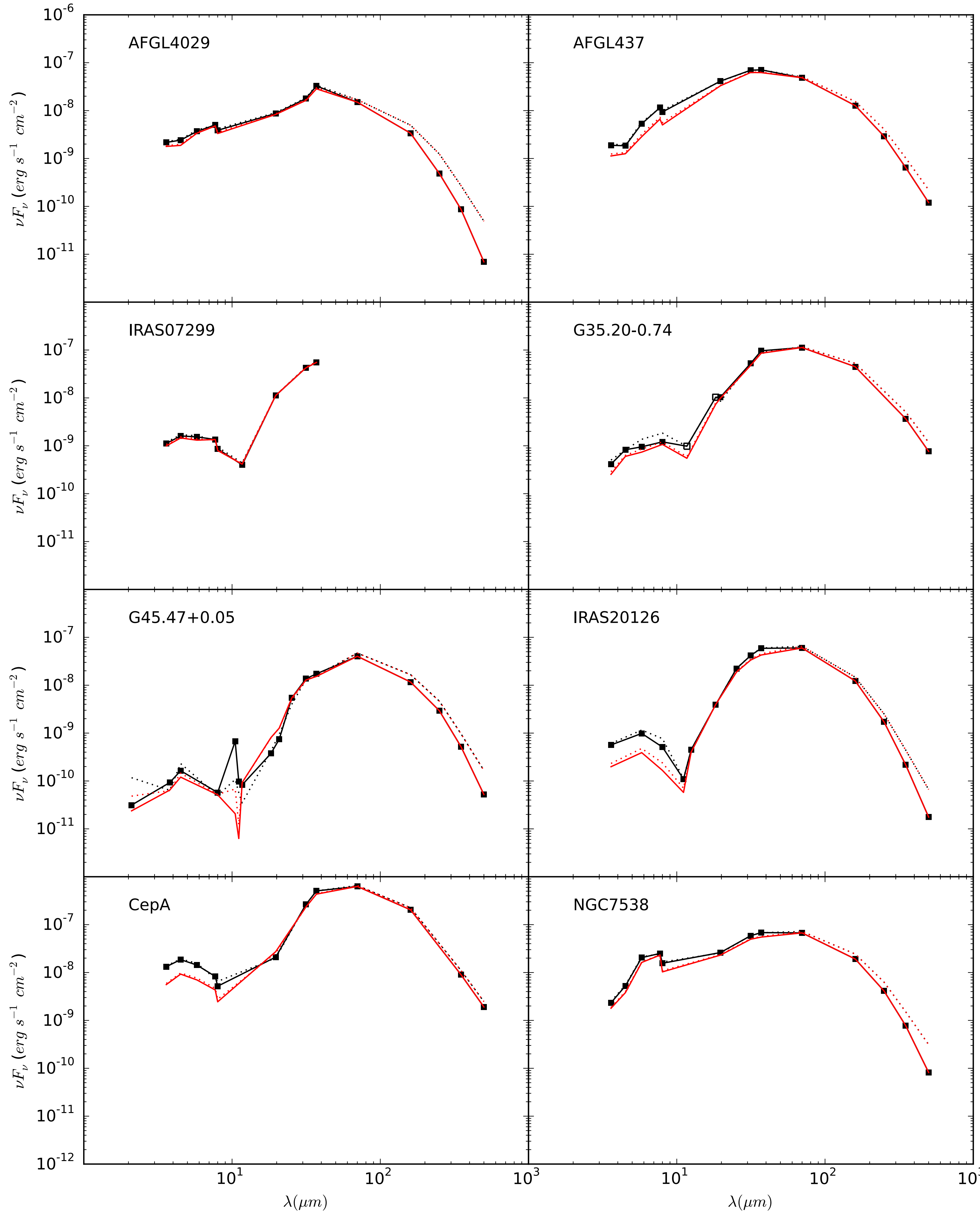

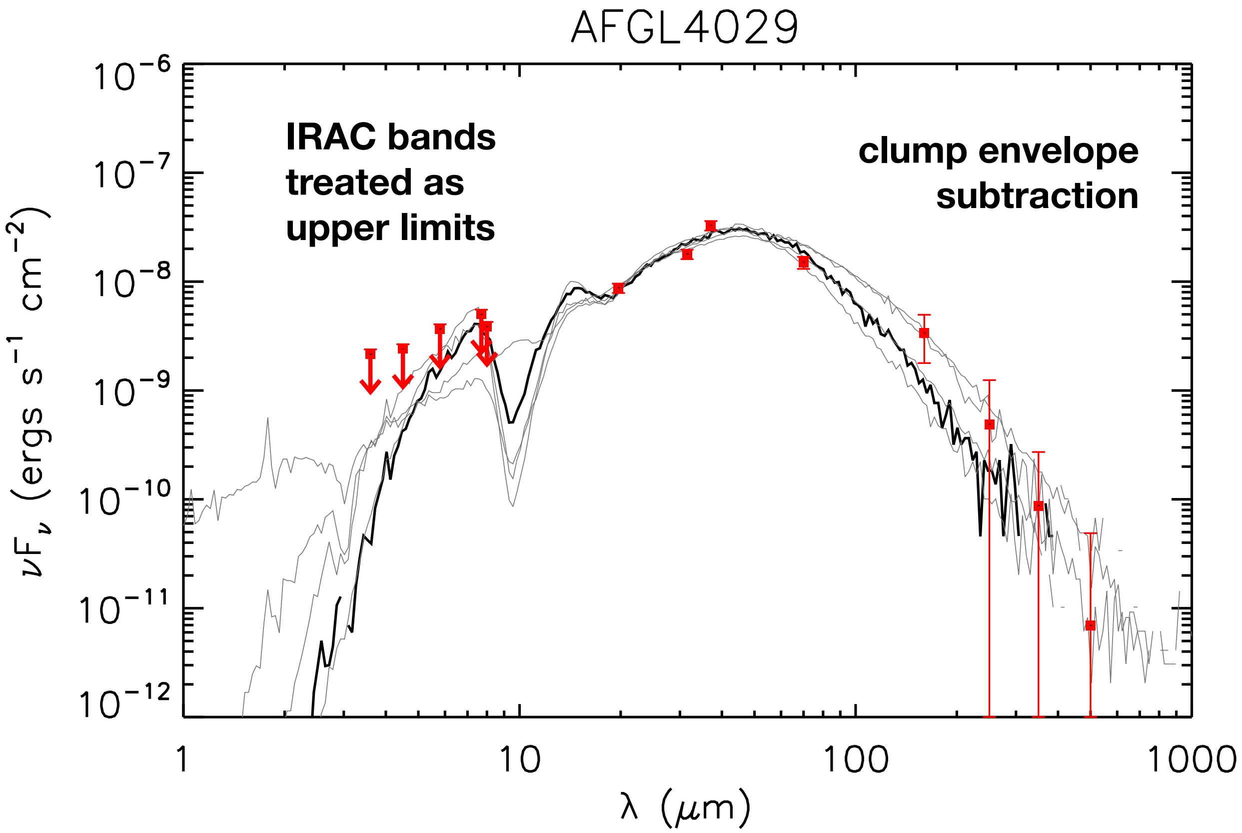


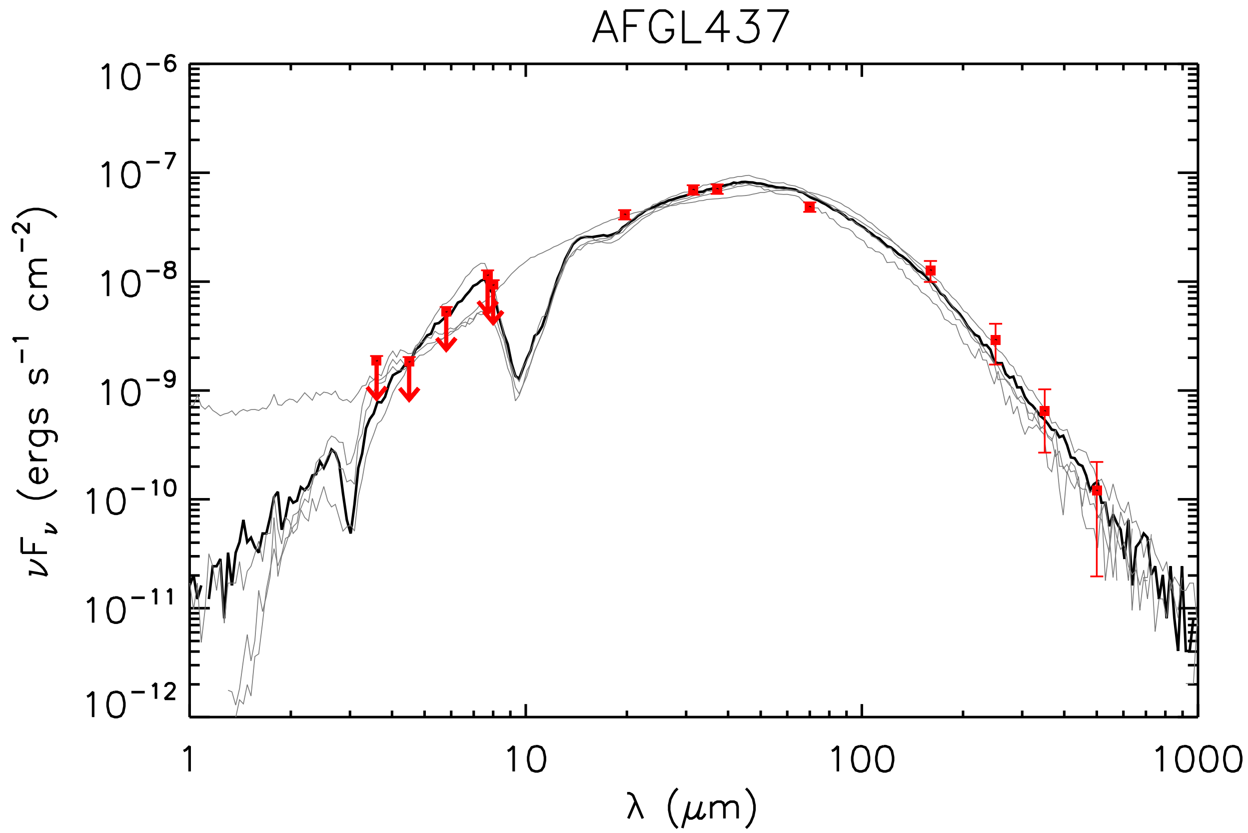


| Source | Zhang & Tan models | | | | | | | | | | |
|---|---|---|---|---|---|---|---|---|---|---|---|
| | $\chi^2$ | $M_c$ $(M_\odot)$ | $\Sigma_{\rm cl}$ (g cm$^{-2}$) | $R_c$ (pc) ($''$) | $m_*$ $(M_\odot)$ | $\theta_{\rm view}$ ($^\circ$) | $A_V$ (mag) | $M_{\rm env}$ $(M_\odot)$ | $\theta_{w,\rm esc}$ ($^\circ$) | $\dot{M}_{\rm disk}$ $(M_\odot/{\rm yr})$ | $L_{\rm bol}$ $(L_\odot)$ |
| AFGL4029 | 1.00 | 100 | 3.2 | 0.04 (4) | 48 | 89 | 64.6 | 2.6 | 71 | 7.1(-4) | 4.6(5) |
| $d$ = 2.2 kpc | 1.15 | 30 | 1.0 | 0.04 (4) | 12 | 62 | 0.0 | 5.7 | 53 | 1.9(-4) | 4.1(4) |
| $R_{\rm ap} = 11.2''$ | 1.28 | 30 | 3.2 | 0.02 (2) | 16 | 65 | 94.9 | 1.0 | 56 | 5.1(-4) | 1.0(5) |
| | 1.34 | 200 | 0.1 | 0.33 (31) | 48 | 89 | 64.6 | 29 | 74 | 5.7(-5) | 3.3(5) |
| | 1.44 | 100 | 0.1 | 0.23 (22) | 16 | 89 | 17.2 | 53 | 45 | 6.2(-5) | 3.0(4) |
| AFGL437 | 0.91 | 160 | 0.1 | 0.29 (30) | 16 | 58 | 0.0 | 116 | 32 | 8.1(-5) | 3.3(4) |
| $d$ = 2.0 kpc | 1.48 | 160 | 0.1 | 0.29 (30) | 24 | 86 | 15.2 | 87 | 45 | 8.5(-5) | 7.8(4) |
| $R_{\rm ap} = 32.0''$ | 1.55 | 50 | 3.2 | 0.03 (3) | 8 | 29 | 0.0 | 35 | 25 | 6.0(-4) | 1.7(4) |
| | 2.02 | 160 | 0.1 | 0.29 (30) | 32 | 89 | 23.2 | 55 | 59 | 7.6(-5) | 1.5(5) |
| | 2.22 | 200 | 0.1 | 0.33 (34) | 12 | 34 | 0.0 | 174 | 20 | 8.0(-5) | 2.0(4) |

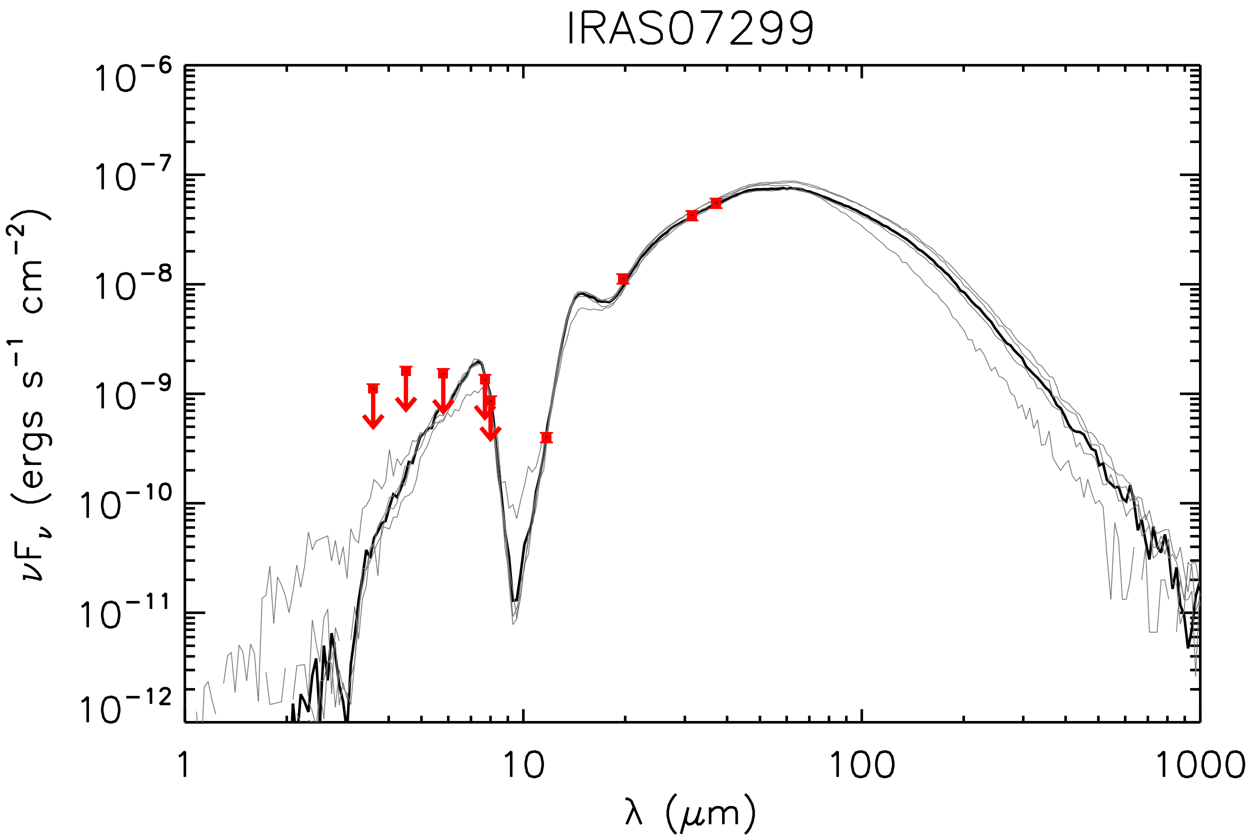


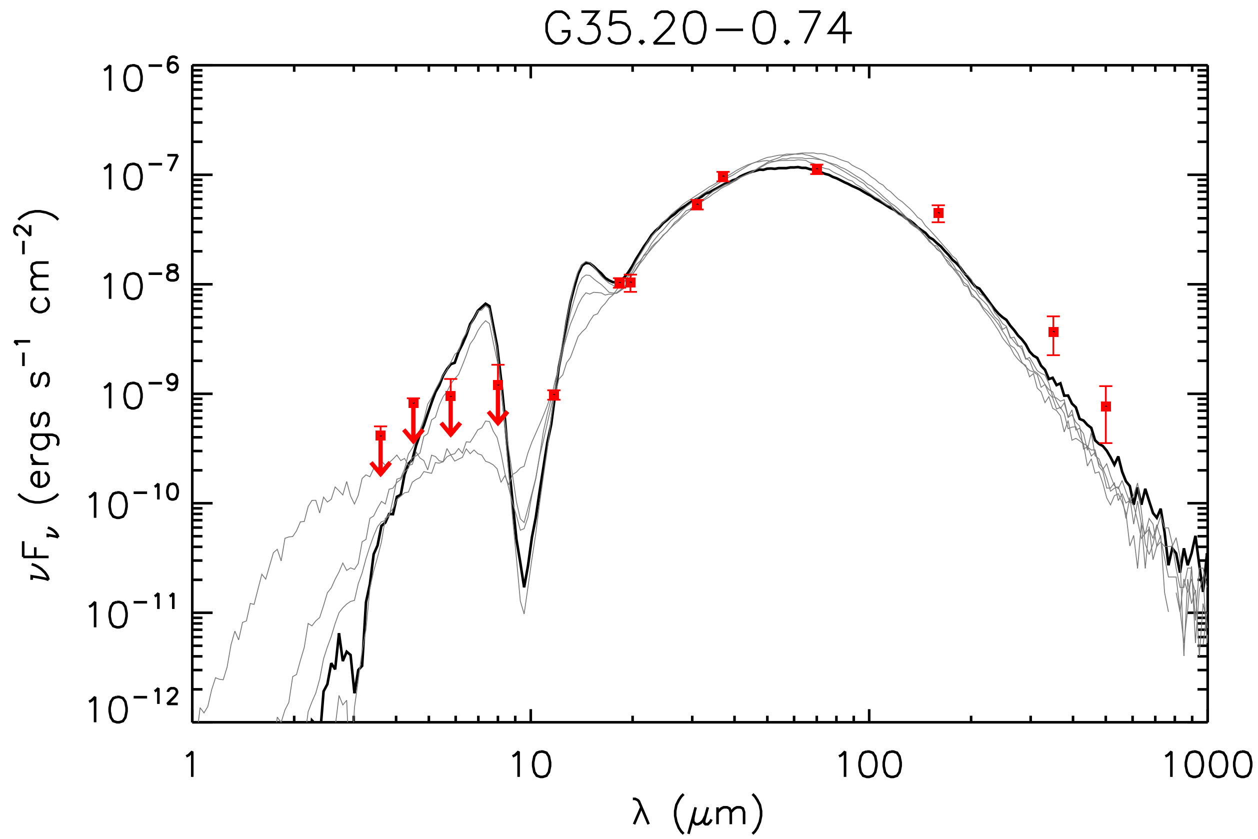


| | Zhang & Tan models | | | | | | | | | | |
|---|---|---|---|---|---|---|---|---|---|---|---|
| Source | $\chi^2$ | $M_c$ ($M_\odot$) | $\Sigma_{\rm cl}$ (g cm$^{-2}$) | $R_c$ (pc) ($''$) | $m_*$ ($M_\odot$) | $\theta_{\rm view}$ ($^\circ$) | $A_V$ (mag) | $M_{\rm env}$ ($M_\odot$) | $\theta_{w,\rm esc}$ ($^\circ$) | $\dot{M}_{\rm disk}$ ($M_\odot$/yr) | $L_{\rm bol}$ ($L_\odot$) |
| IRAS07299 | 0.22 | 200 | 0.1 | 0.33 (48) | 8 | 89 | 20.2 | 181 | 14 | 6.8(-5) | 9.5(3) |
| $d$ = 1.4 kpc | 0.23 | 320 | 0.1 | 0.42 (61) | 8 | 83 | 3.0 | 307 | 11 | 7.7(-5) | 8.8(3) |
| $R_{\rm ap} = 7.7''$ | 0.32 | 240 | 0.1 | 0.36 (53) | 8 | 86 | 22.2 | 226 | 13 | 7.1(-5) | 1.1(4) |
| | 0.59 | 60 | 0.3 | 0.10 (15) | 12 | 77 | 9.1 | 32 | 40 | 1.2(-4) | 2.7(4) |
| | 0.67 | 160 | 0.1 | 0.29 (43) | 8 | 89 | 33.3 | 143 | 17 | 6.3(-5) | 1.1(4) |
| G35.20-0.74 | 2.63 | 480 | 0.1 | 0.51 (48) | 16 | 48 | 40.4 | 440 | 15 | 1.2(-4) | 3.8(4) |
| $d$ = 2.2 kpc | 2.64 | 100 | 3.2 | 0.04 (4) | 12 | 29 | 70.7 | 77 | 20 | 9.4(-4) | 5.2(4) |
| $R_{\rm ap} = 32.0''$ | 2.76 | 320 | 0.1 | 0.42 (39) | 24 | 68 | 81.8 | 256 | 27 | 1.2(-4) | 8.4(4) |
| | 2.76 | 80 | 3.2 | 0.04 (3) | 12 | 39 | 15.2 | 58 | 22 | 8.4(-4) | 5.0(4) |
| | 2.77 | 200 | 0.3 | 0.19 (17) | 12 | 22 | 43.4 | 173 | 17 | 1.9(-4) | 4.0(4) |

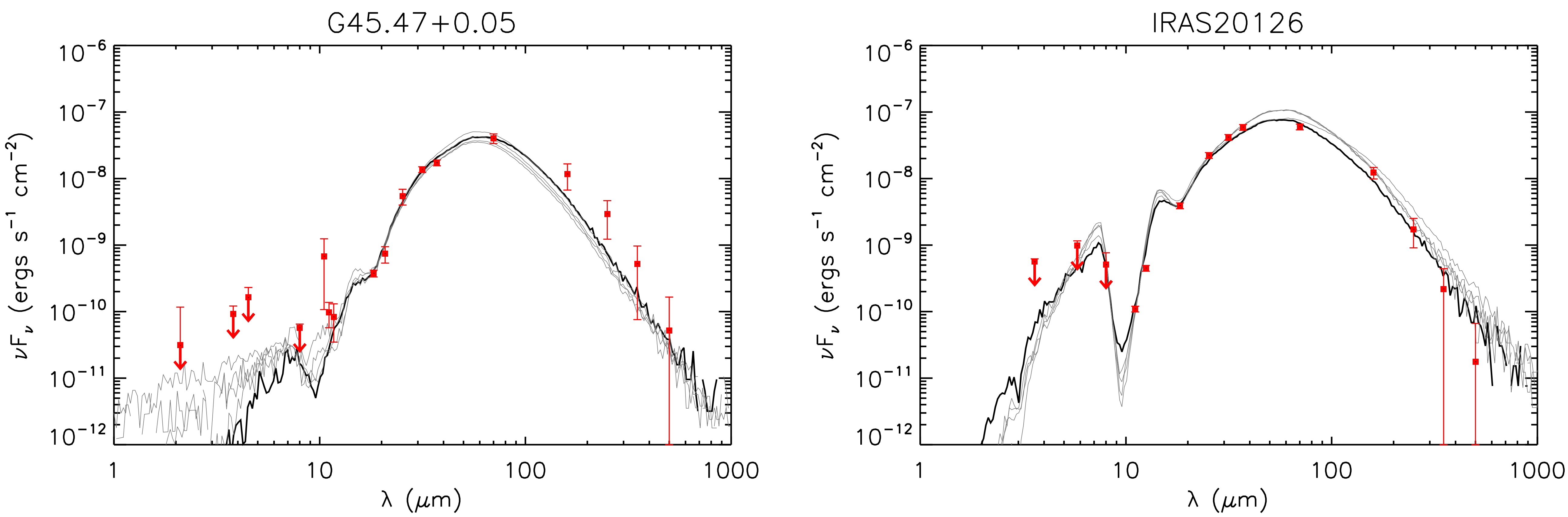


| Source | $\chi^2$ | $M_c$ ($M_\odot$) | $\Sigma_{\rm cl}$ (g cm$^{-2}$) | $R_c$ (pc) ($''$) | $m_*$ ($M_\odot$) | $\theta_{\rm view}$ ($^\circ$) | $A_V$ (mag) | $M_{\rm env}$ ($M_\odot$) | $\theta_{w,\rm esc}$ ($^\circ$) | $\dot{M}_{\rm disk}$ ($M_\odot$/yr) | $L_{\rm bol}$ ($L_\odot$) |
|---|---|---|---|---|---|---|---|---|---|---|---|
| | Zhang & Tan models | | | | | | | | | | |
| G45.47+0.05 | 1.21 | 200 | 3.2 | 0.06 (1) | 32 | 86 | 63.6 | 140 | 25 | 1.7(-3) | 4.6(5) |
| $d$ = 8.4 kpc | 1.34 | 320 | 1.0 | 0.13 (3) | 48 | 89 | 46.5 | 200 | 35 | 9.3(-4) | 5.1(5) |
| $R_{\rm ap}$ = 14.4$''$ | 1.57 | 320 | 1.0 | 0.13 (3) | 32 | 68 | 15.2 | 252 | 24 | 8.2(-4) | 2.7(5) |
| | 1.62 | 240 | 1.0 | 0.11 (3) | 32 | 86 | 1.0 | 170 | 30 | 7.2(-4) | 2.6(5) |
| | 1.75 | 240 | 1.0 | 0.11 (3) | 24 | 55 | 0.0 | 192 | 23 | 6.6(-4) | 1.7(5) |
| IRAS20126 | 1.82 | 80 | 0.3 | 0.12 (15) | 16 | 74 | 37.4 | 42 | 42 | 1.5(-4) | 4.2(4) |
| $d$ = 1.64 kpc | 2.07 | 120 | 0.3 | 0.14 (18) | 24 | 74 | 69.7 | 57 | 47 | 1.8(-4) | 9.3(4) |
| $R_{\rm ap}$ = 12.8$''$ | 2.32 | 80 | 0.3 | 0.12 (15) | 12 | 44 | 73.7 | 53 | 31 | 1.4(-4) | 3.4(4) |
| | 2.33 | 200 | 0.1 | 0.33 (41) | 12 | 86 | 65.7 | 174 | 20 | 8.0(-5) | 2.0(4) |
| | 2.39 | 100 | 0.3 | 0.13 (16) | 16 | 51 | 66.7 | 61 | 36 | 1.6(-4) | 4.5(4) |

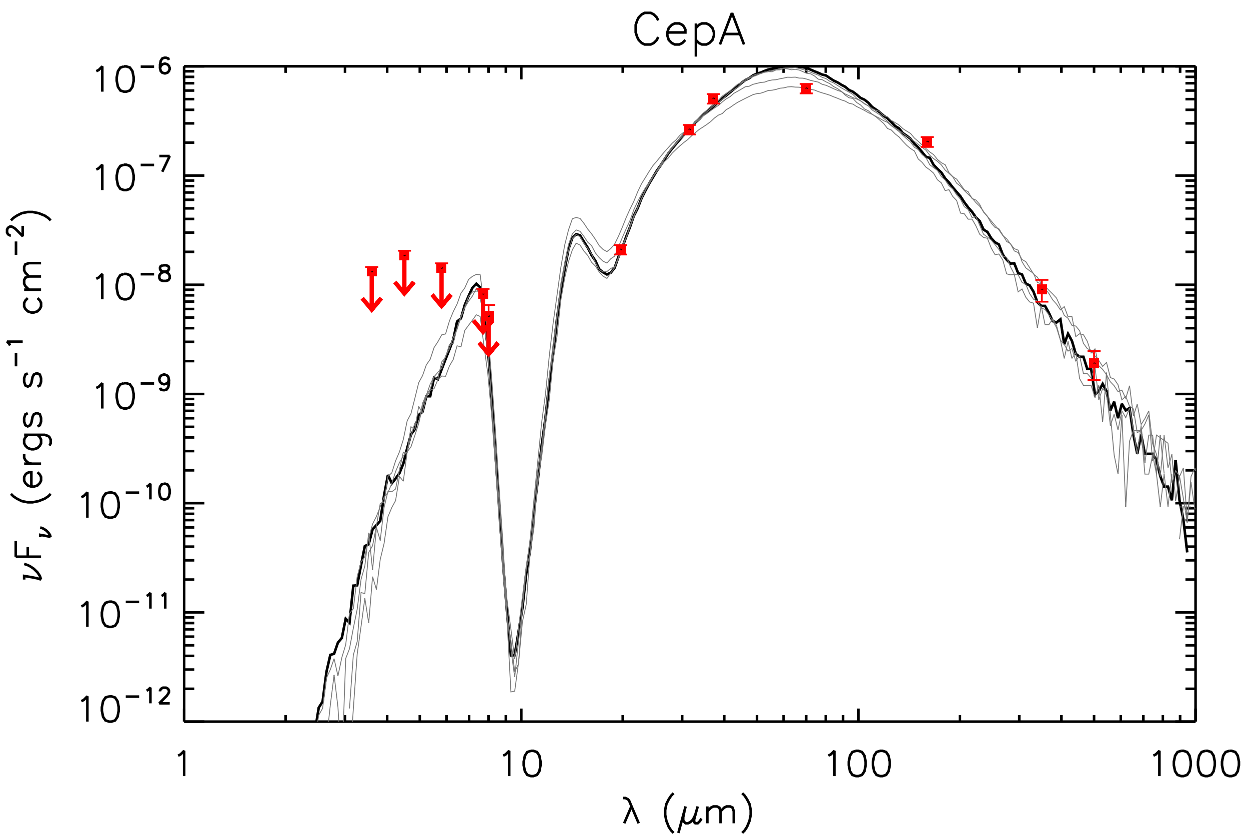


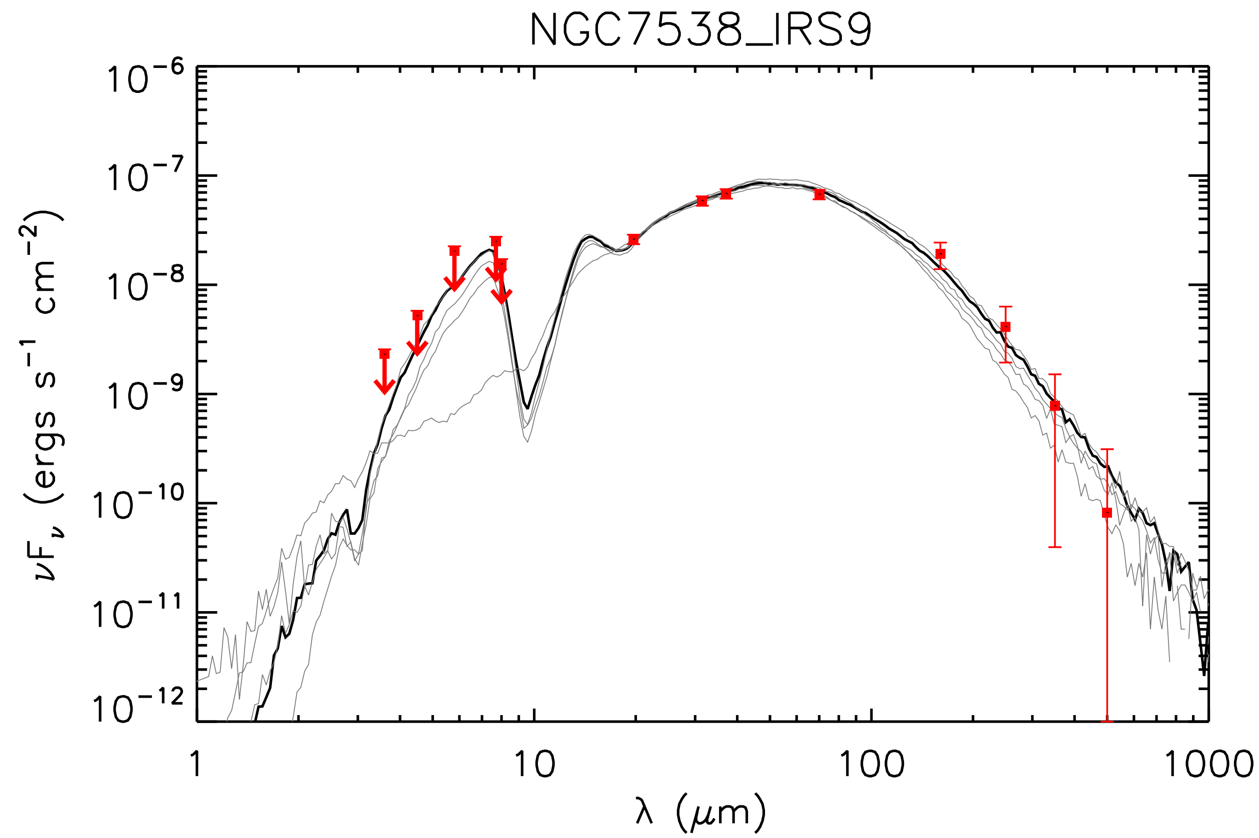


| | Zhang & Tan models | | | | | | | | | | |
|---|---|---|---|---|---|---|---|---|---|---|---|
| Source | $\chi^2$ | $M_c$ ($M_\odot$) | $\Sigma_{\rm cl}$ (g cm$^{-2}$) | $R_c$ (pc) ($''$) | $m_*$ ($M_\odot$) | $\theta_{\rm view}$ ($^\circ$) | $A_V$ (mag) | $M_{\rm env}$ ($M_\odot$) | $\theta_{w,\rm esc}$ ($^\circ$) | $\dot{M}_{\rm disk}$ ($M_\odot$/yr) | $L_{\rm bol}$ ($L_\odot$) |
| CepA | 2.17 | 160 | 0.3 | 0.17 (47) | 12 | 29 | 94.9 | 135 | 20 | 1.8(-4) | 3.8(4) |
| $d$ = 0.725 kpc | 2.21 | 160 | 0.3 | 0.17 (47) | 16 | 39 | 98.0 | 125 | 26 | 2.0(-4) | 5.0(4) |
| $R_{\rm ap}$ = 48.0$''$ | 2.65 | 400 | 0.1 | 0.47 (132) | 16 | 86 | 100.0 | 364 | 17 | 1.1(-4) | 3.8(4) |
| | 2.71 | 480 | 0.1 | 0.51 (145) | 12 | 83 | 80.8 | 460 | 12 | 1.1(-4) | 2.4(4) |
| | 2.81 | 160 | 0.3 | 0.17 (47) | 24 | 74 | 100.0 | 98 | 37 | 2.2(-4) | 9.9(4) |
| NGC7538 | 0.15 | 400 | 0.1 | 0.47 (36) | 16 | 22 | 23.2 | 364 | 17 | 1.1(-4) | 3.8(4) |
| IRS9 | 0.19 | 320 | 0.1 | 0.42 (32) | 16 | 39 | 2.0 | 281 | 19 | 1.1(-4) | 3.7(4) |
| $d$ = 2.65 kpc | 0.35 | 240 | 0.1 | 0.36 (28) | 24 | 39 | 52.5 | 171 | 33 | 1.1(-4) | 8.2(4) |
| $R_{\rm ap}$ = 25.6$''$ | 0.47 | 480 | 0.1 | 0.51 (40) | 16 | 22 | 17.2 | 440 | 15 | 1.2(-4) | 3.8(4) |
| | 0.54 | 60 | 3.2 | 0.03 (2) | 12 | 34 | 22.2 | 38 | 27 | 7.6(-4) | 5.0(4) |

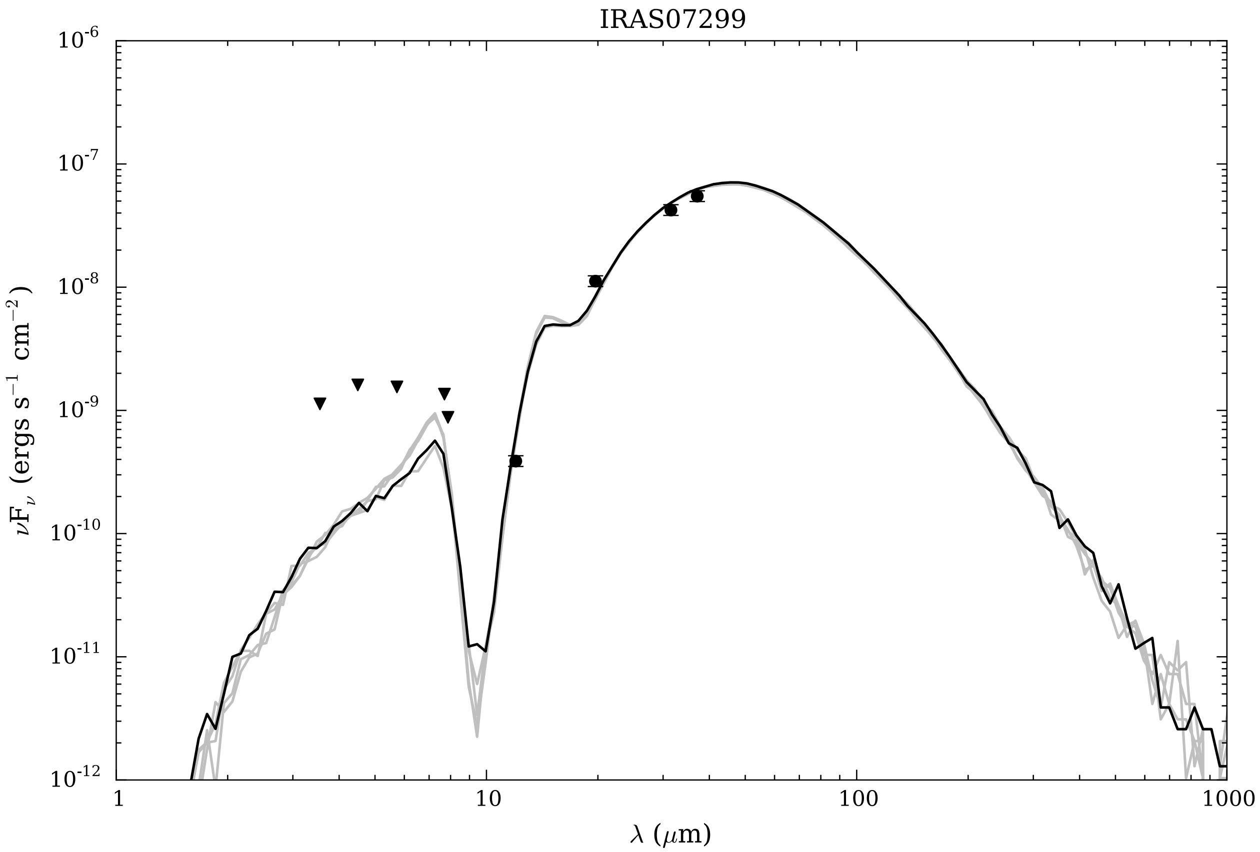


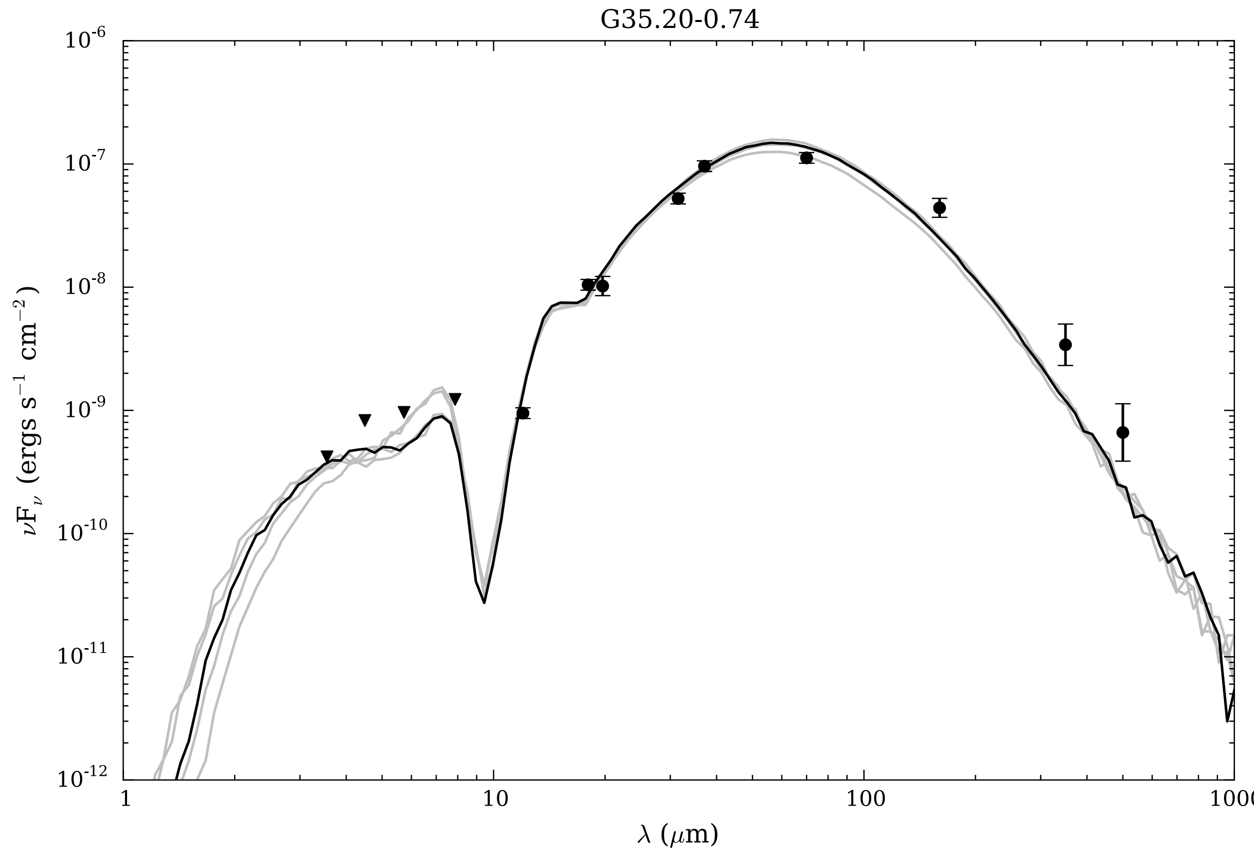


| | Zhang & Tan models | | | | | | | | | | | Robitaille et al. models | | | | | | | | | |
|---|---|---|---|---|---|---|---|---|---|---|---|---|---|---|---|---|---|---|---|---|---|
| Source | $\chi^2$ | $M_c$ ($M_\odot$) | $\Sigma_{\rm cl}$ (g cm$^{-2}$) | $R_c$ (pc) ($''$) | $m_*$ ($M_\odot$) | $\theta_{\rm view}$ (°) | $A_V$ (mag) | $M_{\rm env}$ ($M_\odot$) | $\theta_{w,\rm esc}$ (°) | $\dot{M}_{\rm disk}$ ($M_\odot$/yr) | $L_{\rm bol}$ ($L_\odot$) | $\chi^2$ | $m_*$ ($M_\odot$) | $\theta_{\rm view}$ (°) | $A_V$ (mag) | $M_{\rm env}$ ($M_\odot$) | $R_{\rm env}$ (pc) ($''$) | $\theta_{w,\rm esc}$ (°) | $\dot{M}_{\rm env}$ ($M_\odot$/yr) | $\dot{M}_{\rm disk}$ ($M_\odot$/yr) | $L_{\rm bol}$ ($L_\odot$) |
| IRAS07299 | 0.22 | 200 | 0.1 | 0.33 (48) | 8 | 89 | 20.2 | 181 | 14 | 6.8(-5) | 9.5(3) | 1.10 | 18 | 76 | 13.2 | 171 | 0.39 (57) | 10 | 4.3(-4) | ... | 8.3(3) |
| $d = 1.4$ kpc | 0.23 | 320 | 0.1 | 0.42 (61) | 8 | 83 | 3.0 | 307 | 11 | 7.7(-5) | 8.8(3) | 1.13 | 17 | 76 | 10.0 | 62 | 0.20 (30) | 6 | 4.0(-4) | ... | 6.6(3) |
| $R_{\rm ap} = 7.7''$ | 0.32 | 240 | 0.1 | 0.36 (53) | 8 | 86 | 22.2 | 226 | 13 | 7.1(-5) | 1.1(4) | 1.15 | 17 | 81 | 10.0 | 62 | 0.20 (30) | 6 | 4.0(-4) | ... | 6.6(3) |
| | 0.59 | 60 | 0.3 | 0.10 (15) | 12 | 77 | 9.1 | 32 | 40 | 1.2(-4) | 2.7(4) | 1.16 | 18 | 81 | 12.5 | 171 | 0.39 (57) | 10 | 4.3(-4) | ... | 8.3(3) |
| | 0.67 | 160 | 0.1 | 0.29 (43) | 8 | 89 | 33.3 | 143 | 17 | 6.3(-5) | 1.1(4) | 1.17 | 17 | 87 | 10.0 | 62 | 0.20 (30) | 6 | 4.0(-4) | ... | 6.6(3) |
| G35.20-0.74 | 2.63 | 480 | 0.1 | 0.51 (48) | 16 | 48 | 40.4 | 440 | 15 | 1.2(-4) | 3.8(4) | 2.26 | 20 | 87 | 20.7 | 597 | 0.48 (45) | 34 | 1.6(-3) | 2.8(-7) | 4.7(4) |
| $d = 2.2$ kpc | 2.64 | 100 | 3.2 | 0.04 (4) | 12 | 29 | 70.7 | 77 | 20 | 9.4(-4) | 5.2(4) | 2.40 | 20 | 81 | 24.1 | 597 | 0.48 (45) | 34 | 1.6(-3) | 2.8(-7) | 4.7(4) |
| $R_{\rm ap} = 32.0''$ | 2.76 | 320 | 0.1 | 0.42 (39) | 24 | 68 | 81.8 | 256 | 27 | 1.2(-4) | 8.4(4) | 2.49 | 20 | 76 | 33.0 | 597 | 0.48 (45) | 34 | 1.6(-3) | 2.8(-7) | 4.7(4) |
| | 2.76 | 80 | 3.2 | 0.04 (3) | 12 | 39 | 15.2 | 58 | 22 | 8.4(-4) | 5.0(4) | 2.54 | 19 | 70 | 16.4 | 679 | 0.48 (45) | 27 | 1.5(-3) | 2.6(-7) | 4.3(4) |
| | 2.77 | 200 | 0.3 | 0.19 (17) | 12 | 22 | 43.4 | 173 | 17 | 1.9(-4) | 4.0(4) | 2.70 | 18 | 76 | 16.8 | 560 | 0.48 (45) | 29 | 1.2(-3) | 3.9(-6) | 3.6(4) |

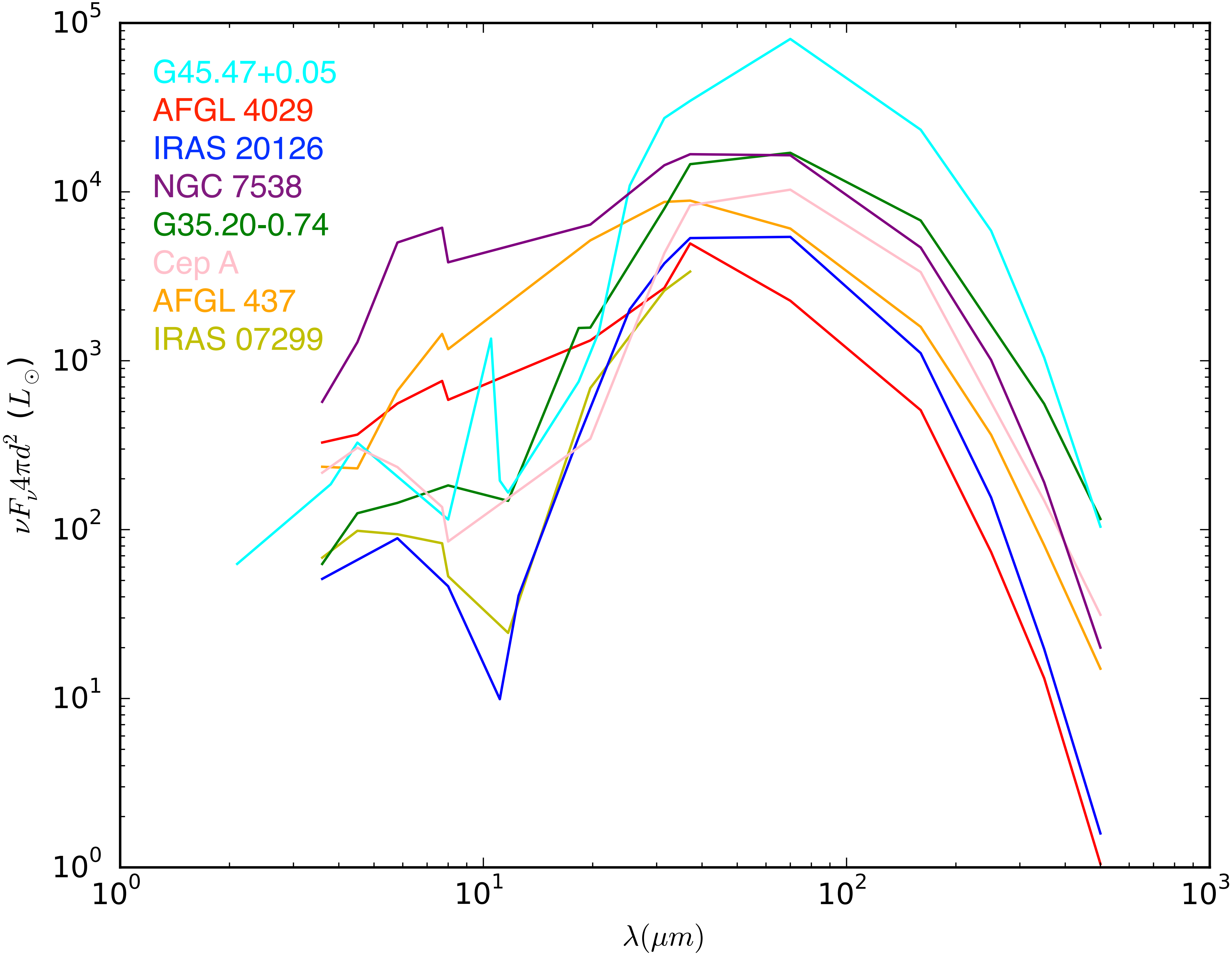
G45.47+0.05
AFGL 4029
IRAS 20126
NGC 7538
G35.20-0.74
Cep A
AFGL 437
IRAS 07299
$\nu F_\nu 4\pi d^2 \ (L_\odot)$
$\lambda(\mu m)$
$10^0$
$10^1$
$10^2$
$10^3$
$10^4$
$10^5$

# SOMA Next Steps

SOMA II. Massive Protostars Across Environments
(Liu et al.)

SOMA III. Model Fitting with SEDs & Image Intensity Profiles
(Zhang et al.)

SOMA IV. HST NIR Follow-up
(Da Rio et al.)

SOMA V. ALMA Outflow Follow-up
(Zhang et al.)

SOMA VI. ALMA Core Follow-up
(Liu et al.)

# Outflow-Confined HII Regions

**Tan & McKee (2003), Tanaka, Tan & Zhang (2016)**

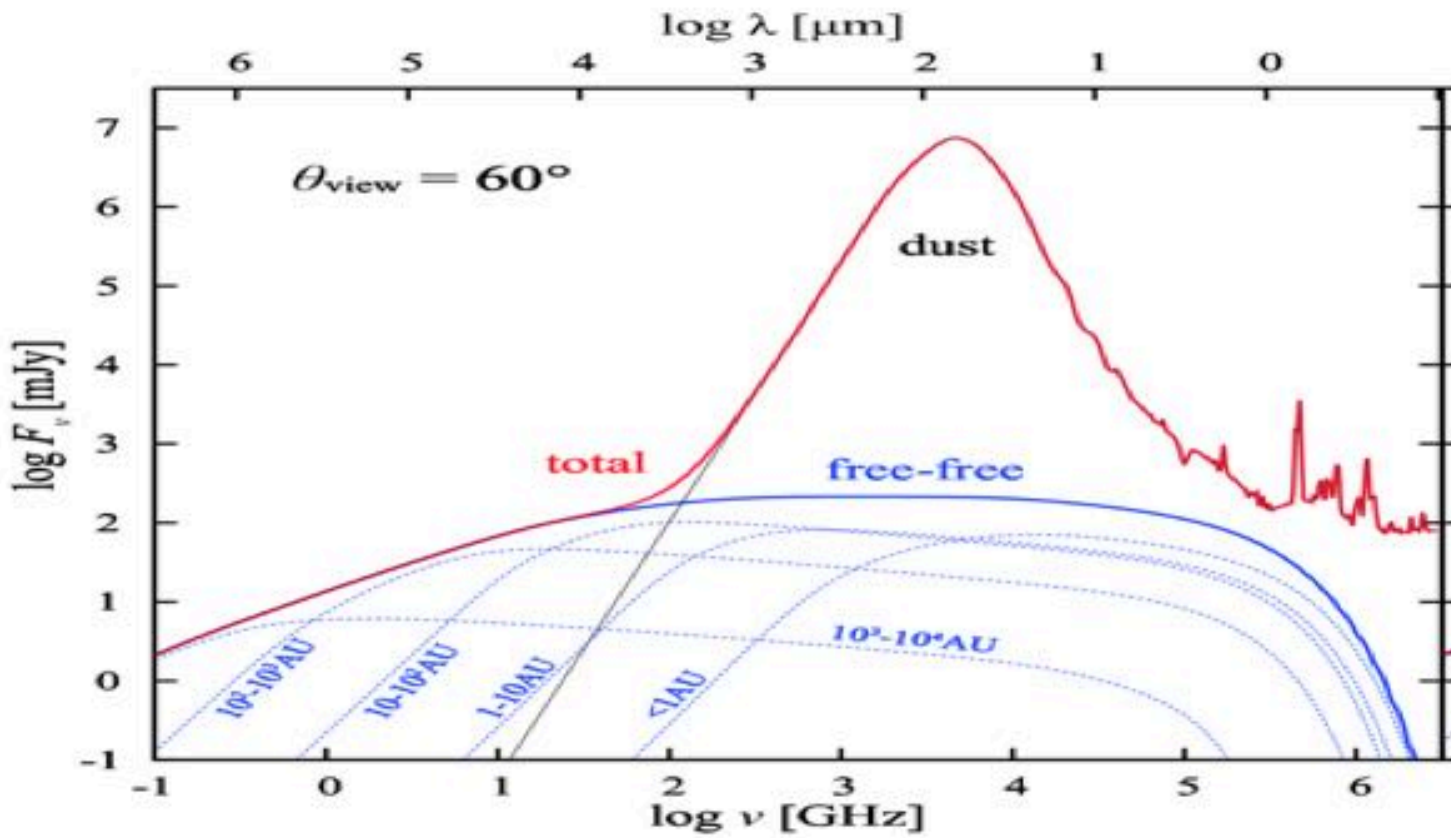


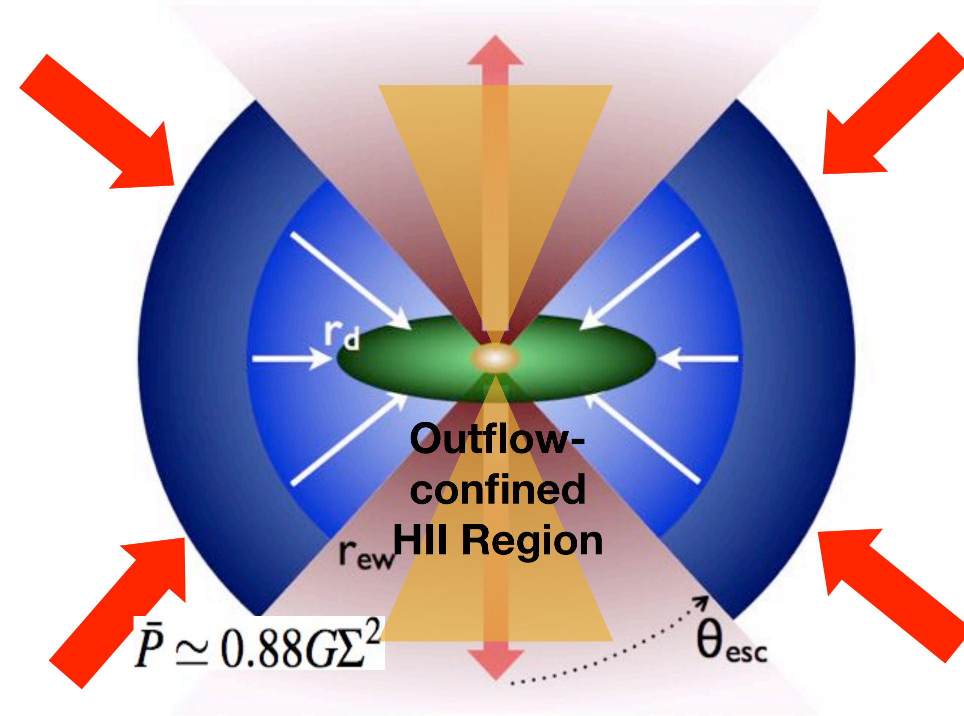


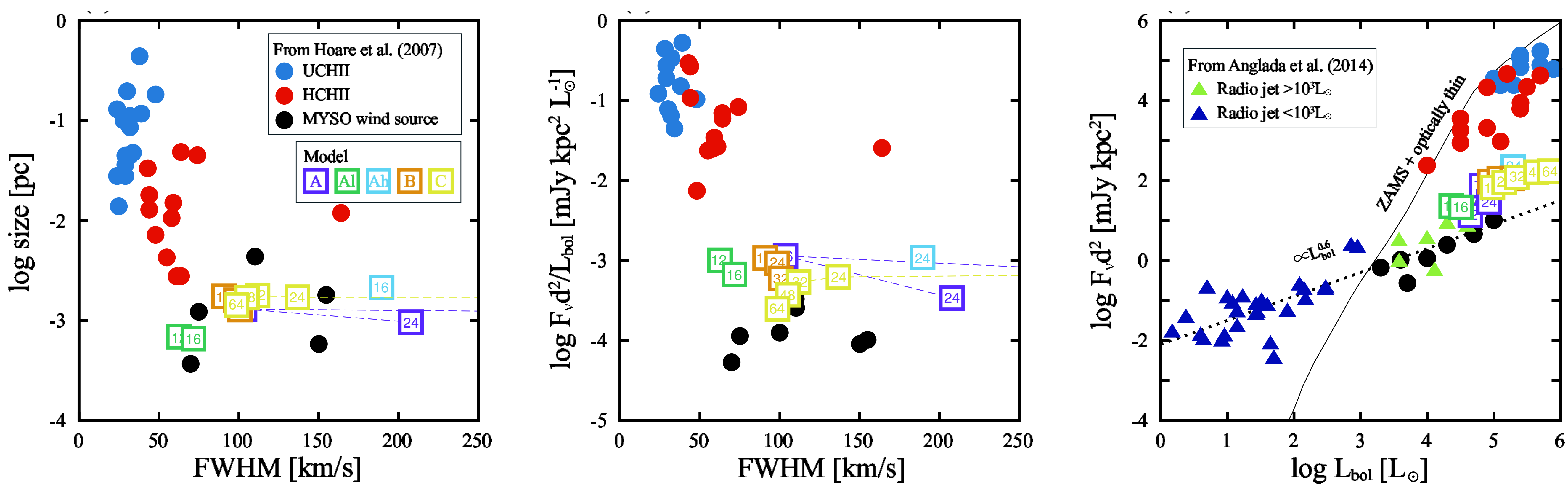

# Feedback During Massive Star Formation

Is there a maximum stellar mass set by by formation processes?

Salpeter (1955)

$dN_*/dm_* = A\, m_*^{-2.35}$

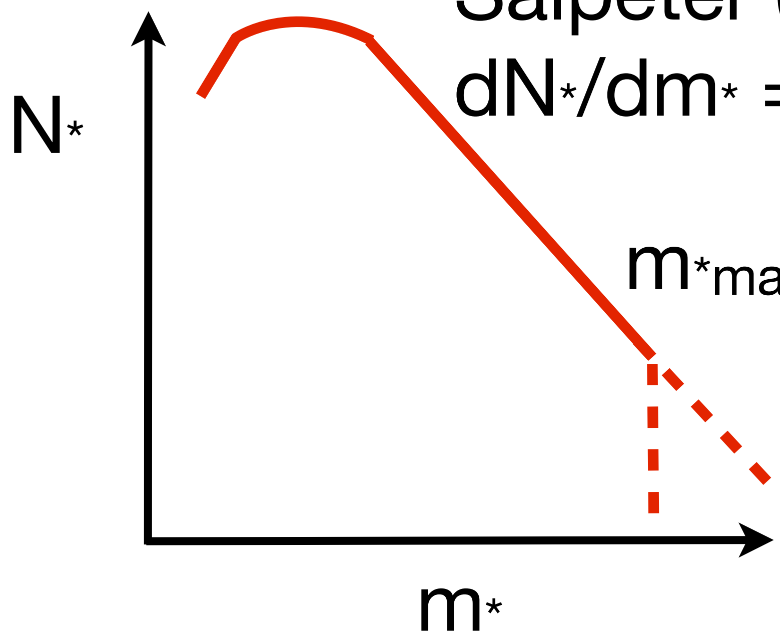



**$m_{*max}$~150 $M_\odot$ (e.g. Figer 2005).**

**But Crowther et al. (2010) claim most massive star to form was initially ~300$M_\odot$, consistent with statistical sampling of Salpeter IMF with no maximum cutoff mass.**

**Feedback processes:**

1. Protostellar outflows
2. Ionization
3. Stellar winds
4. Radiation pressure
5. Supernovae

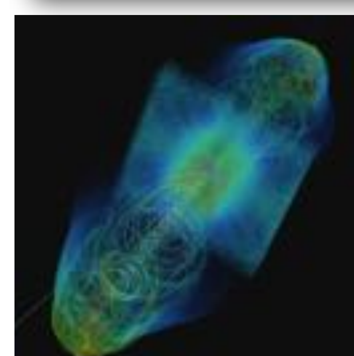

Staff+ (2010); Kuiper+ (2015)

Peters et al. 2010, 2011

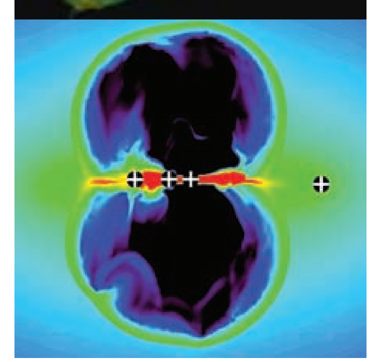

Krumholz+ (2009); Rosen+ (2016)
Kuiper et al. (2012); Klassen+ (2016)

**Accretion processes:** Core/disk fragmentation (Kratter & Matzner 06; Peters et al. 10)

**Stellar processes:** Nuclear burning instabilities/enhanced mass loss

**Currently unclear what sets the shape of the massive star IMF**

# Feedback

Tanaka, Tan, Zhang (2017)

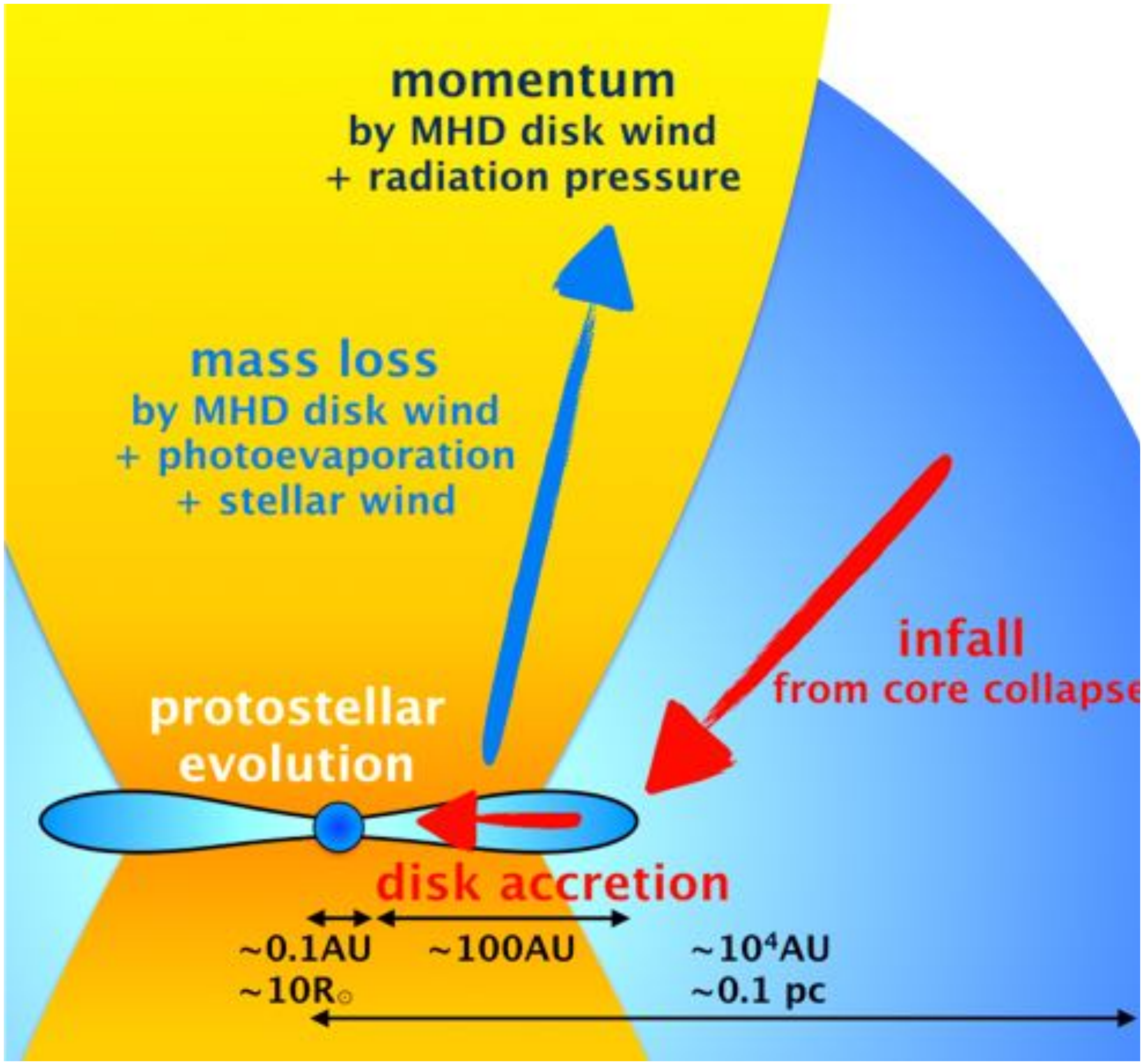


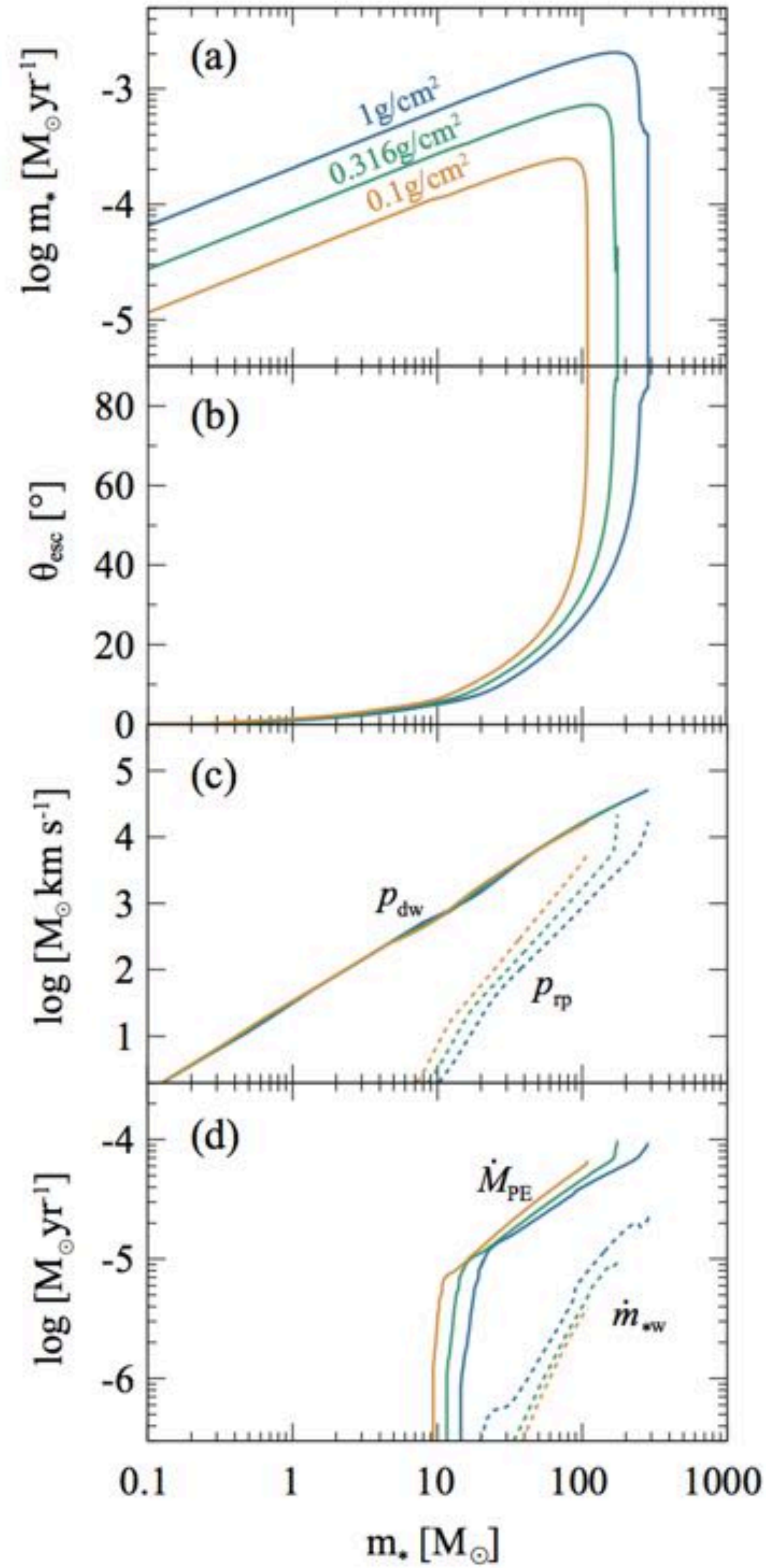

# Feedback

Tanaka, Tan, Zhang (2017)

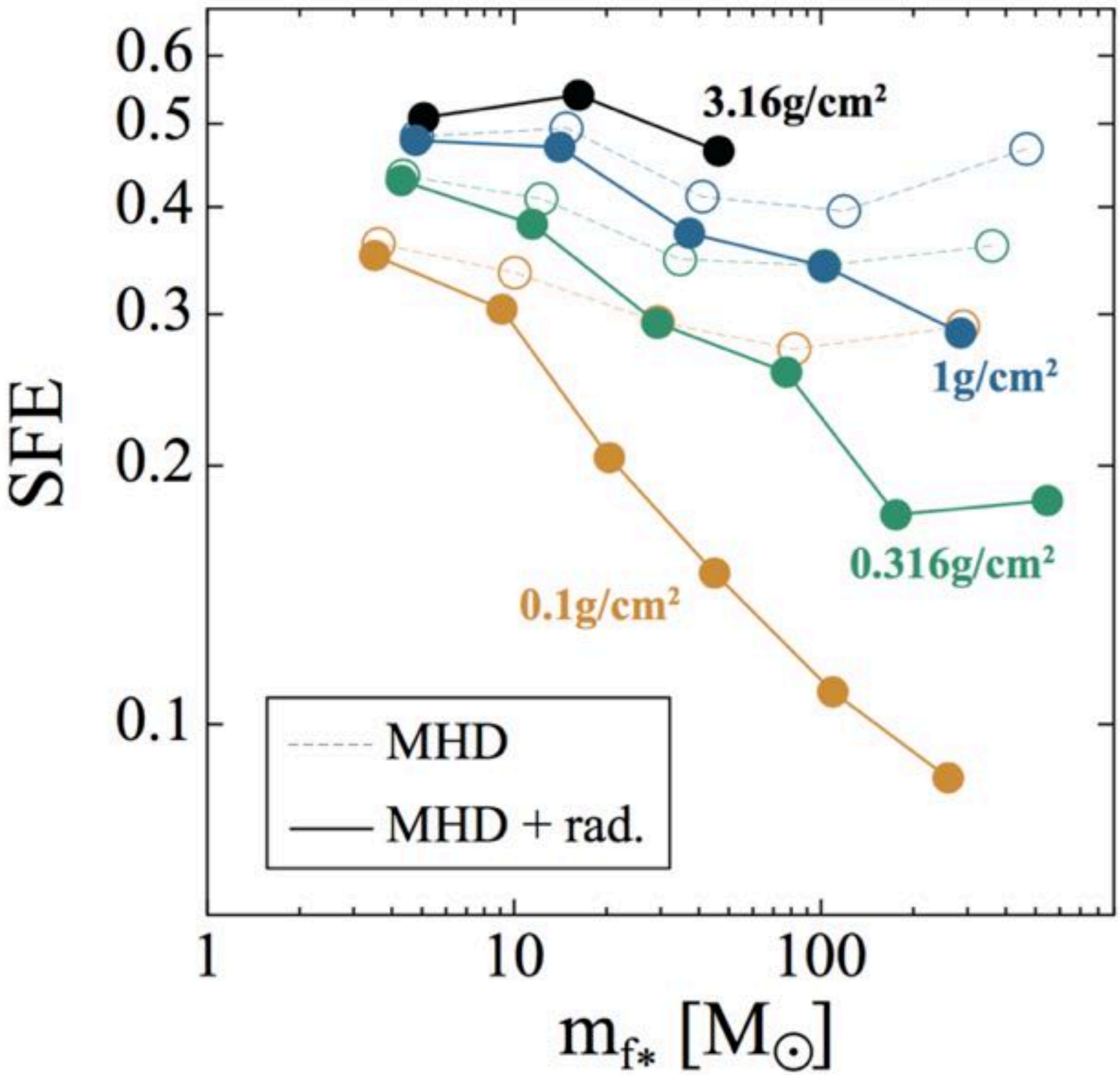


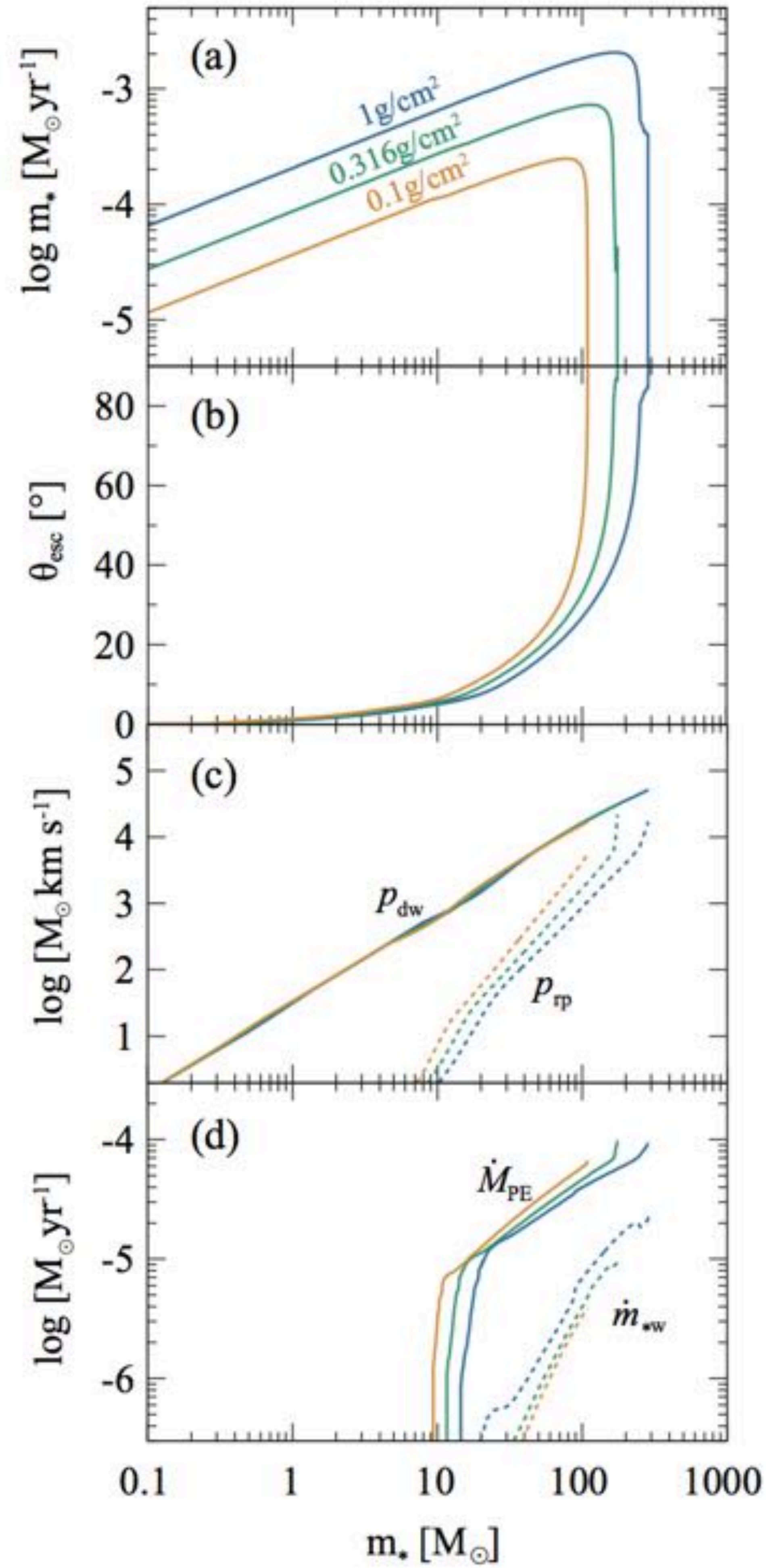

# Conclusions

**Massive Star Formation Theories:**
Core Accretion; Competitive Accretion; Protostellar Collisions

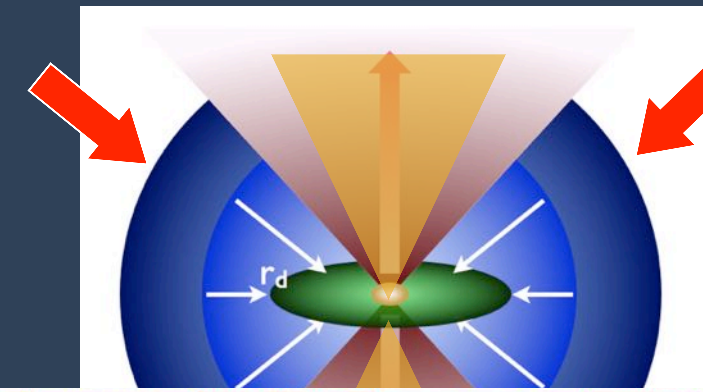


**Theory: “Turbulent Core Model”**:
normalize core surface pressure to surrounding clump pressure, i.e. self-gravitating weight. Core supported by non-thermal pressure (B-fields/turbulence).
Radiative transfer model grid
(Zhang & Tan, in prep.)

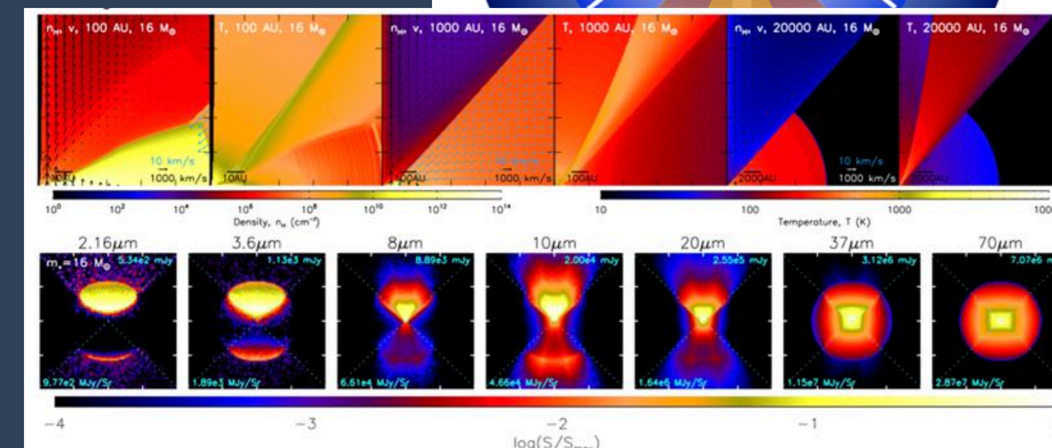


**1: Massive starless/early-stage cores exist in IRDCs (Tan+ 2013; Kong+ 2017b)**

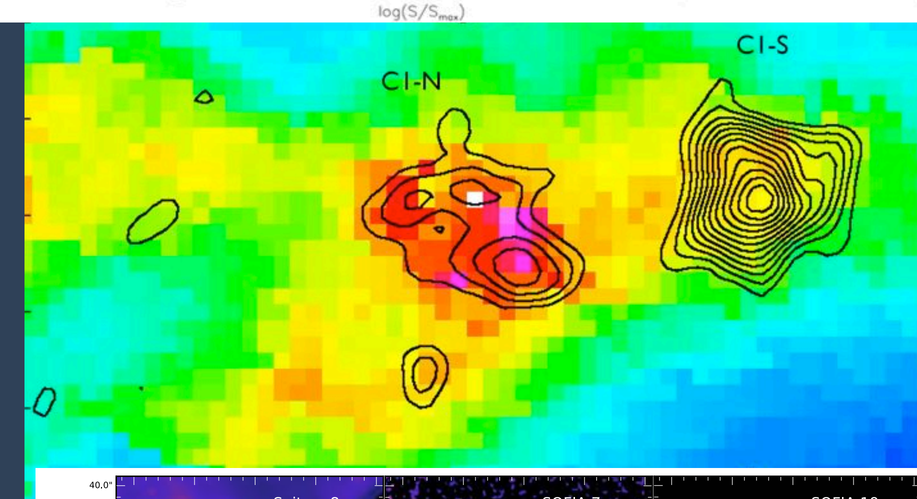


**2: SOMA Survey of Massive Protostars: (De Buizer+ 2017) High- & intermediate-mass protostars often have a similar morphology to low-mass protostars, e.g., collimated outflows. Bipoloar outflow cavities shape MIR to FIR morphology and SEDs. SED fitting alone has significant degeneracies. We expect these to be broken by intensity profile fitting & multiwavelength follow-up.**